D2-118405-1

POSTFLIGHT ANALYSIS OF THE APOLLO 14 CRYOGENIC OXYGEN SYSTEM

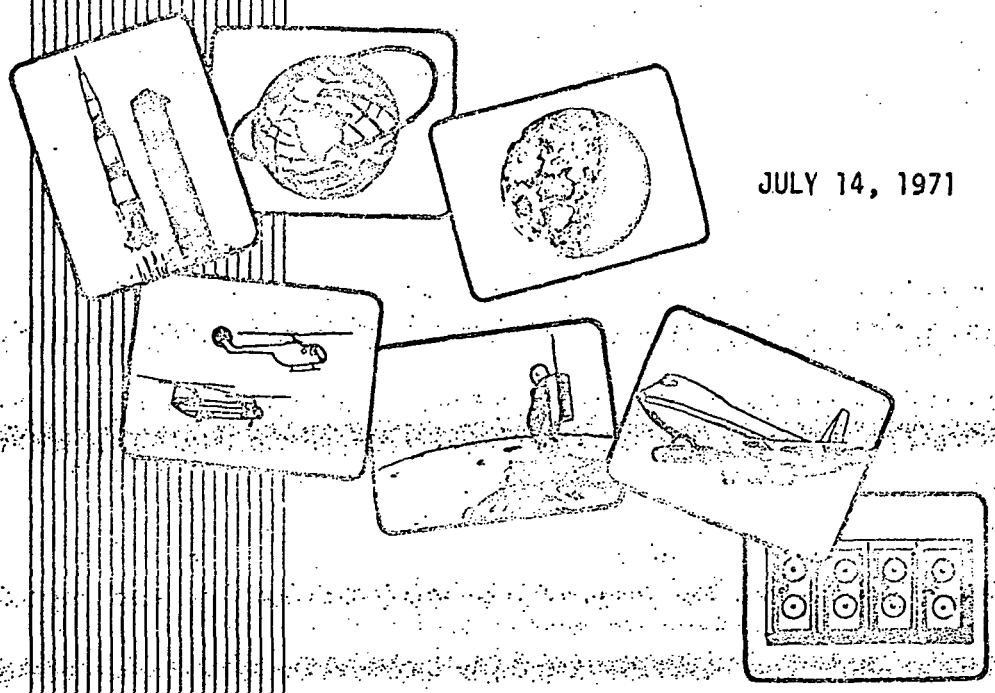

JULY 14, 1971

THE BOEING COMPANY
HOUSTON, TEXAS

II

MSC-04112
Supplement 2

APOLLO 14 MISSION REPORT

SUPPLEMENT 2

POSTFLIGHT ANALYSIS OF THE APOLLO 14 CRYOGENIC OXYGEN SYSTEM

PREPARED BY

Propulsion and Power Division

APPROVED BY

For James A. McDivitt
Brigadier General, USAF
Manager, Apollo Spacecraft Program

NATIONAL AERONAUTICS AND SPACE ADMINISTRATION
MANNED SPACECRAFT CENTER
HOUSTON, TEXAS
MARCH 1972

DOCUMENT NO. D2-118405-1

TITLE POSTFLIGHT ANALYSIS OF THE APOLLO 14 CRYOGENIC OXYGEN SYSTEM

CONTRACT NO. [redacted]

Prepared by:

Propulsion and Power Systems
5-2940

Prepared for:

National Aeronautics and Space Administration
Manned Spacecraft Center
Houston, Texas

July 14, 1971

Prepared by: D. D. Rule
J. E. Barton
H. W. Patterson

Approved by: R. K. Nuno (5-2940)
Program Manager

III

REVISIONS

REV. SYM	DESCRIPTION	DATE	APPROVED

TABLE OF CONTENTS

PARAGRAPH		PAGE
	Revisions	i
	Abstract and Key Words	ii
	Contents	iii
	Illustrations	iv
	Tables	vi
	Nomenclature	vii
	References	x
1.0	Introduction	1-1
1.1	Background	1-1
1.2	Scope	1-1
2.0	Summary	2-1
3.0	Methods of Analysis	3-1
3.1	Stratification and Heat Transfer	3-1
3.2	Tank Flow Rates	3-1
3.3	Tank Accelerations	3-5
4.0	Preflight Predictions	4-1
4.1	Nominal Conditions	4-1
4.2	DTO Tests	4-1
4.3	Real Time Flight Analysis	4-1
5.0	Postflight Analysis	5-1
5.1	Stratification Model Simulations	5-1
5.1.1	Nominal Heater Cycle	5-1
5.1.2	Maximum Quantity for EVA Flow Rates	5-2
5.1.3	Minimum Quantity for EVA Flow Rates	5-4
5.1.4	Maximum Pressure Decay	5-6
5.1.5	Short Heater Cycles	5-7
5.1.6	Heater Temperature at Low Quantity	5-10
5.2	Determination of Model Parameters	5-11
5.3	Results of Heater Temperature Correlation	5-13
6.0	Conclusions	6-1
7.0	Recommendations	7-1
	Appendix A - The Pressure Change Equation for a Cryogenic Tank	A-1
	Appendix B - Stratification Math Model	B-1
	Appendix C - Heater Temperature Correlations	C-1

ILLUSTRATIONS

FIGURE	TITLE	PAGE
3-1	Apollo 14 Oxygen System Flow Schematic	3-9
3-2	Oxygen Heat Exchanger Restrictor Performance	3-10
3-3	Oxygen Tank Heat Leak at Zero Expulsion	3-11
3-4	Tank 3 Pressure and Flow Response During High Flow Test	3-12
3-5	Tank 1 Pressure and Flow Response During High Flow Test	3-13
3-6	Vehicle Angular Motion During High Flow Test	3-14
4-1	Potential Pressure Decay Comparisons	4-3
4-2	Effect of Acceleration on Potential Pressure Decay	4-4
4-3	Attitude Hold Heater Cycle - 0.95 ft^2 Heater Area	4-5
4-4	Attitude Hold Heater Cycle - 0.475 ft^2 Heater Area	4-6
4-5	Real Time High Flow Test Simulation	4-7
5-1	PTC Heater Cycle Simulation	5-14
5-2	PTC Heater Cycle Convergence	5-15
5-3	Tank 1 Test Simulation - 0.95 ft^2 Heater Area	5-16
5-4	Tank 1 Test Simulation - 0.475 ft^2 Heater Area	5-17
5-5	Tank 1 Transient Pressure and Flow Response	5-18
5-6	Plumbing System Pressure Response with High Flow Rates	5-19
5-7	Tank 1 Test Simulation with Pressure Dependent Flow Rate	5-20
5-8	Tank 1 Test Convergence with Pressure Dependent Flow Rate	5-21
5-9	Tank 1 Potential Pressure Decay During the High Flow Test	5-22
5-10	Convergence of Maximum Potential Pressure Decay During the High Flow Test	5-23
5-11	Tank 3 Test Simulation	5-24
5-12	Tank 3 Test Convergence	5-25
5-13	Simulation of Heater Cycle at AET 5:15	5-26
5-14	Potential Pressure Decay, .95 ft^2 Heater Area	5-27

ILLUSTRATIONS (Continued)

FIGURE	TITLE	PAGE
5-15	Potential Pressure Decay, .475 ft^2 Heater Area	5-28
5-16	Heater Sensor Temperature Simulation, AET 5:15 to 5:44	5-29
5-17	Convergence of Maximum Potential Pressure Decay at AET 5:44	5-30
5-18	Convergence of Heater Sensor Temperature at AET 5:44	5-31
5-19	Length of Equilibrium Heater Cycle at 92% Quantity	5-32
5-20	Effect of Acceleration on Heater Cycles, AET 10:30 12:30	5-33
5-21	Effect of Acceleration on Heater Sensor Temperature AET 10:30-12:30	5-34
5-22	Simulation of AET 10:30 to 12:00 Using 100 x 10 Grid	5-35
5-23	Effect of Stratification on Length of Heater Cycle	5-36
5-24	Effect of Stratification on Heater Sensor Temperature	5-37
5-25	Convergence of Heater Sensor Temperature at AET 11:50	5-38
5-26	Convergence of Length of Cycle Time at AET 11:45	5-39
5-27	Build-Up of Potential Pressure Decay from AET 10:30 to 12:30	5-40
5-28	Convergence of Maximum Potential Pressure Decay at AET 12:30	5-41
5-29	Low Density Heater Cycle Simulation	5-42
5-30	Low Density Heater Cycle Convergence	5-43
5-31	Radiant Heat Transfer During Low Density Heater Cycle	5-44
5-32	Temperature Comparisons Summary	5-45
5-33	Empirical Heater Response, 97% Quantity	5-46
5-34	Empirical Heater Response, 15% Quantity	5-47
5-35	Empirical Heater Response, 17% Quantity	5-48
5-36	Empirical Heater Response, 43% Quantity	5-49
5-37a-f	Parametric Heater Response	5-50 thru 5-55

TABLES

TABLE	TITLE	PAGE
5-1	Stratification Model Parameter Summary	5-11

NOMENCLATURE

Symbols

A	Area
b	Tank wall thickness
C_k	Constant in heater temperature sensor lag equation
C_p	Specific heat at constant pressure
C_s	Stefan Boltzman constant
C_{ra}	Constant in Rayleigh heat transfer equation (equal 0.525)
D	Diameter
E	Young's modulus
F	Impulse Function or Thrust
$\overline{F}$	Thrust vector
$\overline{g}$	Acceleration in Earth gravity units
GM	Product of gravitational constant and attracting body mass
h	Enthalpy
I	Vehicle inertia matrix
K	Thermal conductivity
L	Length
M	Mass
MC	Heater thermal mass
N	Polytropic exponent
P	Pressure
Q	Quantity of heat
R	Gas constant
$\overline{R}$	Position vector
R_a	Rayleigh number
r	Tank radius
T	Temperature
t	Time
U	Internal energy
V	Volume
v	Velocity
$\dot{W}$	Weight flow rate
$\overline{\alpha}$	Vehicle angular acceleration vector
β	Coefficient of thermal expansion

NOMENCLATURE (Continued)

Symbols

γ	Ratio of specific heats
ε	Heater emissivity (0.2 assumed)
ρ	Density
ϕ	Thermodynamic property, $\frac{1}{\rho \frac{\partial U}{\partial P}}$
θ	Thermodynamic property, $-\rho \frac{\partial h}{\partial \rho}$
σ	Poisson's ratio
μ	Viscosity
$\bar{\omega}$	Vehicle angular velocity vector

Subscripts

b	Bulk fluid
cg	Center of gravity
d	Demand
f	Thrust
g	Attracting body (earth or moon)
h	Heater
L	Lines
o	Reference stagnation state
t	Tank
s	Sensor
∞	Condition or state at infinite expansion

NOMENCLATURE (Continued)

Acronyms

AET	Apollo Elapsed Time
CSM	Command Service Module
DAP	Digital Auto-Pilot
DTO	Detailed Test Objectives
EVA	Extra-Vehicular Activity
GET	Ground Elapsed Time
LM	Lunar Module
MSC	Manned Spacecraft Center
PTC	Passive Thermal Control
RCS	Reaction Control System
SRU	Sperry Rand Univac

REFERENCES

1. C. K. Forester, Pressurized Expulsion of Non-Isothermal Single Phase Cryogen, paper at the NASA-MSC Cryogenic Symposium, May 20 and 21, 1971.

2. C. K. Forester, D. D. Rule, and H. W. Patterson, Apollo Oxygen Tank Stratification Analysis, The Boeing Company, D2-118357-1, November 30, 1970.

3. Apollo 14 Flight Data for Tank Accelerations and Miscellaneous Cryogenic System Variables.

4. A. H. Shapiro, The Dynamics and Thermodynamics of Compressible Fluid Flow, Volume 1, The Ronald Press Company, 1953.

5. Task Summary, Apollo 14 Oxygen Tank Tests (DTO) Predictions, The Boeing Company, January 29, 1971.

6. Apollo Fuel Cell and Cryogenic Gas Storage System Flight Support Handbook, NASA-MSC Document, February 18, 1970.

7. H. W. Patterson, Correlation of Apollo Oxygen Tank Thermodynamic Performance Predictions, paper at the NASA-MSC Cryogenic Symposium, May 20 and 21, 1971.

1.0 INTRODUCTION

The Apollo 13 incident resulted in the removal of the mixing fans from the oxygen tanks for the Apollo 14 and subsequent spacecraft. Since the performance of such tanks in the low-g flight environment cannot be duplicated on the ground, flight performance could not be firmly established from ground test data. Thus, the Apollo 14 mission provided the first flight data on the performance of the oxygen tanks.

Accurate prediction of tank performance capability is necessary to satisfy mission planning requirements for Apollo 15 and subsequent flights because the oxygen tanks will be used to the maximum extent of their performance capability . Therefore, the post-flight analysis of the Apollo 14 spacecraft tank performance was conducted not only to establish the adequacy of the tanks for these future flights, but to determine if the existing stratification model for low-g oxygen thermodynamic behavior was adequate to predict flight performance for Apollo 15 and subsequent flights.

1.1 Background

Comprehensive stratified performance analyses of the Apollo oxygen tanks were not conducted prior to the Apollo 13 incident since mixing fans were available to reduce the effects of stratification on tank operation. After the Apollo 13 incident, an oxygen stratification model was developed (References 1 and 2) and verified by analysis of data obtained for one period of the Apollo 12 mission. This analysis verified the model ability to predict pressure collapses which could occur as a result of stratification. The ability to predict heater temperatures could not be verified since the Apollo 12 tanks did not contain heater temperature sensors.

The resulting stratification model was used to produce pre-flight predictions for the Apollo 14 oxygen tanks performance. These predictions, however, would not be adequate for later missions, which would include tank conditions (flow rates, quantities, and accelerations) for which the model had not been verified.

1.2 Scope

The Apollo 14 post-flight analysis consisted of stratification model simulations of tank performance for six different conditions of flow rate, tank quantity, and acceleration. The six conditions, selected with the concurrence of the Technical Monitor, included two periods of passive thermal control, two periods of attitude hold, and the two high flow EVA simulation tests (DTO). Quantities from 15 to 97% and

1.2 Scope (Continued)

flow rates from approximately 1.5 lbs/hour to more than 4.5 lbs/hour were included in these simulations. The results (tank pressures, heater temperatures, and heater cycles) of the simulations based on actual accelerations and flow rates are compared with the best available flight data. The comparisons of flight data with simulation results are discussed and the flight stratified performance of the redesigned tanks evaluated. The simulation accuracies obtained from varied model parameters are evaluated and model parameters are selected for the best prediction capabilities. Simulations of heater temperatures based on empirical heat transfer equations are also compared with flight data, and parametric temperature predictions are presented. The ability of the redesigned tanks to satisfy future mission requirements is assessed based on the combined stratification model and empirical heat transfer equation data.

2.0 SUMMARY

The Apollo oxygen tanks were redesigned and the mixing fans removed after the Apollo 13 incident. The ability of the redesigned tanks to provide all mission flow requirements was not demonstrated in a flight environment prior to the Apollo 14 mission. Pre-flight predictions of tank performance for the Apollo 14 mission were made with a stratification math model validated by analysis of one Apollo 12 condition. These predictions provided confidence that the Apollo 14 mission could be successfully performed, but did not adequately evaluate tank performance for conditions such as EVA expected during later missions.

The post-flight analysis of the Apollo 14 mission was performed to better evaluate the redesigned tank performance in the flight environment, and the ability of the stratification math model to predict flight performance. The math model was evaluated by simulating tank pressures and heater temperatures with the model and comparing the results with flight data for six different conditions. The ability to satisfy future mission requirements was evaluated on the basis of potential pressure decay data resulting from the simulations. The heater temperature data from the simulations was supplemented with data generated from empirical heat transfer relationships to evaluate heater performance for the full range of flight conditions.

The simulations included nominal attitude hold and passive thermal control (PTC) tank acceleration conditions, as well as abnormally high (5×10^{-6} g) acceleration conditions caused by the planned oxygen venting during the high flow DTO tests. Tank quantities from 15% to 97% and flow rates to more than 4.5 lbs/hour during these conditions were included in these evaluations.

The simulated maximum heater temperatures were in excellent agreement with flight data for the attitude hold and PTC periods as shown below.

QUANTITY, CONDITION	ASSUMED HEATER AREA	TEMPERATURE ERROR
97%, Attitude Hold	0.95 Ft^2	+ 2°F
92%, Attitude Hold	0.95 Ft^2	-12°F
70%, (DTO)	0.95 Ft^2	+31°F
54%, PTC	0.475 Ft^2	- 9°F
20%, (DTO)	0.95 Ft^2	-45°F
	0.475 Ft^2	+60°F
15%, PTC	0.475 Ft^2	-10°F

The best accuracies were obtained by using the larger heater area for high quantities. The heater area for best accuracy did not depend on the flight condition. The reduced accuracy of the DTO simulated temperatures may have been caused by abnormal accelerations which were

2.0 SUMMARY (Continued)

not perpendicular to the heater as assumed by the model. Heater temperatures simulated with empirical heat transfer relationships were within 50°F of flight for all conditions investigated except the 20% DTO condition. These results, which agreed favorably with the stratification model results, were used to generate parametric heater temperature data and to evaluate mission capabilities.

The only significant pressure decay resulting from stratification during the Apollo 14 mission occurred at 97% tank quantity. The math model estimated decay of 86 psi was in agreement with flight data. The actual flight decay was between 59 and 100 psi. No other pressure decay occurred during the flight. The evaluation of the model decay simulation capability was severely limited by the lack of flight decays and resulting data. Since pressure decays and heater temperatures are closely and fundamentally related by the model, the demonstrated accurate heater temperature simulations adequately validated the model for predictions of pressure decays.

It was concluded from the Apollo 14 preflight and postflight analyses that the redesigned oxygen tanks could supply the known required flow rates for the Apollo missions. The worst case pressure decay during a three hour EVA period will be less than 230 psi. The stratification model was found to be adequate for predictions of the most important tank performance variables (pressure decays and heater temperatures).

3.0 METHODS OF ANALYSIS

3.1 Stratification and Heat Transfer

The constant grid stratification math model (References 1 and 2) was used to simulate the overall oxygen tank stratified performance (pressure, pressure decay, heater temperature, etc). A brief description of the model equations and assumptions is included in Appendices A and B. Heater temperature sensor response was calculated by an empirical method developed to model heat transfer in supercritical oxygen. This method uses a Rayleigh number convection correlation with the fluid properties treated by averaging as described in Appendix C.

3.2 Tank Flow Rates

The oxygen flow distribution system is shown by Figure 3-1. The system includes check valves which are intended to prevent flow into the tanks during normal operation. The isolation valve between tanks 2 and 3 is normally open and for the Apollo 14 mission was closed only during the high flow test. The flow restrictors are capillary tubes with flow pressure drop characteristics as shown by Figure 3-2. The restrictors are the only significant source of pressure drop in the system.

The data available from the system include fluid quantity and pressure, and heater temperature for each of the three cryogenic tanks. The surge tank is instrumented to provide pressure data only. The flow rate to the environmental control system is measured downstream of the surge tank and, therefore, includes contributions from all four of the tanks. The flow rate to the fuel cells is also measured, but can be more accurately determined from the electrical current.

The total flow from the three tanks during the Apollo 14 mission was determined from the fuel cell usage and the pressure drop across the restrictors to the environmental control system (ECS). The flow rate to the fuel cells was computed using the fuel cell current, because this method is more accurate than the use of the fuel cell flow meters. The flow rate across the restrictors during high flow periods was based on the restrictor pressure drop calibrations. During low flow periods, the average restrictor flows were obtained from the ECS flow rate (measured downstream of the restrictors) and the net change of mass in the surge tank during the period. The net change of mass in the surge tank was calculated from only the surge tank pressure; thus, differences in calibration of the surge tank and oxygen tank pressure transducers did not affect the results.

The flow rates from the individual cryogenic tanks were not measured; therefore, it was necessary to divide the total system flow among the three tanks. The individual tank flow rates were determined from the total system flow on the basis of equilibrium tank thermodynamics. The pressure differences between tanks were used to determine the check valve configuration and to constrain the thermodynamic calculations.

3.2 Tank Flow Rates (Continued)

The flow distribution is affected by the heat input to the separate tanks. Individual tank heat leaks were estimated from flight data. The tank 1 and tank 3 heat leaks were found to be nominal at zero flow rate at 90% and 10% quantities, respectively (Figure 3-3). The tank 2 heat leak was not verified, but is believed to have been slightly greater than nominally expected. The tank 2 heat leak could not be determined for a zero flow condition because the check valve provided to isolate the tank was found to be leaking, thus causing abnormal pressure rise rates within the tank with the heaters off. The check valve also permitted warm fluid to flow back into the tank causing warming of the insulation and increasing the heat leak.

The flow rate distributions were obtained by simultaneous solution of the pressure change equations (see Appendix A) for the tanks supplying the system flow. The calculations included the effects of tank elasticity, a factor strongly affecting the relative pressure change rates within the tanks. The simultaneous solution of the pressure change equations for the tanks supplying the system demand related the individual tank flow to the total flow. The total flow used for this calculation included the flow rate required to pressurize the external line volumes. These calculations are simplified if the pressure change rate is known and used with the nominal heat leak to determine the individual tank flows. The flow rates from this method are in the same ratio as those provided by simultaneous solution of the equations.

The tank 2 check valve leak required special consideration to determine the flow into the tank which caused the tank 2 pressurization rate with heaters off to be the same as the tank 3 rate with heaters on. The flow rate into the tank was determined from the volume change required to produce the observed pressure change. Using equation A-13 from Appendix A and considering the volume change due to a hot bubble as well as tank elasticity, the pressure change is:

$$\frac{dP}{dt} = \frac{\phi}{V}\left(\frac{dQ}{dt} + \theta\frac{dM_d}{dt}\right) - \frac{1}{V}\rho_t\theta\phi\left[\left(\frac{dV}{dt}\right)_t + \left(\frac{dV}{dt}\right)_L\right] \qquad (1)$$

where $\left(\frac{dV}{dt}\right)_L$ is the volume change due to a bubble of fluid at the line density

3.2 Tank Flow Rates (Continued)

During pressurization, the demand flow $\frac{dM_d}{dt}$ is zero. Substituting $-\frac{1}{\rho_L}\frac{dM}{dt}$ for $\left(\frac{dV}{dt}\right)_L$ and solving for $\frac{dM}{dt}$ results in

$$\frac{dM}{dt} = \frac{\rho_L}{\rho_t}\frac{V}{\phi\theta}\left[\frac{dP}{dt} - \frac{\phi}{V}\frac{dQ}{dt} + \frac{1}{V}\rho_t\phi\theta\left(\frac{dV}{dt}\right)_t\right] \qquad (2)$$

This method of determining tank 2 inflow during the tank 3 heater cycle at 26 hours AET showed the check valve leakage rates to be approximately 0.05 lbs/hour which is believed to be realistic. The tank 2 inflow is an additional demand flow for tank 3 when the check valve is presumably closed, but the small additional flow is within the accuracy of the data and was neglected in subsequent analyses.

The flow rate distribution calculations were accomplished in a subroutine of the stratification math model for simulation of periods with several heater cycles. The surge tank pressure in the model was calculated from the initial pressure and the net mass inflow determined from the restrictor and ECS flow rates. The restrictor flow rate was determined from an equation approximating the restrictor pressure drop calibration data (Figure 3-2). The surge tank pressure change equation was switched from an isothermal approximation to an adiabatic approximation when the pressure change rate exceeded 4 psi/minute.

The flow rate subroutine treated the inactive tanks with equilibrium thermodynamics. The inactive tanks did not share the system flow when the active (stratified) tank pressure was above the inactive tanks pressure. When the active tank pressure was not greater than the inactive tanks, the total flow was distributed among all tanks. Switching between these two flow configurations resulted in some instability; as, for example, when the active tank(s) was (were) capable of pressurizing with all tanks flowing, but depressurized when only the active tank(s) was (were) flowing. This instability persisted for a few time steps and caused erratic pressure change rates, but did not affect heater temperatures. The instability was most significant when the inactive tanks were capable of supplying the total flow with little pressure change. The instability affected the pressure rise rate for the simulation of the heater cycle at AET 185 and the pressurization time for this simulation was manually corrected during the period of instability. The instability did not significantly affect the results of other simulations.

3.2 Tank Flow Rates (Continued)

Thermodynamic analyses were not required to distribute the flows during the high flow tests, since the isolation valve was closed and the system flow logic determined each of the tank flow rates. The tank 3 flow rates during the tests were determined from the restrictor pressure drop while the surge tank valve was open (Figure 3-4). Flow rates were assumed constant while the surge tank valve was closed. The tank 1 flow rates (Figure 3-5) were also determined from the restrictor pressure drop, but included the fuel cell flow rate when the tank 1 pressure was greater than the tank 2 pressure. The flow rates from both tanks 1 and 3 increased by approximately 0.35 lbs/hour at AET 168:40 when the urine dump valve was opened. The tank 2 pressure rise after 168:40 was apparently caused by a leak of 0.08 lbs/hour through both the fuel cell valve module check valve and the tank 2 check valve. This estimated leak rate is small compared to the total tank flow and was neglected.

3.3 Tank Accelerations

The sources of accelerations in a space vehicle in drifting flight include vehicle rotations, thrusts caused by fluid venting, gravity gradients and solar pressure. The solar pressure is approximately 10^{-7} lbs/ft^2 and produces an acceleration of less than 5×10^{-9} "g" for the Apollo vehicle. The acceleration due to solar pressure was an order of magnitude smaller than the accelerations produced by vehicle rotations during typical attitude hold periods and was, therefore, neglected.

The procedure for the analysis of accelerations during attitude hold conditions used rotation rates from guidance data directly for the centripetal acceleration. The rotation rates were numerically differentiated for the angular acceleration term. The total acceleration due to rotation is:

$$32.174\ \bar{g} = \bar{\omega} \times \bar{\omega} \times (\bar{R}_t - \bar{R}_{cg}) + \bar{\alpha} \times (\bar{R}_t - \bar{R}_{cg}) \qquad (3)$$

Telemetry data from the digital auto pilot used for the analysis includes the three components of the rotation vector and the calculation is, in principle, straightforward. Some difficulty does, however, arise due to the angular acceleration. The angular acceleration terms tend to dominate the centripetal terms, because the centripetal acceleration depends on the square of the rotation area. The acceleration term also introduces questions of significance due to the short durations of application. Typically, the reaction control system jet firings cause angular accelerations greater than 2×10^{-4} radians/second^2, but the duration is of the order of 10 milliseconds. This acceleration results in a movement of the oxygen tank of about 10^{-7} inches during the time the acceleration is applied. This small displacement would appear to be negligible; however, the angular accelerations should certainly not be entirely ignored. The approach used was to distribute the angular acceleration over time intervals of 10 seconds or greater by numerical differentiation of the observed angular rates at the end points of the time interval. The time intervals were selected on the basis of engineering judgement to adequately characterize the accelerations events. Although this procedure is arbitrary, the results appear to be satisfactory and a better method has not presented itself.

The tank accelerations during stable periods of passive thermal control (PTC) were calculated without consideration of angular accelerations. During PTC flight modes, the reaction control system is deactivated and the vehicle is essentially spin stabilized. For this condition, angular accelerations are generally negligible and the centripetal acceleration only is significant.

3.3 Tank Accelerations (Continued)

When the vehicle is in attitude hold in the near vicinity of the earth or moon, the gravity gradient acceleration is significant. This term, which must be added to the rotational accelerations, is:

$$32.174\ \bar{g} = \frac{2\ GM\ (\bar{R}_g \cdot \bar{R}_t)\bar{R}_g}{\bar{R}_g^{\ 4}\ |\bar{R}_g|} \tag{4}$$

The gravity gradient term is of the order of 10^{-7} "g" for a 100 mile altitude earth orbit. Since the magnitude of the gravity gradient is proportional to $1/|\bar{R}_g|^3$, the term becomes negligible at distances of 2 to 3 earth radii. The radius vector to the attracting body in the vehicle coordinate system is necessary to the gravity gradient calculation. This vector can only be determined from the vehicle trajectory and inertial platform data. A computer program for the calculation of the acceleration including the gravity gradient term derived from trajectory data was developed by NASA-MSC for the Apollo 14 mission. The tank accelerations from this program (Reference 3) were used for nominal attitude hold and passive thermal control (PTC) periods analyzed.

The high flow oxygen tank tests during the Apollo 14 mission were not in nominal flight "g" conditions due to overboard dumping of oxygen. The oxygen dumped overboard through a convergent nozzle in the command module entry hatch produced a significant thrust and vehicle acceleration. A preflight estimate of the tank accelerations during the high flow test was made by analyzing the vent nozzle thrust and vehicle dynamics.

The thrust from the oxygen vent was calculated as the thrust from a convergent nozzle exhausting to vacuum. The choked nozzle thrust is

$$F_N = \frac{F_\infty}{\left(\frac{F}{F^*}\right)_\infty} \tag{5}$$

where $\left(\frac{F}{F^*}\right)_\infty$ is the ratio of the impulse function with expansion to zero pressure to the impulse function at the sonic throat. The impulse function ratio is 1.4289 at zero pressure from the isentropic tables (Reference 4) with a specific heat ratio of 1.4 for oxygen. The thrust resulting from expansion to zero pressure is:

$$F_\infty = \frac{V_\infty \dot{W}}{32.174} \tag{6}$$

and for a perfect gas

$$V_\infty = \sqrt{\frac{(2)(32.174)\gamma RT}{\gamma - 1}} \tag{7}$$

3.3 Tank Accelerations (Continued)

Therefore:

$$F_{\infty} = \frac{\dot{W}}{32.174}\sqrt{\frac{64.348\ \gamma RT}{\gamma-1}} \tag{8}$$

The nozzle thrust is then:

$$F_N = \frac{\dot{W}}{(1.4289)(32.174)}\sqrt{\frac{64.348\ \gamma RT}{\gamma-1}} \tag{9}$$

The vent flow at 0.00172 lbs/sec or 6.2 lbs/hour resulted in a thrust of 0.091 pounds. The calculated thrust of 0.091 pounds is a lower limit since no expansion downstream of the throat or plume effects were considered.

The 0.091 pounds thrust produced a linear "g" of 3.65×10^{-6} for the 24,985 pounds vehicle weight at the time of the test. The thrust vector was not through the vehicle center of mass, therefore, rotational accelerations were also produced. The equation for the angular accelerations is:

$$\overline{R}_f \times \overline{F} = I\overline{\alpha} \tag{10}$$

and solving

$$\overline{\alpha} = I^{-1}\ (\overline{R}_f \times \overline{F}) \tag{11}$$

The moments of inertia obtained from preflight mass properties data were used with equation (11) to predict angular acceleration rates. The rotation rates were then calculated from the time required to rotate the vehicle through the 5° dead band. Finally, rotational tank accelerations were calculated from equation (3). The total tank 3 "g" was found to be 4.9×10^{-6} and for tank 1 a "g" of 4.7×10^{-6} was obtained. These accelerations neglected the effects of reaction control system firings as well as plume effects and should be somewhat lower than actually experienced.

The basic guidance data from the Digital Auto Pilot (DAP) was used for the postflight analysis to determine if the preflight acceleration prediction was valid. The vehicle attitude errors for a 14 minute period analyzed are shown by Figure 3-6. These data indicate that the vehicle was oscillating primarily about the y axis, and the oscillation amplitude was less than 0.3 degrees. The oscillations result from the steady torque of the vented oxygen increasing the attitude error to the deadband limit (approximately ± 5°) and the RCS correction firings driving the vehicle back inside the dead band.

3.3 Tank Accelerations (Continued)

Rotational accelerations were calculated from the angular error amplitudes and time between RCS firings assuming the accelerations were constant between the RCS firings. The torque caused by the vented oxygen was inferred from the rotational accelerations and the vehicle moments of inertia. The thrusts were in turn calculated from the torques and the locations of the vent and the center of gravity.

The average vent thrust calculated from these data were approximately 0.06 pounds, but variations of more than a factor of 2 occurred between successive vehicle oscillations. Since a vent thrust of .09 pound was used for the preflight acceleration estimate, it was concluded that the 4.9×10^{-6} "g" used for the simulations could not be significantly improved. The 0.09 pound thrust calculated for a choked nozzle is believed to be more accurate than the 0.06 pound estimated from the guidance data. A thrust lower than .09 pound could only be obtained if the flow was significantly less than 6 pounds per hour.

The guidance data indicates RCS firings about once per minute. Each of the firings causes a high acceleration of very brief duration. This acceleration contribution was neglected in the estimated acceleration. Including an average value for this term would raise the "g" level by less than 30% resulting in less than 10°F change in heater temperature. It was concluded that the 4.9×10^{-6} "g" estimate was sufficiently accurate for use in all postflight analyses of the high flow test.

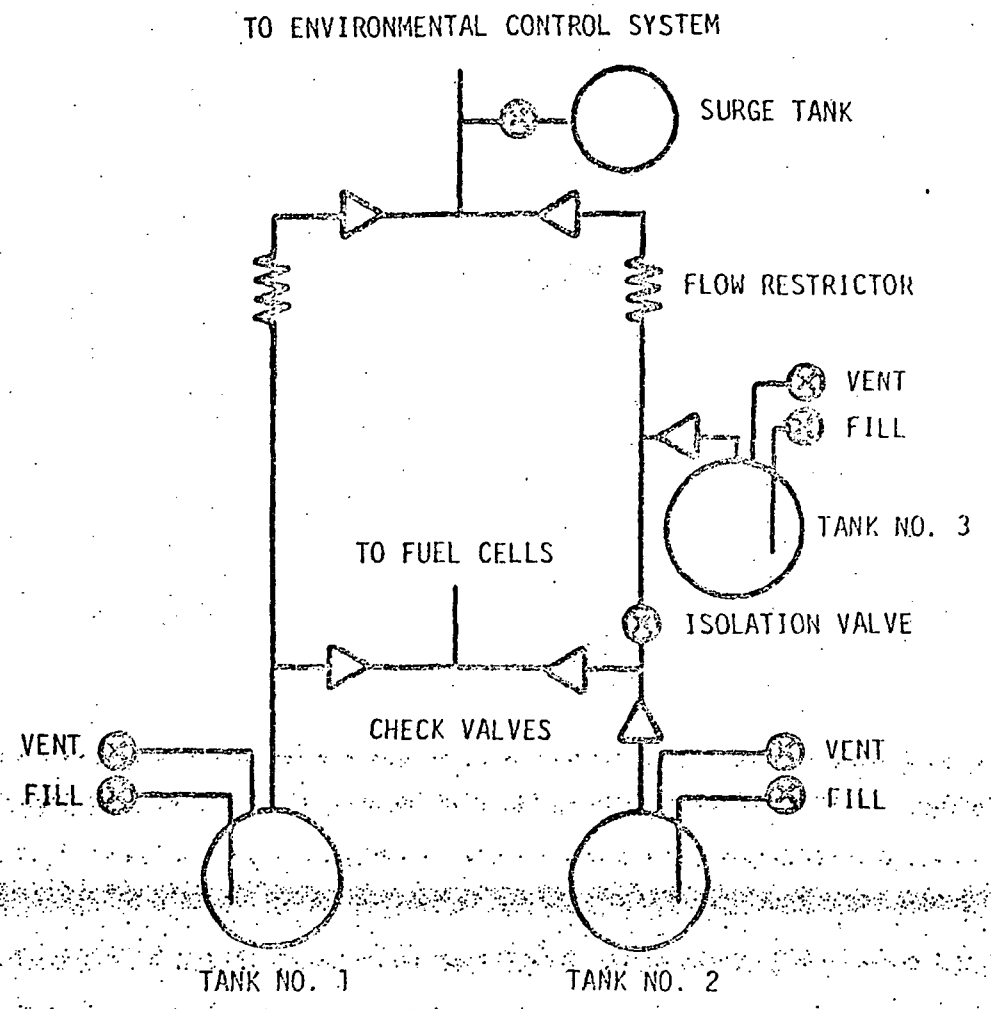

FIGURE 3-1 - APOLLO 14 OXYGEN SYSTEM FLOW SCHEMATIC

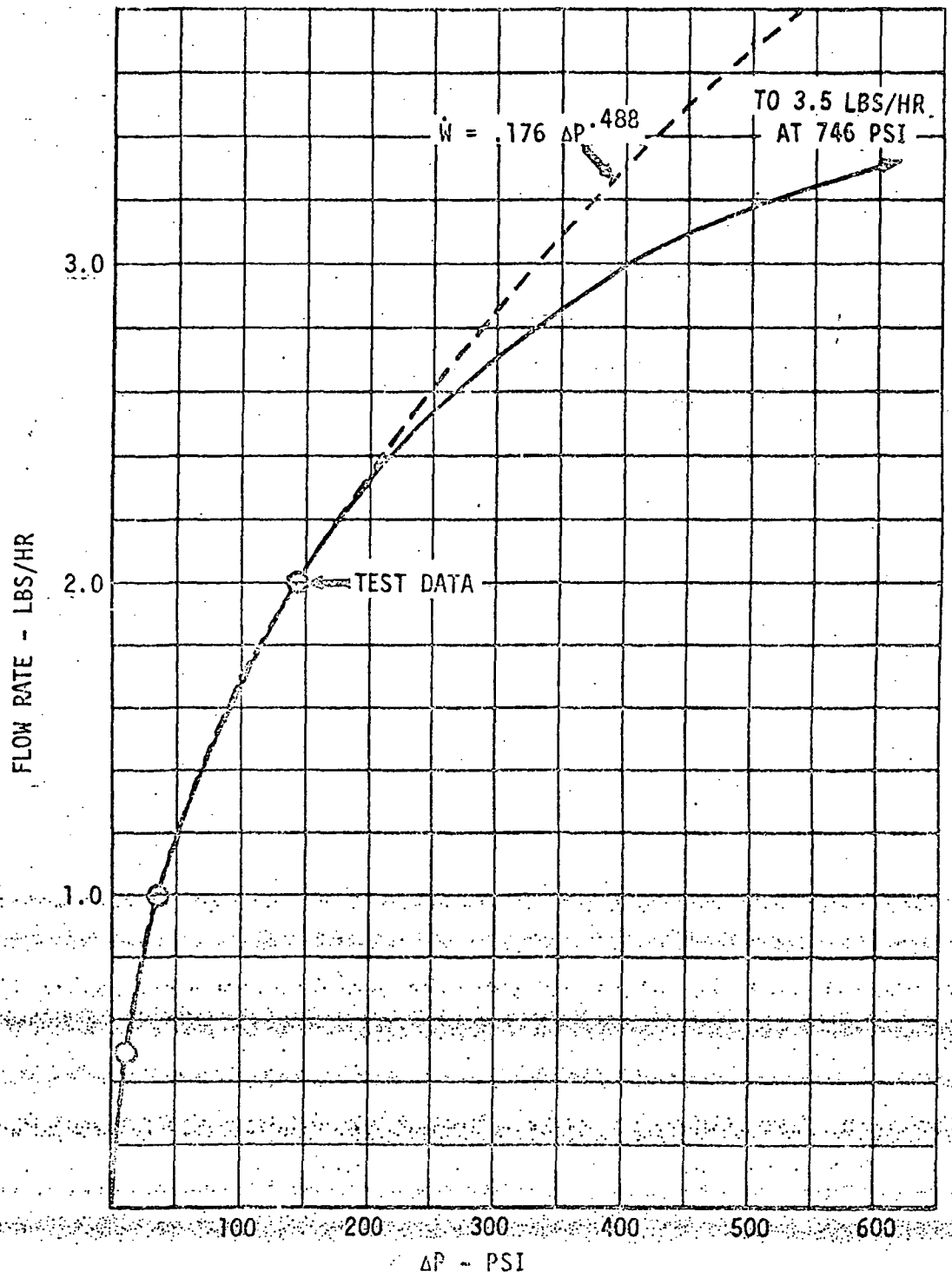

FIGURE 3-2 - OXYGEN HEAT EXCHANGER RESTRICTOR PERFORMANCE

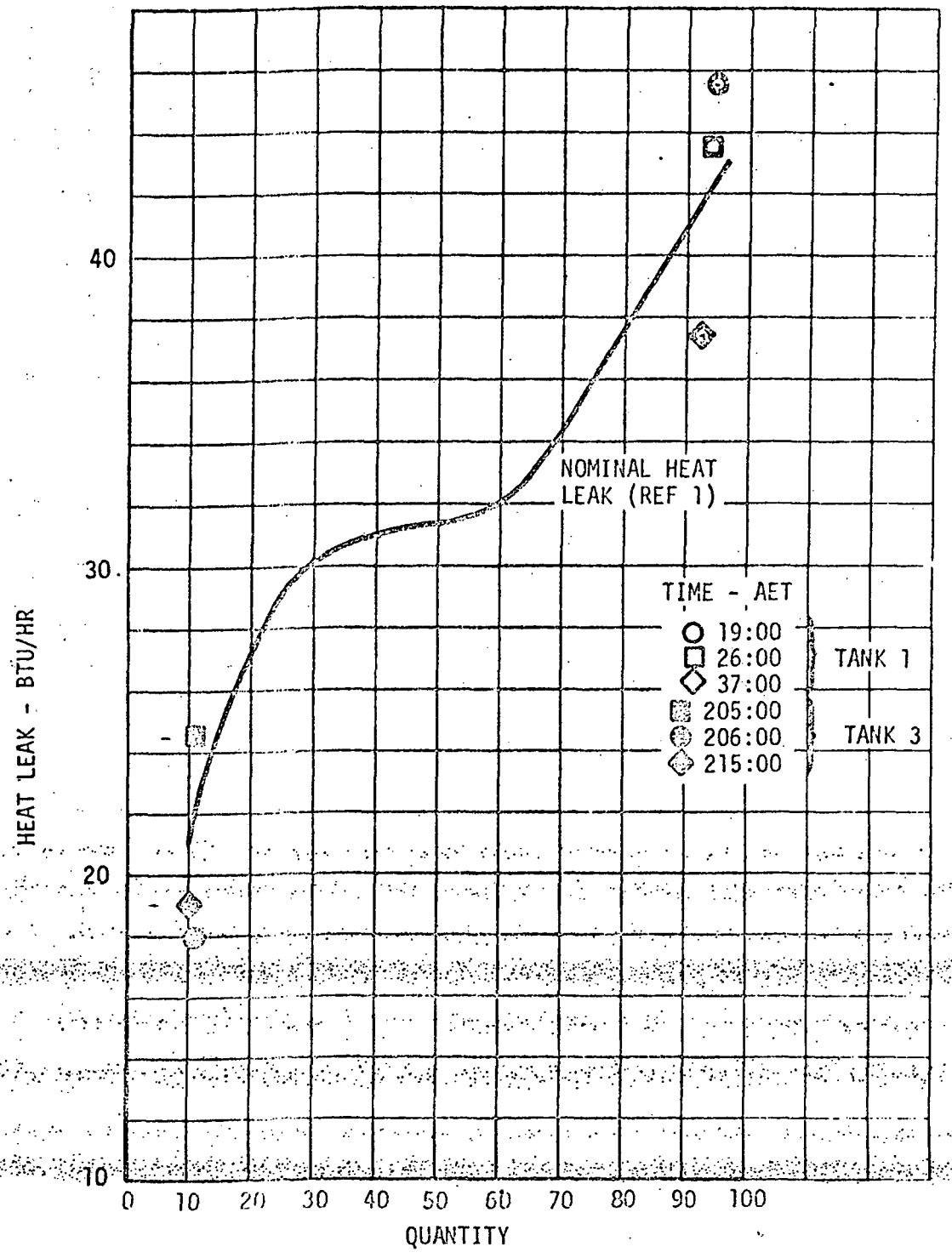

FIGURE 3-1 - OXYGEN TANK HEAT LEAK AT ZERO EXPULSION

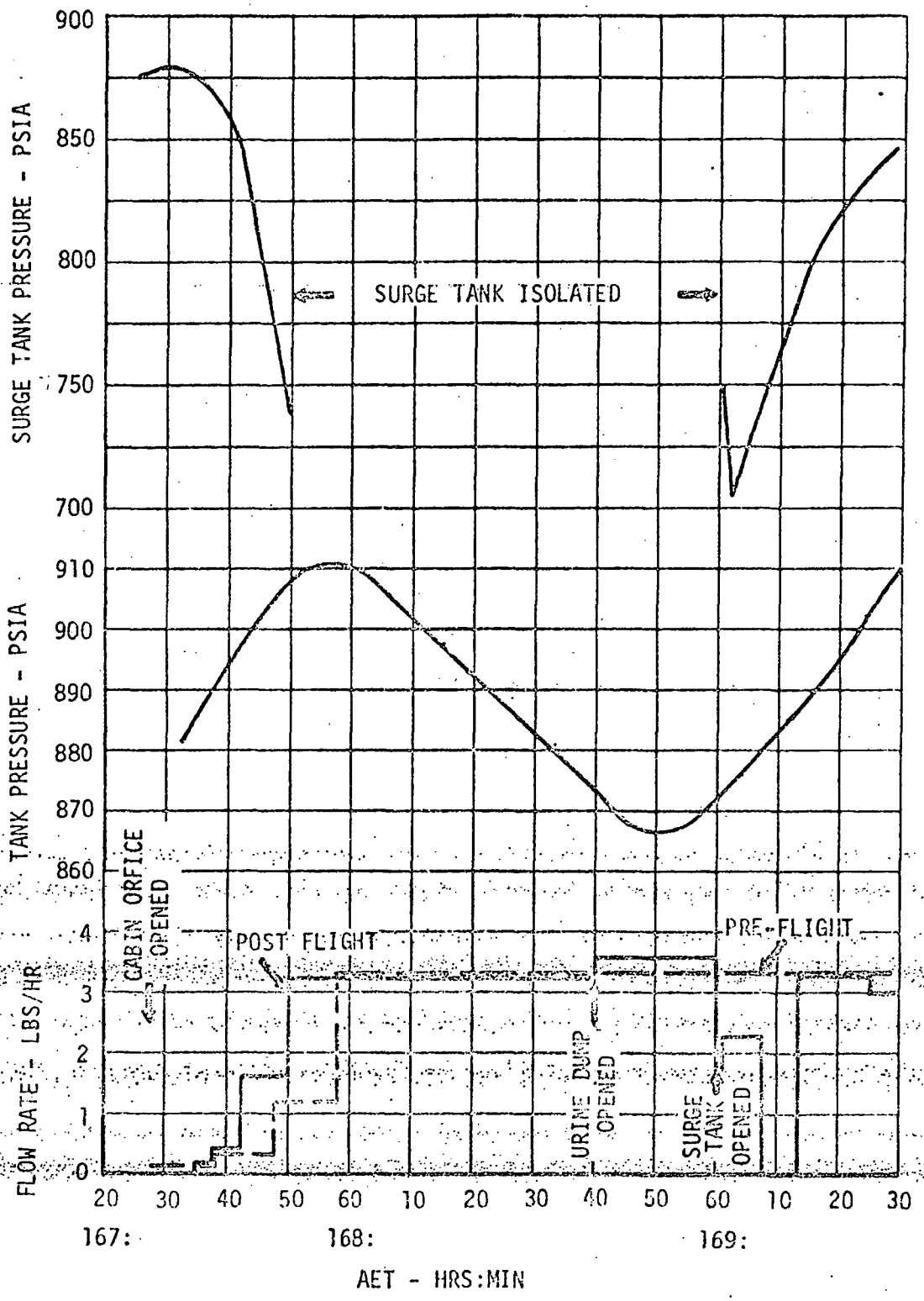

FIGURE 3-4 - TANK 3 PRESSURE AND FLOW RESPONSE DURING HIGH FLOW TEST

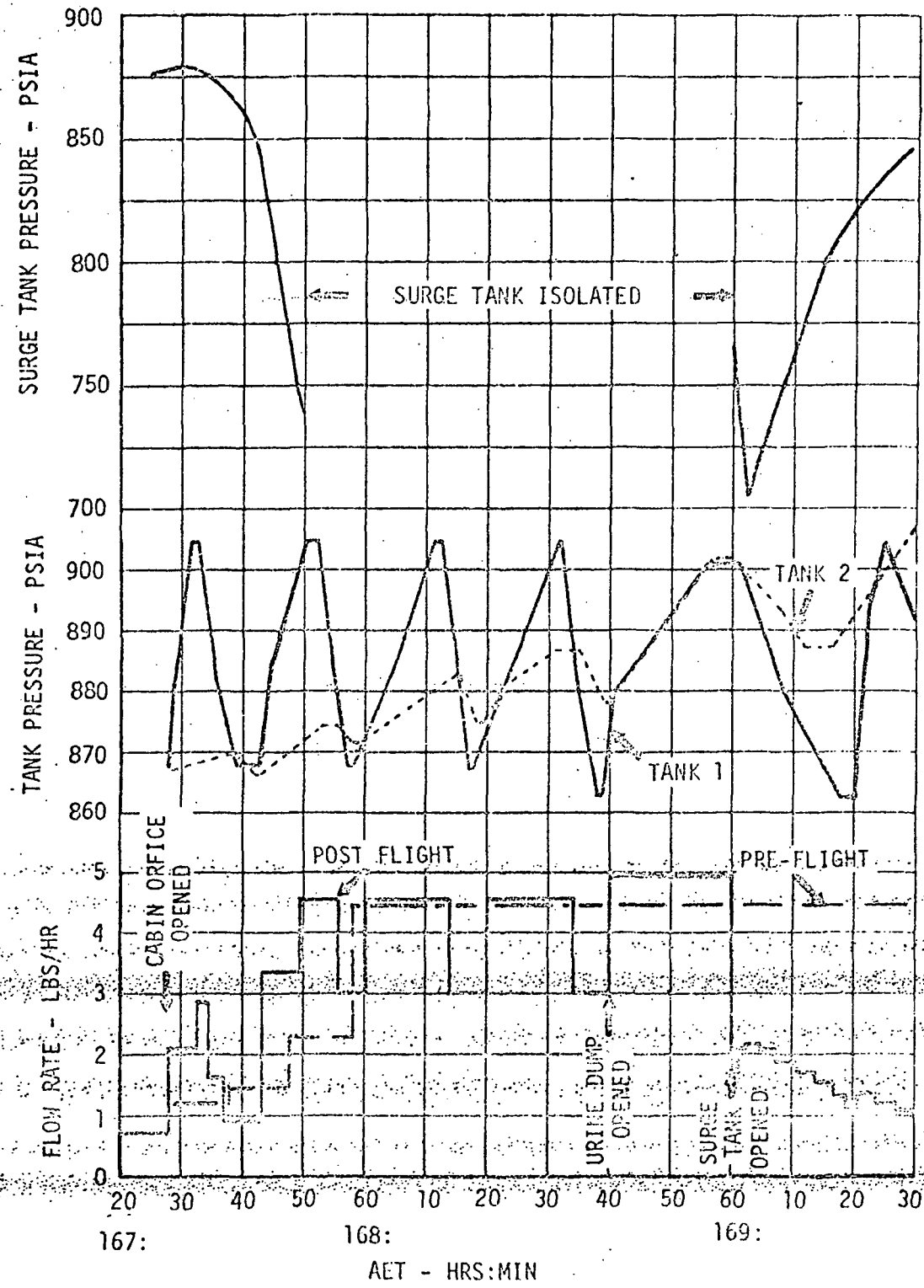

FIGURE 3-5 - TANK 1 PRESSURE AND FLOW RESPONSE DURING HIGH FLOW TEST

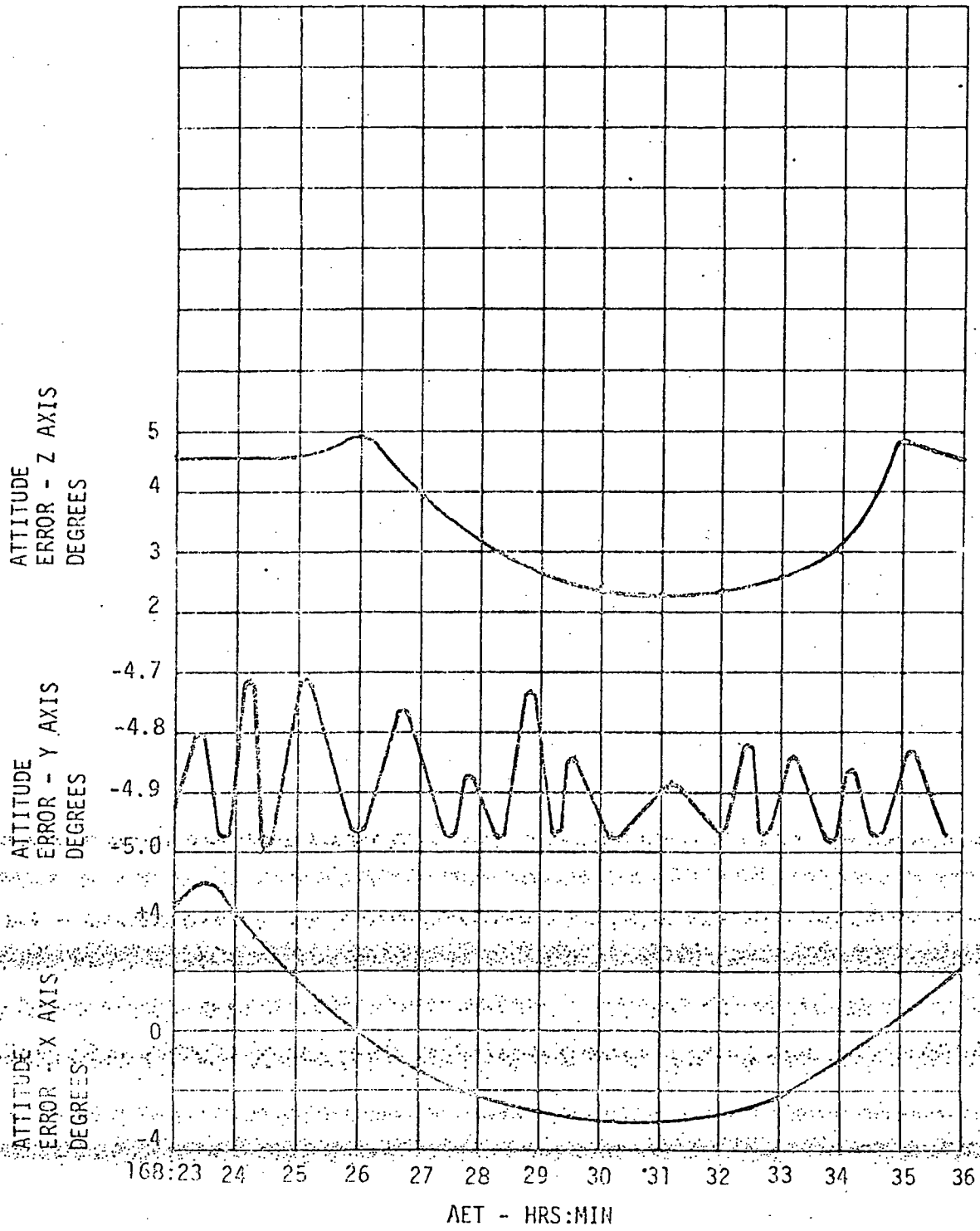

FIGURE 3-6 - VEHICLE ANGULAR MOTION DURING HIGH FLOW TEST

4.0 PREFLIGHT PREDICTIONS

4.1 Nominal Conditions

The analysis of nominal flight conditions was primarily directed towards predicting pressure decays which could occur during normal system operation with relatively low tank flow rates. These analyses indicated that no pressure decays in excess of 100 psi would occur as a result of normal system operation (Figure 4-1). The high flow rates required for the Command Module purge early in the mission were not included in the analyses, since this condition was previously analyzed (Reference 2) for Apollo 12. The maximum pressure decay resulting from stratification during the Apollo 14 mission was less than 100 psi and occurred at an Apollo Elapsed Time (AET) of 5 hours 45 minutes. No other significant pressure decays occurred during the mission.

4.2 DTO Tests

Test predictions (Reference 5) were made to determine the tanks ability to provide the high flow rates required for the EVA simulation, and the nominal flows required for emergency return with low tank quantity. The high flow EVA simulation test included overboard oxygen venting which produced significant vehicle and tank accelerations. The vent configuration was not firmly established when the analyses were initiated, therefore, two accelerations were used for the tank 1 pressure decay predictions (Figure 4-2). The accelerations estimated from the vent configuration and flow were 4.7×10^{-6} "g" for tank 1 and 4.9×10^{-6} "g" for tank 3. The predicted pressure decay due to the fluid properties at the 20% quantity condition was predicted for tank 3. No decay was observed for either tank 1 or 3 because the test was prematurely terminated, and a maneuver to stir the fluid did not occur for a considerable time until after the end of the test.

The emergency return test condition, tank 3 depletion from 20% to 5% quantity, pre-flight prediction determined that the heater temperature would approach, but not exceed 500°F for three heater element operation. The heater temperature red-line was set at 350°F during the mission and only two heater elements were used during the test period. Flight heater temperature data are, therefore, not available for the conditions analyzed and meaningful comparisons can not be made.

4.3 Real Time Flight Analysis

The tank 3 high flow test at 20% quantity was conducted with two heater elements which invalidated the original test prediction. The stratification model was also modified prior to the mission to include the heater thermal mass which was neglected in the first predictions. Analyses were performed during the mission to verify the modified model heater temperature predictions and to provide realistic predictions of the tank 3 test before the test was started. Analysis of the heater cycle at AET 78:20

4.3 Real Time Flight Analysis (Continued)

verified that a heater area of 0.95 ft^2 predicted the peak heater temperature within 30°F (Figure 4-3) while the heater area of 0.475 ft^2 provided less accurate results (Figure 4-4). Revised predictions for the tank 3 high flow test were, therefore, made with 0.95 ft^2 effective heater area (Figure 4-5). The predicted peak heater temperature for the first heater cycle was in excellent agreement with flight data. The predicted heater temperatures and tank pressures remained in good agreement with flight data until the test was terminated at GET 169:38:57. Deviations between predicted temperatures and flight data immediately after the start of the heater cycle were caused by the temperature sensor lag which was not included in the model used for these analyses.

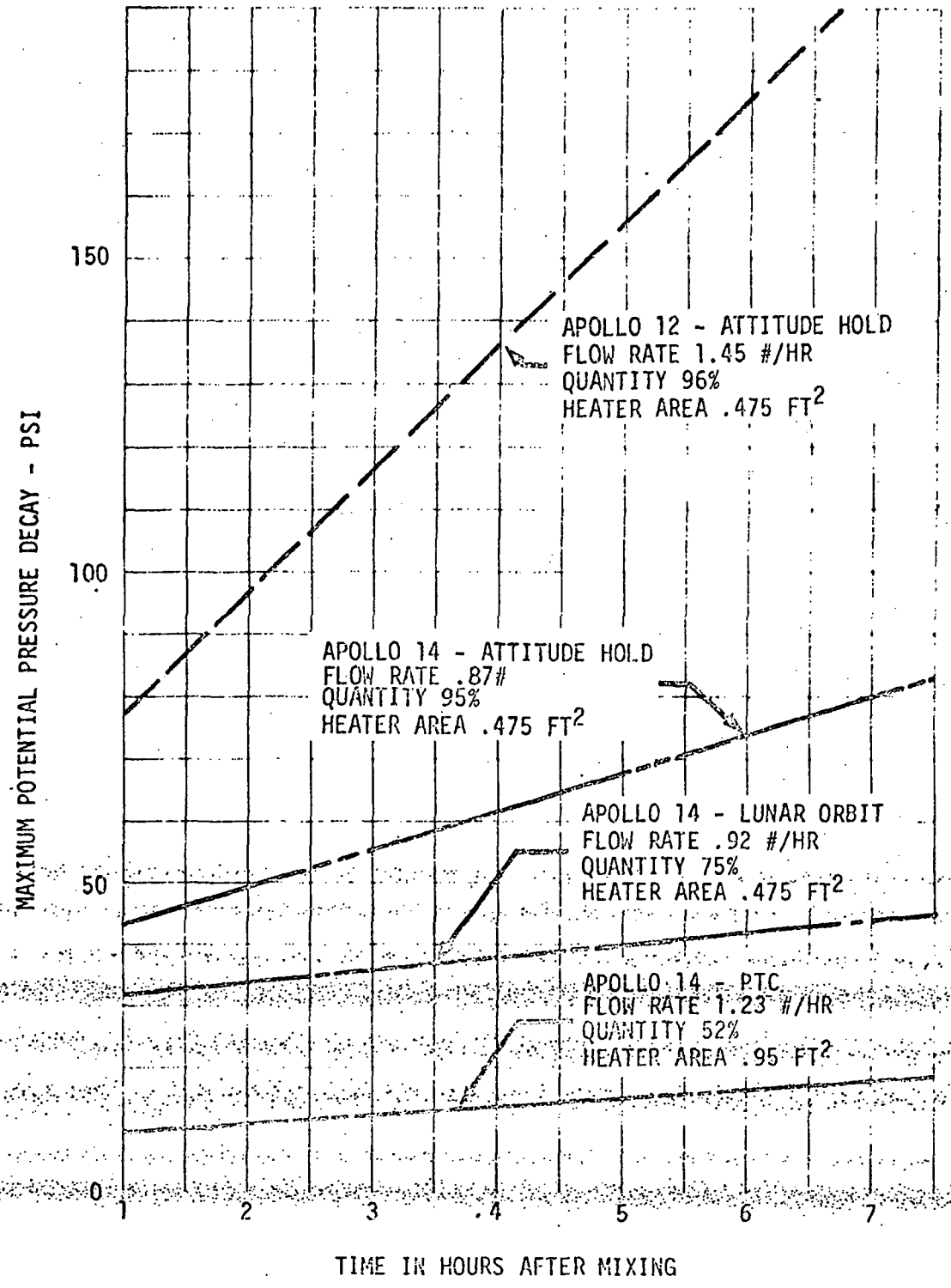

FIGURE 4-1 - POTENTIAL PRESSURE DECAY COMPARISONS

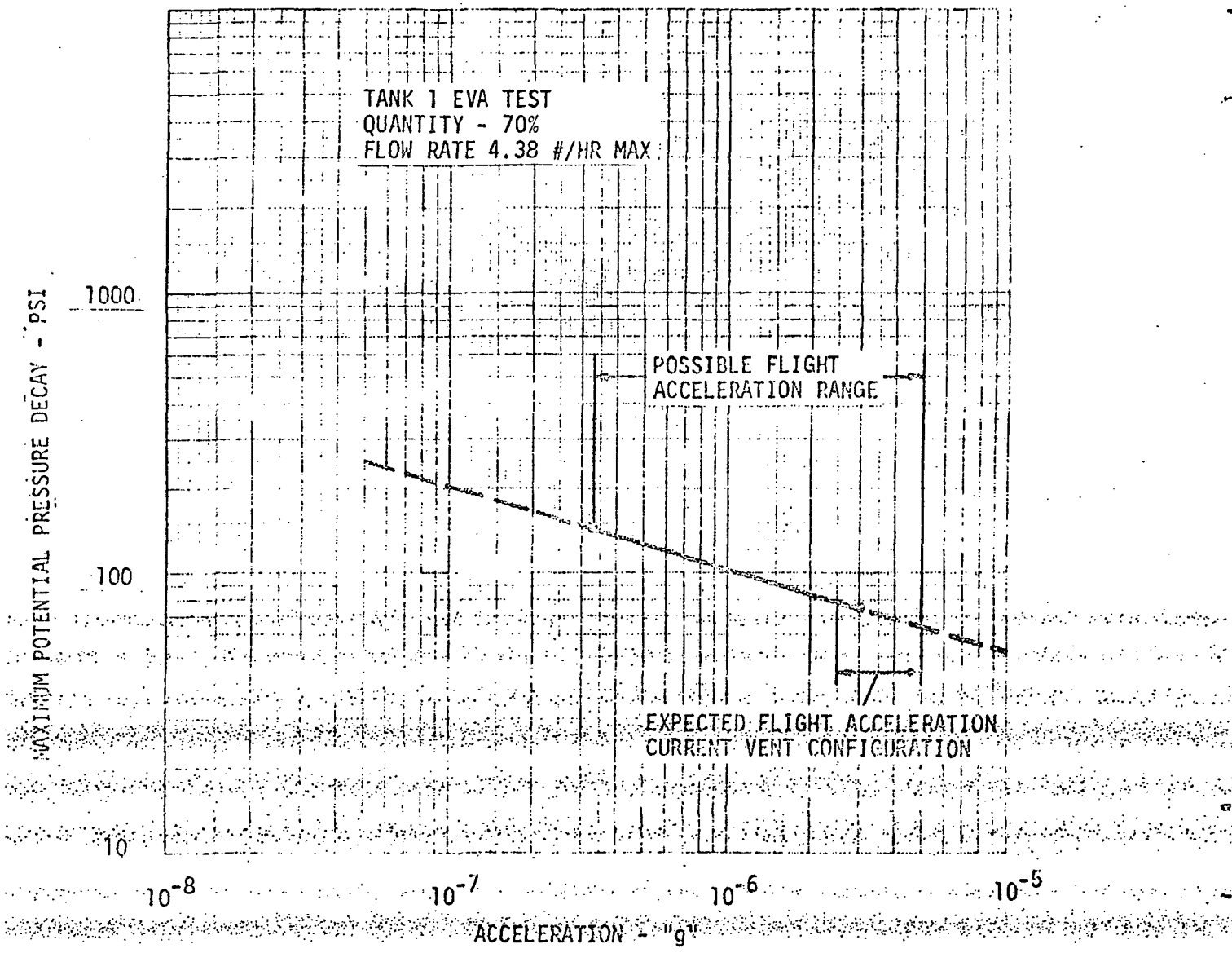

FIGURE 4-2 - EFFECT OF ACCELERATION ON POTENTIAL PRESSURE DECAY

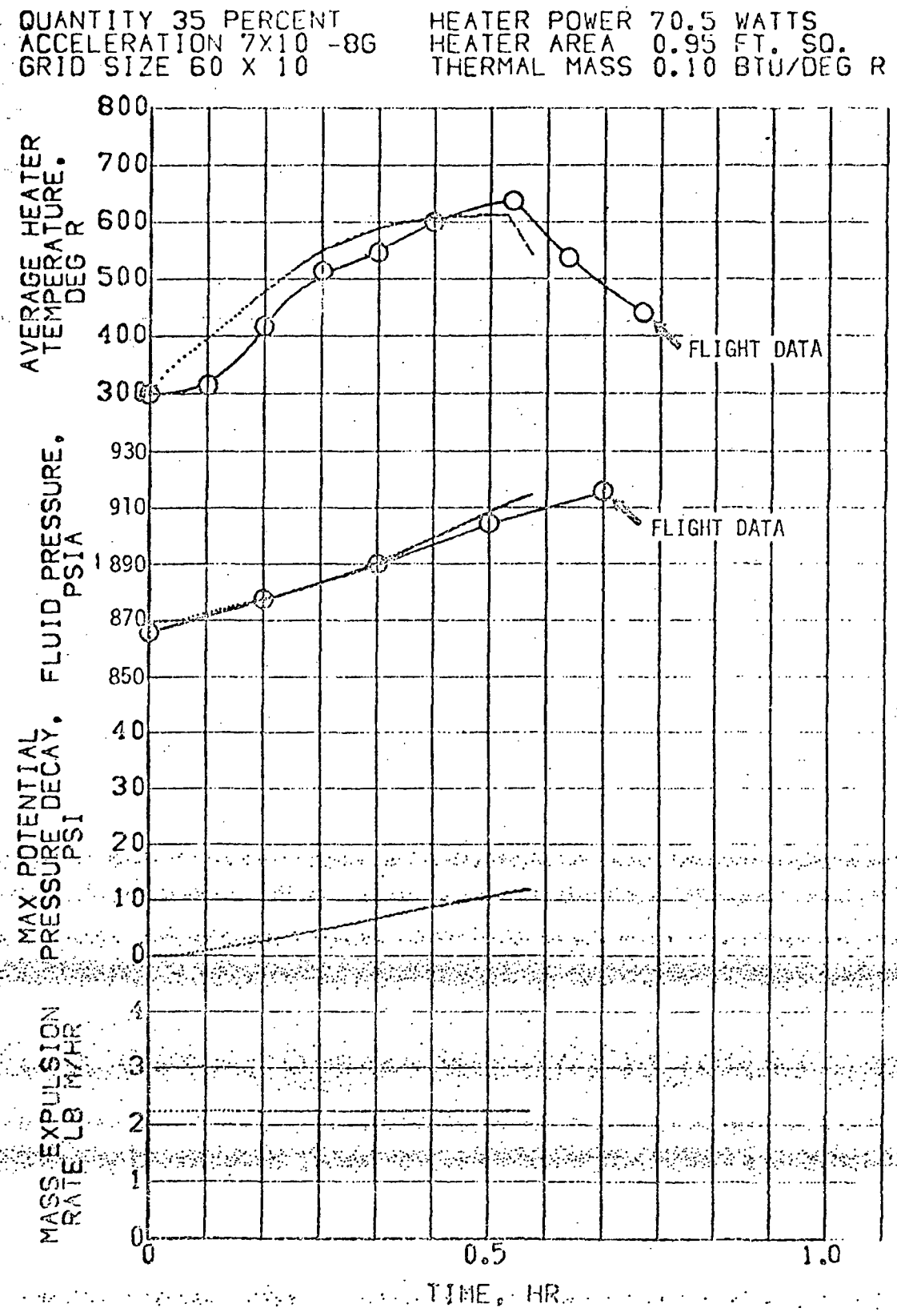

FIGURE 4-3 - ATTITUDE HOLD HEATER CYCLE - 0.95 FT^2 HEATER AREA

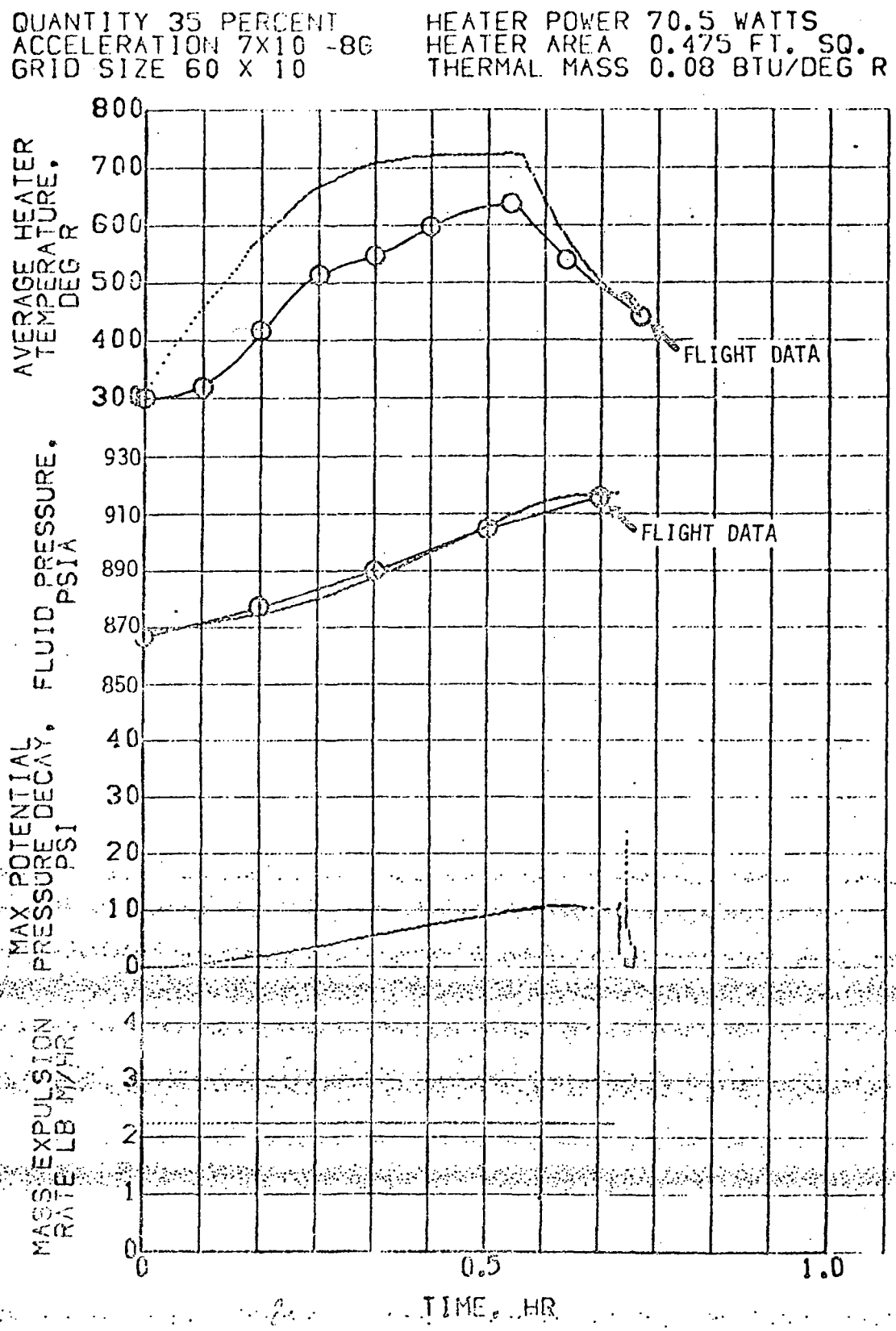

FIGURE 4-4 - ATTITUDE HOLD HEATER CYCLE - 0.475 FT^2 HEATER AREA

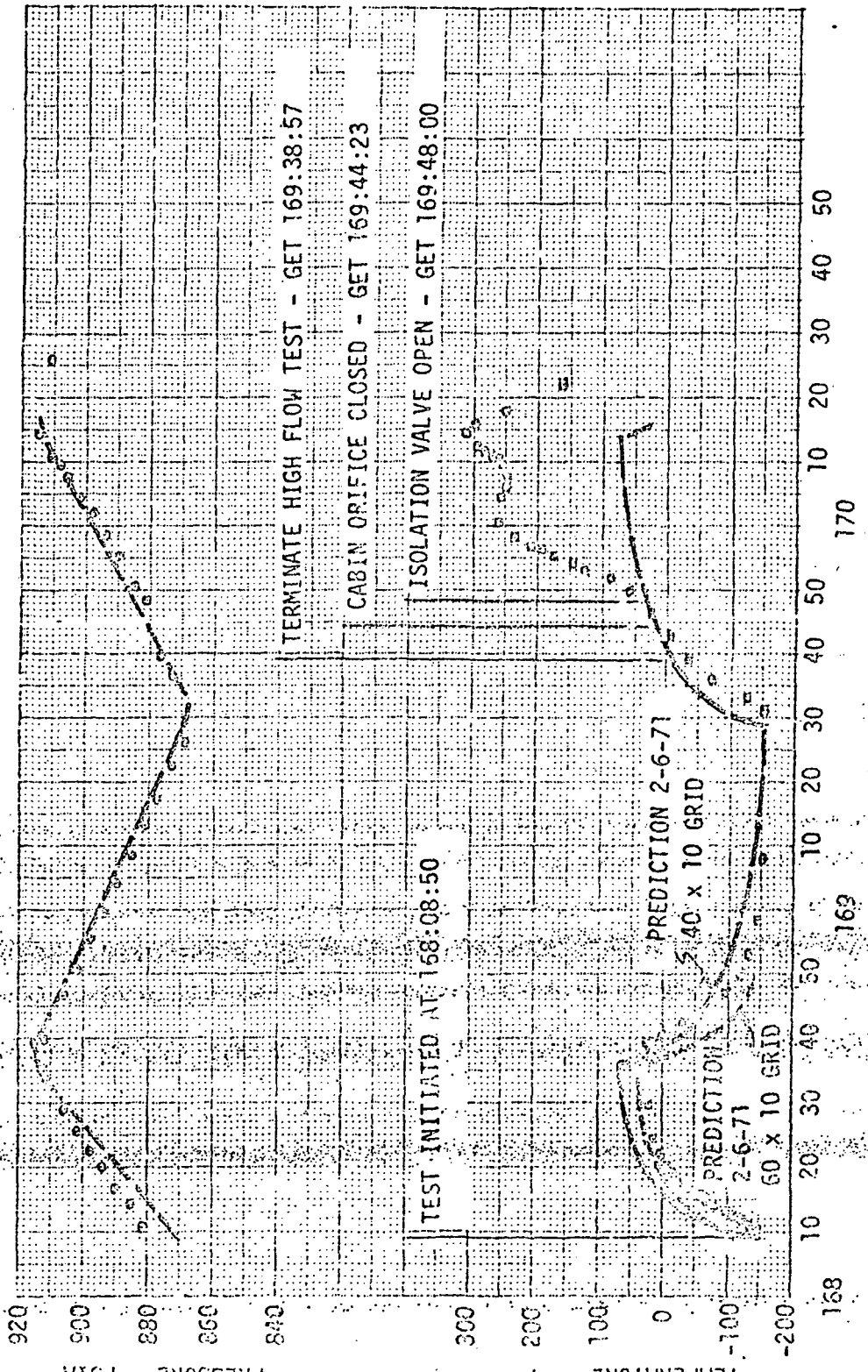

FIGURE 4-5 - REAL TIME HIGH FLOW TEST SIMULATION

5.0 POSTFLIGHT ANALYSIS

5.1 Stratification Model Simulations

Flight periods for simulation were selected with the concurrence of the technical monitor in order to demonstrate prediction capabilities for important tank performance parameters. The selected periods included the most critical flight conditions, flow rates and tank quantities. The bases for selecting the six flight periods analyzed are summarized by the table below.

BASIS FOR PERIOD SELECTION	FLIGHT CONDITION	TANK QUANTITY	AET
Nominal Heater Cycle	PTC	54%	26:00
Maximum Quantity for EVA Flow Rates	DTO	72%	167:00
Minimum Quantity for EVA Flow Rates	DTO	20%	167:00
Maximum Pressure Decay	Attitude Hold	97%	5:00
Short Heater Cycles	Attitude Hold	92%	11:00
Heater Temperature at Low Quantity	PTC	15%	186:00

These flight periods were simulated on the NASA-MSC SRU-1108 computers using the stratification math model. As discussed in Section 3, the simulations used input parameters either measured or computed from flight data. These included acceleration levels, initial tank pressures, initial heater temperatures, percent quantity of fluid, and fluid flow rates. The simulations resulted in heater cycles, potential pressure decay and heater temperature; these were then compared to actual values of these parameters demonstrated in flight. The comparison showed that the Apollo 14 cryogenic oxygen system operated satisfactorily. In addition, this effort showed that the stratification math model could accurately predict system performance with certain limitations. The results of the simulation and discussions of math model adequacy are presented in the following paragraphs.

5.1.1 Nominal Heater Cycle

A PTC heater cycle at AET 26:00 was simulated to verify nominal system operation. The results of this analysis established a baseline for selecting model parameters for other flight periods simulated. This analysis was initiated before postflight "g" data were available, and an acceleration of 3.0×10^{-6} "g" was estimated from available data for guidance rotation rates. The flight acceleration data (Reference 3) confirmed that the average acceleration was within about 10% of the estimate. The average tank flow rate during the pressurization cycle was 2.67 lbs per hour including ECS and fuel cell flow rates of .94 and 1.45 lbs/hour, respectively, and .28 lbs/hour into the surge tank.

5.1.1 Nominal Heater Cycle (Continued)

Simulation results for heater sensor temperature and tank pressure for two different heater areas bracketed flight data (Figure 5-1). The small area simulation was made with a heater area of 0.475 ft^2, which is the flat plate area equivalent to the 0.59 ft^2 outer surface of the cylindrical heater tube. Since the heater tube is perforated, flow through the tube could provide a flat plate area equal to the areas of the inner and outer tube surfaces, a total of 0.95 ft^2. Analyses were conducted for both heater areas to determine which provided the most accurate simulation of sensor temperature and pressurization time. The large heater area reduced the heater sensor temperature, and the time required to pressurize was also reduced; because the small heater at higher temperature stored more thermal energy. Simulated pressure results lag behind flight data early in the stroke due to averaging the flow into the surge tank over the cycle. The actual flow rates increase as the difference in pressure between the oxygen and surge tanks increases. Therefore, an average surge tank flow over-estimates the flow immediately after the heater turns on and and causes the simulation pressure to rise more slowly.

The asymptotic limit for the heater temperature with the 0.475 ft^2 area is within 9°F of the flight data, while the heater on time for the same area is within 40 seconds of the flight data (Figure 5-2). These results are within the accuracy of the data itself. The asymptotic sensor temperature and heater on time with the larger heater area are not in good agreement with flight data, which implies that the inside of the heater tube was not an effective heat transfer surface. The effect on convergence of the number of cells in the Y-direction was also investigated by repeating simulations with a heater area of 0.95 ft^2 and grid sizes of 40 x 10 and 40 x 15. These simulations produced essentially identical results with pressurization times of sixteen minutes and a sensor temperature of 46°F. These results imply that at lower quantities, nominal tank performance can be closely simulated with a heater area of 0.475 ft^2. Satisfactory convergence in this quantity range can be obtained with maximum grid sizes of 60 x 10 with convergence not dependent upon the number of cells in the Y-direction.

5.1.2 Maximum Quantity for EVA Flow Rates

Simulations of the tank 1 high flow test at AET 167:00 were performed with time dependent flow rates calculated from ECS and fuel cell demands. The tank acceleration was calculated from the oxygen vent thrust (Paragraphs 3.2 and 3.3). Abrupt changes in tank flow rates (Figure 5-3) occurred during the test period because tank 2 and tank 1 alternately supplied fuel cell flow rates (Paragraph 3.2). The heater cycles simulated with 40 x 10 grids and heater areas of 0.95 ft^2 and 0.475 ft^2 are in poor agreement with flight data early in the simulation (Figures 5-3 and 5-4). The tank flow rates were investigated to determine if they could differ from the fixed demands used to perform the simulation enough to cause the error in heater cycles. Flow rates calculated from the actual tank

5.1.2 Maximum Quantity for EVA Flow Rates (Continued)

pressure change rates by equilibrium thermodynamics indicated negative flow rates (flow into the tank) during part of the period (Figure 5-5). The large differences between flow rates based on demands and flow rates based on tank pressures indicated that flow rate errors caused the simulation inaccuracy.

The plumbing system thermodynamic behavior was investigated as a possible source of flow rate errors. When the demand flow rapidly increases, a cold, dense slug of fluid is drawn from the tank into the warm tubing. The density of the fluid inside the tank is approximately ten times the density of the fluid at the ambient temperature in the system plumbing. If no heat transfer is assumed between the hot and cold fluid, then to maintain pressure in the lines an equal volume of cold fluid must replace the volume of hot fluid. The tank flow rates will exceed the average system demand for some period of time to fill the lines with cryogenic fluid after the demand increases. This phenomena was investigated by using the existing math model to simulate the plumbing response to sudden high flow demands. The simulation outflow rate was 2.5 lbs/hour at 60°F and the inflow rate was 25 lbs/hour at the tank temperature of -195°F.

The simulated line pressure decreased for the first 15 seconds even though the inflow was an order to magnitude higher than the outflow (Figure 5-6). The pressure decrease with the high flow into the line confirms that the plumbing system could cause gross variations in tank outflow. After the lines were initially filled with cold cryogenic fluid the thermal capacitance of the system could cause sufficient pressure rise in the line to cause flow back into the tank. No attempt was made to analyze this effect for the duration of the high flow test, because computer time requirements are prohibitive with the existing model. The simulation of the line response for 18 seconds required more than one hour of computer time. It was concluded that large variations in the tank 1 flow rates occurred during the first few heater cycles of the high flow test as a result of plumbing system thermodynamics.

The tank flow rates could be adequately established for simulations for only the last heater cycle during the high flow test when the plumbing was near thermal equilibrium. Simulations of the last heater cycle were made with the model flow rate adjusted on the basis of pressure to properly include the fuel cell flow demands. Under these conditions, fair agreement was obtained with the flight pressure response for the 80 x 10 grid with a heater area of 0.95 ft^2 (Figure 5-7). The heater sensor temperature asymptotic estimate was 30°F above flight data (Figure 5-8). The heater-on time however, did not converge, indicating that the heater boundary layer was not adequately resolved. The resolution obtained was adequate for asymptotic extrapolation of the heater temperature which was in satisfactory agreement with flight data.

5.1.2 Maximum Quantity for EVA Flow Rates (Continued)

Potential pressure decay is a function of total heater-on time only and simulations of this variable were valid for the duration of high flow test. The potential pressure decay as a function of time is shown in Figure 5-9. When the oxygen vent was closed at AET 169:05 the acceleration decreased by an order of magnitude. This change in "g" level caused some model instability and the potential decay was not valid for later times. The maximum potential pressure decay during the heater cycle immediately preceeding termination of the high flow test was 32.3 psi (Figure 5-10). A pressure decay was not observed in flight because the tank 1 heater was turned off at 169:34 and no significant vehicle maneuver occurred to abruptly mix the fluid before the potential pressure decay had dissipated. Extrapolation of the potential pressure decay history shown by Figure 5-9 indicates that the potential pressure decay dropped to less than 10 psia approximately 30 minutes after the heater was turned off.

5.1.3 Minimum Quantity for EVA Flow Rates

Detailed simulations of the tank 3 high flow tests at AET 167:00 were performed with heater areas of 0.95 and 0.475 ft^2. Expulsion rates were based upon ECS and fuel cell demands and the acceleration level was calculated from the thrust produced by the oxygen being vented overboard during the test (Paragraph 3.2 and 3.3). The DTO was terminated at the end of one and one-half hours instead of the planned three hours. When the cabin orifice was closed, terminating high flow, the vehicle acceleration dropped from approximately 4.9×10^{-6} "g" to 7.2×10^{-8} "g". Post flight analysis indicated that the estimate of 4.9×10^{-6} "g" cannot be significantly improved, but the acceleration level after the termination of the high flow test may have been as much as an order of magnitude higher than 7.2×10^{-8} "g". The saturated heater temperature at either acceleration is much higher than the observed heater temperature (Figures 5-37c and 5-37d). Heat transfer rates at temperatures far below saturation are low and most of the energy is being stored in the heater thermal mass. The temperature rise rate at this quantity is dominated by the heater tube thermal response, therefore, the temperature simulation is not in significant error.

The heater power was manually changed from 70 watts (2 elements) to 110 watts (3 elements) near AET 169:09. The stratification math model simulates the effects of the high flow, the decrease in "g" level, and the change in heater power. Figure 5-11 compares the results of a simulation with a heater area of 0.95 ft^2 and a grid of 40 x 10 with flight data. Since the surge tank flow rate was treated as a time averaged value over the cycle, as previously discussed, the simulated pressure lags flight data early in the upstroke. Furthermore, tank 3 pressure was initialized at 876 psia because the heater had already been activated by the pressure switch at 868 psia prior to the initiation of high flow. This particular combination of grid size and heater area predicted a heater sensor temperature 23°F

5.1.3 Minimum Quantity for EVA Flow Rates (Continued)

above the observed temperature at end of the first high flow cycle. During the second pressurization cycle, the test was terminated and the simulation tank acceleration dropped almost two orders of magnitude. Instead of saturating at a temperature comparable to the first cycle, the heater sensor continued to rise. When the heater power was stepped up from 70 to 110 watts, the temperature rise rate increased even more. The sensor continued to rise to 310°F showing no tendency to saturate, when the heater was turned off by the pressure switch at 169:34.

When a convergence study of heater sensor temperature and heater-on time was performed (Figure 5-12), the results for either heater area were not in as good agreement with flight data as the 40 x 10 grid with the large heater. By comparing the results of combinations of grid and heater area with flight data (Figure 5-12), the 40 x 10 grid and larger heater simulates the high flow test pressure and temperature response better than any other combination. However, the asymptotic heater temperature with the 0.95 ft^2 heater area converged 45°F below flight data while the temperature with 0.475 ft^2 area converged 60°F above flight data. Convergence of time to pressurize also span flight data. Previous analyses of a PTC heater cycle at GET 26:00 indicated that a low quantity, a heater tube area of 0.475 ft^2 produced better agreement with flight data when the external variables of "g" level and flow rate were accurately defined. This implies that these variables may not be as well defined during the high flow tests as they were during the nominal PTC cycle.

The average acceleration level during the DTO is apparently not significantly different than that used for the simulation; (Reference Section 3.4), however, the effect of the high "g", low time duration, RCS acceleration spikes may not be accurately modeled by averaging over time. As shown previously by Figure 3-6 these firings occur at a rate of about one per minute during the DTO and these spikes could significantly affect heater temperatures and pressurization times. The two dimensional model assumes an acceleration perpendicular to the heater; which is not valid during the high flow test, when the linear acceleration due to the venting oxygen caused the acceleration vector to be inclined about 57° to the heater tube. Either of these phenomena could significantly affect the results of the high flow test simulation. No satisfactory method of modeling these effects is available.

5.1.4 Maximum Pressure Decay

The only significant pressure drop during the flight of Apollo 14 due to stratification occurred during LM/CSM separation at AET 5:47. The tank 1 pressure dropped to 804 psia from an initial pressure in the control band of 868 to 905 psia. Prior to this at AET 4:57, docking caused the oxygen tanks to assume an equilibrium state which was maintained until the beginning of the next heater cycle at AET 5:14. The purpose of the simulation of this period is to predict the build-up of potential decay during this heater cycle.

The only available data for oxygen tank pressure and temperature during this period was that taken by hand during the Apollo 14 flight. Thus, it was difficult to determine the exact starting conditions of the period to be simulated, the exact length of the heater on cycles, and the pressure in the tanks at LM/CSM separation.

This difficulty led to the use of different initial conditions for each of the two sets of simulations performed to analyze the pressure drop. The first simulation, which was run with a heater area of .95 ft^2, used an initial pressure in tank 1 of 872 psia, while a second simulation (which was run with a heater area of .475 ft^2) was initiated with tank pressure at 864 psia. This caused a difference of approximately one minute in the heater-on times for the two simulations. Although the potential decay and heater temperature depend directly upon the heater on time, this difference in the two simulations does not lead to significant error in predicting the potential decay or maximum heater temperature.

Another difference between the two simulations was the surge tank volume used. Due to the repressurization of the LM/CSM beginning at AET 5:14 the surge tank pressure dropped to 414 psia. The first simulation used tank flow rates derived from the assumption that only the surge tank volume and LM/CSM were being repressurized. Later, it was found that the repress bottles were also depleted at the beginning of the period to be simulated. Thus, the second simulation used a surge tank volume of twice that of the first simulation. Flow rates used in both simulations, however, were lower than those experienced in flight (See Figure 5-13). Since both the potential decay and the heater temperature are independent of tank outflow, this discrepancy is not important for the analysis of these parameters.

Some difficulty with the stratification model stability was encountered during the simulation of this heater cycle. The instability was caused by a step down in acceleration level that occurred during the upstroke of the heater cycle (See Figure 5-13). Because of a lack of sufficient computer core in the MSC 1108, a fine enough grid could not be utilized to avoid oscillation in the predicted potential decay after the step down in "g" level. The simulation instability caused

5.1.4 Maximum Pressure Decay (Continued)

the rise in the potential decay to be invalid after the acceleration change. The residual flows from the high "g" period during the first part of the period should cause the growth in potential pressure decay to be constant through the low "g" period. Therefore, since potential decay is a linear function of heater on time, the decay just before the "g" change was extrapolated to predict the later potential decay for each grid size (Figures 5-14 and 5-15). These predictions along with predictions for maximum heater temperature (Figure 5-16) were then extrapolated to an asymptotic value (Figures 5-17 and 5-18).

The simulation using a heater area of .95 ft^2 is in very good agreement with the flight values for maximum heater temperature and potential pressure decay. The maximum heater temperature for this cycle was -115°F at AET 5:44 while the extrapolated simulation temperature for an equal heater-on time was -113°F (Figure 5-18). The pressure drop in flight can not be exactly determined due to the limitations of the available data, but is is estimated to be between 59 and 100 psi. The maximum potential decay predicted by the simulation using the larger heater size was 86 psia which again agrees well with the flight data (Figure 5-17).

While the pressure response of the tank during this period was not of primary interest to this analysis, the initial pressure rise rate of tanks 1 and 2 was investigated. An equilibrium calculation indicates that pressure can not be maintained in tank 1, but must decrease at least -1.06 psi/min because of the high flow rate of 3 lbs/hour during this period. However, flight data indicates that the tank pressure rose at 1.1 psi/min during the initial portion of the heater cycle (Figure 5-13). At AET 5:25, the pressure leveled off for a period of 20 minutes after which the pressure rose to a peak of 906 psia and the heater shut off. The effect of stratification of the fluid does not explain this initial sharp pressure rise and subsequent leveling off. Nor does the stratification model indicate a rise in pressure immediately after the beginning of the heater cycle. This discrepancy is partially due to the difficulty in reading the hand plotted data. The flight pressure rise rate computed above could be significantly in error because of inaccuracies in the determination of the pressure-time response. Other possible explanations for this unusual pressure response are discussed further in Section 5.2.2.

5.1.5 Short Heater Cycles

During the period AET 10:30 to 12:30, oxygen tanks 1 and 2 were cycling in the automatic mode in attitude hold. At the start of this period, the total cycle time was approximately ten minutes, but by AET 11:30 the cycle time had shortened to six minutes. The minimum cycle time derived from equilibrium thermodynamics, however, is 12.3 minutes (Figure 5-19). Because these unusually short cycle times were felt to be due to the effects of stratification, this period was chosen for analysis.

5.1.5 Short Heater Cycles (Continued)

An examination of "g" data for this period indicated that an average acceleration level for this time period was 3×10^{-7} "g". Since this value is higher than was expected; and because noise in the "g" data could have caused the average to be high, an 80 x 10 simulation run was made for this "g" level to compare it to an earlier 80 x 10 run at 7×10^{-8} "g". The results, which are presented in Figure 5-20 and 5-21, did not indicate that the higher "g" level was valid. Therefore, the simulation was performed at an acceleration of 7×10^{-8} "g".

It was initially felt that the math model would stabilize into the steady state cycles in one hour of simulation time. Using the initial conditions for tank 1 at AET 11:30, the simulation was run for a range of grid sizes. The heater cycles did not in fact stabilize fast enough for an accurate simulation of the short heater cycles due to the inclusion in the present math model of the effects of thermal mass. In the previous analysis of Apollo 12 flight data, a math model which neglected thermal mass was used. The simulations conducted at high quantity heater cycles using the previous model stabilized into very short cycles in much less time than is evident with the present mode.

To enable the one hour simulation to be extrapolated to the steady short cycle state, a 100 x 10 grid simulation was run to simulate one and one-half hours of flight time (Figure 5-22). Using this simulation as a guideline, the values for the pressure fall time, pressure rise time, maximum heater sensor temperature, and minimum heater sensor temperature for the one hour simulation runs were extrapolated to values that would have been observed for one and one-half hour simulations (Figures 5-23 and 5-24).

It was realized that the initial conditions used for the one hour simulation runs did not produce the proper average flow rates to simulate exactly the full one and one-half hour period. An examination of the relationship between total cycle time and average flow rate, however, indicated that small variations in flow rate did not significantly affect the cycle time for flow rates between .9 lb/hour and 2.0 lb/hour and a tank quantity of 92% (Figure 5-19). Since the average flow rate during this period was approximately 1.2 lb/hour, the one hour simulation was extrapolated to one and one-half hours.

The results of the extrapolation indicate good agreement with flight data from AET 11:30 to 12:30 for the minimum and maximum heater temperatures. Since the 80 x 10 grid values for the minimum heater temperature were quite close to those predicted by the 100 x 10 grid run, an extrapolation to an infinite grid asymptote was made (Figure 5-25). The predicted minimum heater temperature was thus found to be within 1°F of the flight data. Further, assuming a linear extrapolation of the maximum heater temperature (Figure 5-25), the asymptotic value for the temperature after one and one-half hours was within 12°F of the flight

5.1.5 Short Heater Cycles (Continued)

value. This last figure, however, could be significantly in error because of the coarseness of the extrapolation for the maximum heater temperature.

The results of the simulation of total cycle time was not in good agreement with flight data. The extrapolated values for pressure rise time shown in Figures 5-20 and 5-23, for instance, did not converge. The trend of these extrapolations, however, indicate that if sufficient core were available on the MSC 1108 to adequately resolve the boundary layer, an asymptotic value near flight data would be observed.

The asymptote for the pressure fall time, on the other hand, converges to a value significantly higher than observed in flight (Figure 5-26). Since the 80 x 10 grid fall time is quite close to the 100 x 10 grid time, the asymptote of 5.5 minutes is felt to be accurate. The discrepancy between the simulation and flight is due to the flow rate predicted for tank 1 by the math model being too low during the heater cycle down stroke. Tank 3 begins to flow along with tanks 1 and 2 when the pressure in tank 3 becomes equal to that in tanks 1 and 2. The point in the down stroke where these pressures become equal is determined by the pressure rise in tank 3 due to heat leak. The heat leak into tank 3 used in the math model was equal to the zero flow rate heat leak given in Figure 3.4.5 of Reference 6. The heat leak value listed in this reference is now felt to be too high. Further, the zero flow rate heat leak into tank 3 should not have been used for the short heater cycles because of the retention of cold fluid in the vapor cooled shield during the short up strokes. Before this fluid is allowed to heat up enough to allow the heat leak to be equal to that listed in Reference 6, another downstroke occurs allowing more cold fluid to enter the vapor cooled shield. Thus, a much smaller heat leak should have been used in the analysis.

Because of the assumption of too large a value for the heat leak, tank 3 pressurized faster in the simulation than actually occurred. Therefore, tank 3 began to flow with tanks 1 and 2 earlier in the heater cycle downstrokes than it actually would. This caused a discrepancy in the flow from tank 1 since the quantity in tank 3 was nearer the minimum dQ/dM level and thus provided more of the required flow than either tanks 1 or 2. As a result, the downstrokes of the simulation were lengthened significantly.

Another parameter investigated was the maximum potential pressure decay developed during the two hour period from AET 10:30 to 12:30. The maximum potential pressure decay begins to build up linearly with time after the heater cycles reach a relatively steady stratified state (Figure 5-27). Since the 80 x 10 grid simulation is quite close to the 100 x 10 grid prediction, the extrapolation of the 100 x 10 grid pressure decay build up to AET 12:30 was taken to be the asymptotic

5.1.5 Short Heater Cycles (Continued)

value (Figure 5-28). This extrapolation indicates that the potential pressure decay at AET 12:30 when the heaters in tanks 1 and 2 were turned off was 94 psi. Over the next hour the magnitude of the potential decay decreased until it was negligible when PTC was initiated at AET 13:44.

5.1.6 Heater Temperature at Low Quantity

A heater cycle at AET 186:00 with 15% quantity was chosen for analysis to verify satisfactory heater-tank performance and the capability of the model to simulate performance at very low density. During this period, the vehicle was in a very weak PTC maneuver. Flight data show the acceleration on tank 3 to be 3.3×10^{-7} "g". Fuel cell oxygen demands were calculated from post flight current data, while ECS and surge tank flows were calculated during this period with the flow distribution subroutine described in Section 3.2. The total tank 3 expulsion was approximately 2.0 lbs/hour. Heat input was set at 70 watts to match the two heater element configuration.

The sensor temperature response for the 40 x 10 and 60 x 10 grids (Figures 5-29 and 5-30) are almost identical, indicating satisfactory convergence of the 60 x 10 grid at this low quantity. The heater sensor temperature results for the 0.475 ft^2 heater area converged to within 10°F of the observed flight maximum temperature of 325°F. Simulating the cycle with the larger heater area would have resulted in a sensor prediction significantly below flight data, and it was decided not to repeat the simulation for the larger heater.

Instability in the flow distribution subroutine caused the simulated tank pressure to be in significant error during the first ten minutes of the upstroke. The pressure change rate response was manually constructed from the output and integrated to form the pressure response presented in Figure 5-29. A total pressurization time eleven minutes shorter than the observed fifty-three minutes was calculated. This discrepancy is explained by the manner in which the stratification model treats radiant heat transfer. To calculate pressure rise rates it is assumed that the total heat to the fluid includes radiation. The heater convects energy into the fluid while it simultaneously radiates energy to the tank wall. This radiated energy raises the wall temperature and is convected back into the fluid. An alternate way of modeling the radiant energy would be to have it totally absorbed by the tank wall and not available to raise the fluid pressure. For a heater temperature of 300°F, radiation accounts for 50 BTU/hour or 21% of the total two element heater power (Figure 5-31). By reducing the fluid heat input by this 50 BTU/hour, the pressurization time is lengthened to fifty minutes (Figure 5-29). This result is within 6% of flight data and well within the 10% granularity of pressure data over this range. The results imply that for many problems where radiation is important, the radiant energy is absorbed by the tank wall and

5.1.6 Heater Temperature at Low Quantity (Continued)

is not convected into the fluid for some length of time. The error in calculating pressurization times can be no greater than the fraction of radiant energy to total heater power. This discrepancy in the treatment of radiant energy does not affect the heater temperature sensor time response. Furthermore, these effects are negligible for the problems of interest at lower heater temperatures. For example, for the two element heater cycle during the tank 3 DTO at 20% quantity, the heater sensor reached a maximum of 27°F. Radiation only accounted for about 8 BTU/hour or 3% of the total heater power (Figure 5-31). This error is even less significant during the other simulations.

5.2 Determination of Model Parameters

The simulations discussed in Paragraphs 5.1.1 to 5.1.4 correlated tank pressure and heater temperature results from the stratification model with flight data. These correlations were for a range of quantities from 15% to 97%, accelerations from 7×10^{-8} "g" to 4.9×10^{-6} "g", and flow rates from nominal system usage to the maximum of approximately 5 pounds per hour. Good agreement was obtained between simulation results and flight data when the model heater area was properly selected, and the grids were fine enough for convergence of the solution.

The heater area which resulted in the best heater temperature predictions was 0.95 ft^2 for tank quantities greater than 60% (Table 5-1). A heater area of 0.475 ft^2 resulted in better agreement with heater temperature data for tank quantities less than 60% with the exception of the Tank 3 high flow test at 20% quantity. Simulation of the tank 3 high flow test with a 0.475 ft^2 heater area produced a temperature of 60°F too high while the 0.95 ft^2 heater temperature prediction was 45°F too low. Since these inaccuracies are nearly the same with the smaller heater predicted temperature being conservative, use of the smaller heater area is recommended for all quantities less than 60%.

The number of cells or grids required for adequate simulations is affected by the tank quantity. Approximately 100 cells are required in the X direction of the model for greater than 60% tank quantity. For less than 60% tank quantity 60 cells in the X direction are sufficient. The convergence of the solution must be investigated for a range of grids to determine the prediction accuracy and parameters of interest extrapolated to asymptotic values. Approximately 10 cells are adequate in the Y direction of the model for the full range of quantities. The results obtained with 10 and 20 cells in the Y direction with 40 cells in the X direction are essentially identical. The number of Y direction cells may affect the results when more than 100 cells are used in the X direction. The available SRU-1108 core storage is not adequate to investigate convergence in the Y direction with greater than 100 cells

TANK QUANTITY PERCENT	ACCELERATION "g"	HEATER TEMPERATURE ERROR - °F FLIGHT	SIMULATION RESULTS HEATER AREA - FT^2 .475	.95	BEST HEATER AREA FT^2	TEMPERATURE ERROR °F
97.0	5×10^{-7}	-115	+5	-113	.95	+2
92.60	7×10^{-8}	-155	---	-167	.95	-12
72.16	4.7×10^{-6}	-115	---	-84	.95	+31
54.61	3×10^{-6}	38	29	-57	.475	-9
20.8	4.9×10^{-5}	27	87	-18	.95	-45
15.23	3.3×10^{-7}	325	315	---	.475	-10

TABLE 5-1 STRATIFICATION MODEL PARAMETER SUMMARY

5.2 Determination of Model Parameters (Continued)

in the X direction. The simulations which can be conducted are, therefore, effectively limited to 100 cells in the X direction and 10 cells in the Y direction.

Model parameters used for simulations and verified by correlations of tank pressure and heater temperature include:

Model Dimensions	
Height (Y)	2 ft
Width (X)	1 ft
Depth	1.1875 ft
Heater Area	.95 ft^2 above 60% quantity
	.475 ft^2 below 60% quantity
Heater Emissivity	0.2
Heater Temperature Sensor Lag	.26 $minutes^{-1}$
Heater Thermal Mass	0.1 BTU/°F

5.3 Results of Heater Temperature Correlation

An empirical correlation using Rayleigh equation was developed to supplement the stratification model predictions for heater temperatures. This simplified model was used to provide predictions over a wide range of expected flight "g" levels, tank quantities, and heater powers. These predictions were compared to flight data from 20 Apollo 14 heater cycles (Figure 5-32). The average temperature deviation between flight data and prediction was 18.5°F while the standard deviation was 21.9°F. The individual predicted temperatures were within 50°F of flight data except for the data point taken from the tank 3 DTO (see Figure 5-32). This discrepancy may have been caused by the abnormal inclination of the "g" vector to the heater tube during the DTO. Typical examples of the heater cycles simulated are shown in Figures 5-33 through 5-36. These examples include heater powers of 70 and 120 watts, accelerations from 3.0×10^{-6} "g" to 7.5×10^{-7} "g" and tank quantities from 15.6% to 97%. In each case, the agreement between predicted heater temperature and flight data was within 50°F for the full length of the heater cycle.

Parametric heater response data were generated using the Rayleigh correlation for two heater powers, 80 and 120 watts (Figure 5-37). These data provide heater temperature response as a function of quantity for PTC (3×10^{-6} "g"), lunar orbit (5×10^{-7} "g"), and altitude hold (7.2×10^{-8} "g") for each heater power.

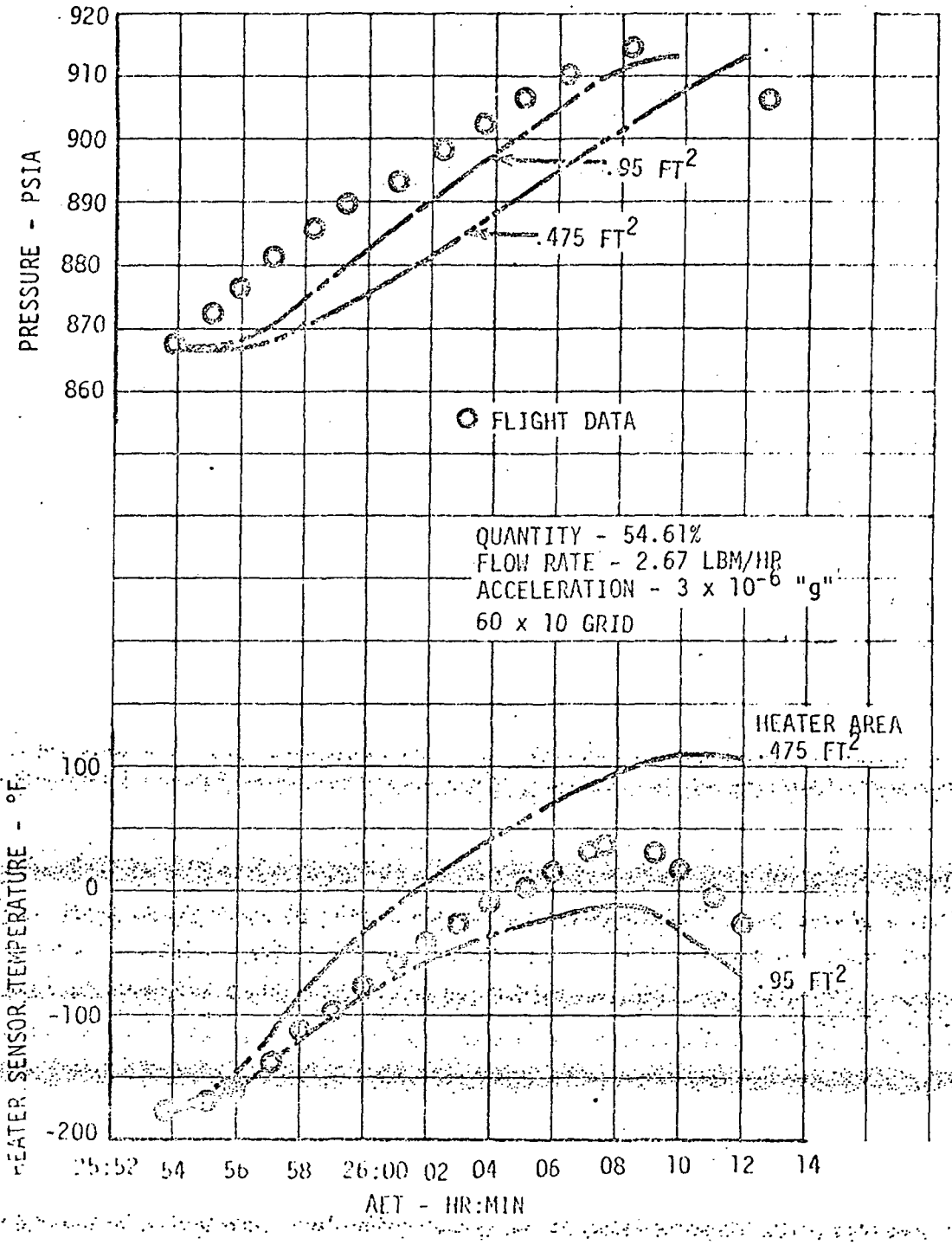

FIGURE 5-1 - PTC HEATER CYCLE SIMULATION

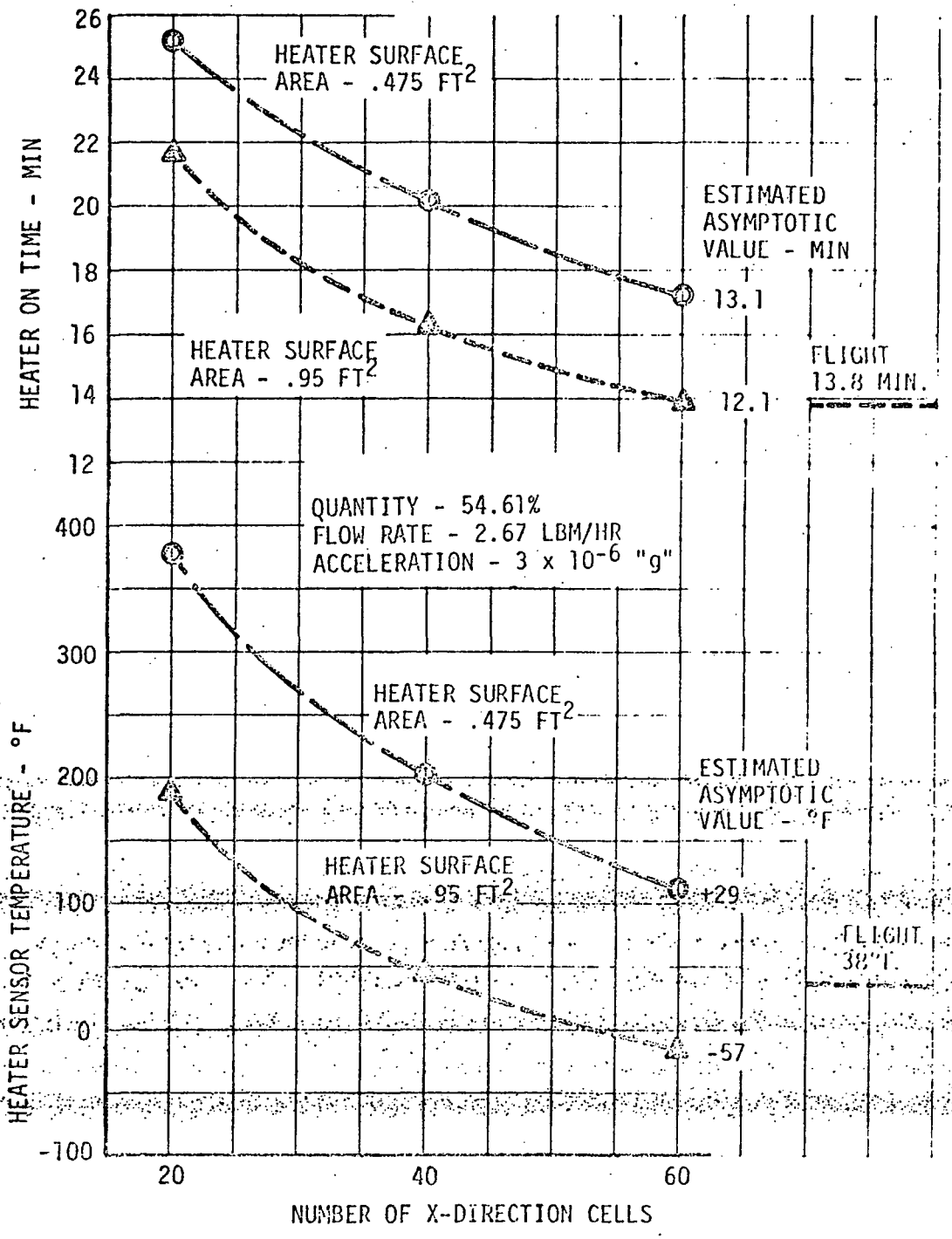

FIGURE 5-2 - PTC HEATER CYCLE CONVERGENCE

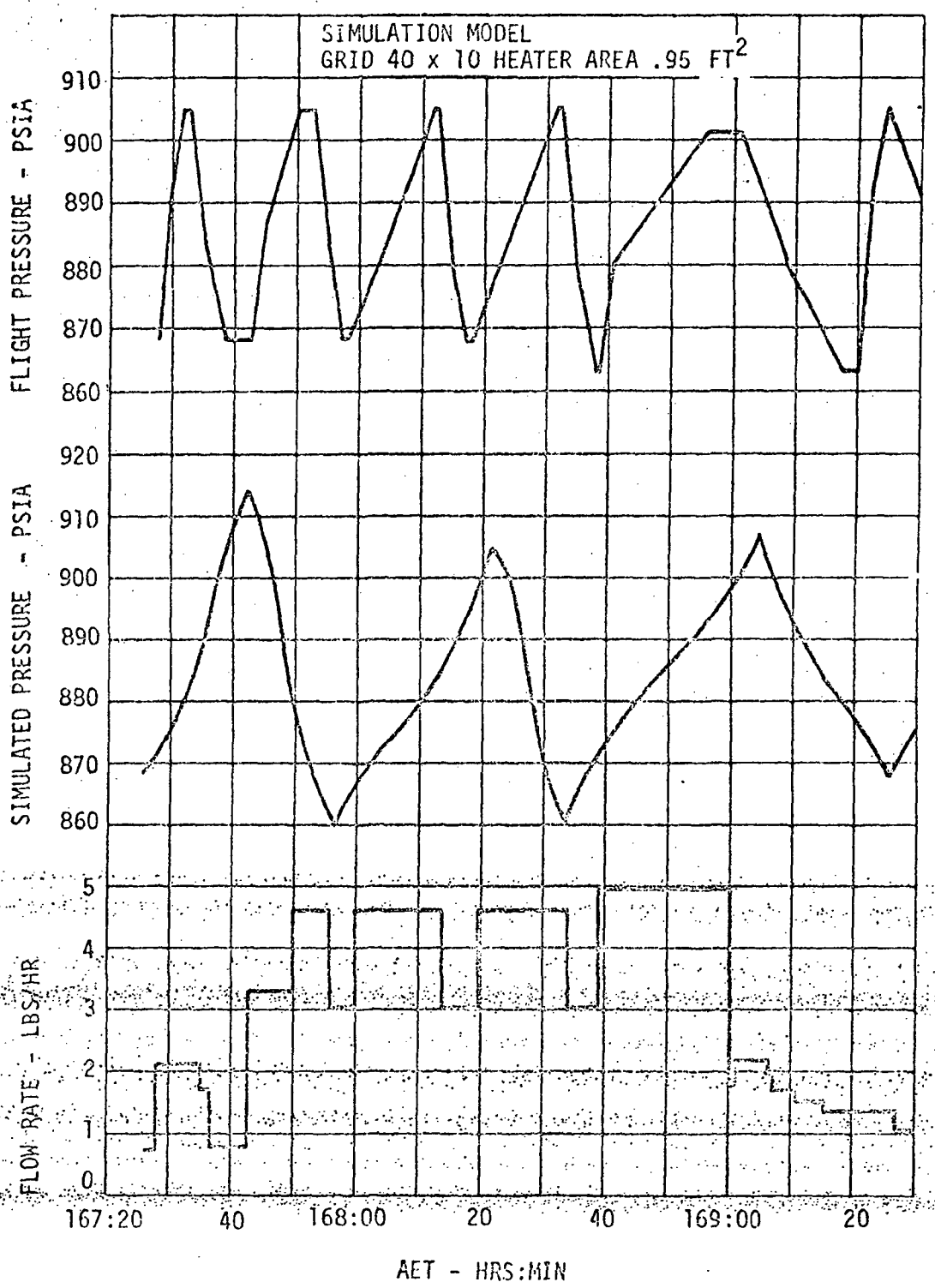

FIGURE 5-3 - TANK 1 TEST SIMULATION - 0.95 FT^2 HEATER AREA

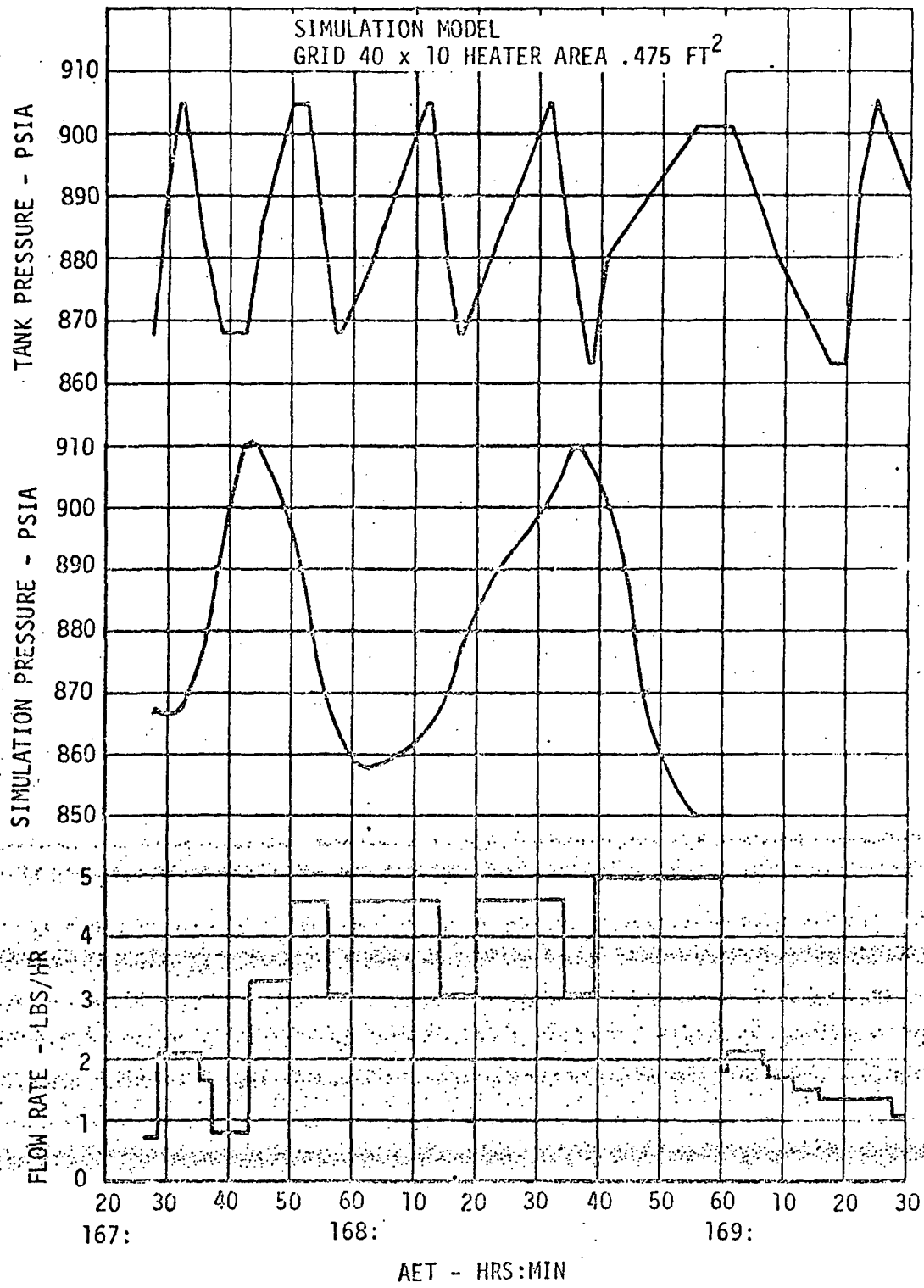

FIGURE 5-4 - TANK 1 TEST SIMULATION - 0.475 FT^2 HEATER AREA

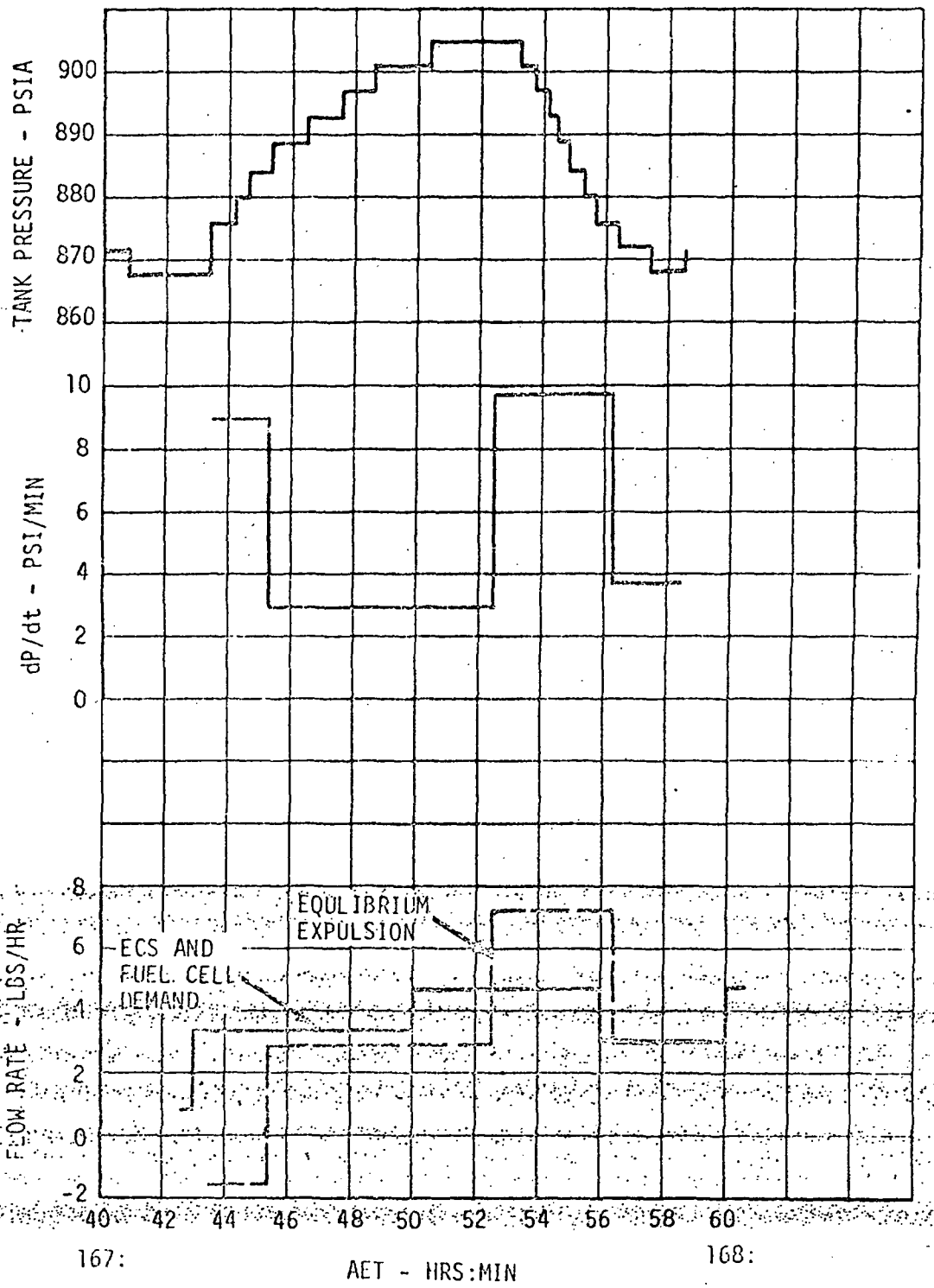

FIGURE 5-5 - TANK 1 TRANSIENT PRESSURE AND FLOW RESPONSE

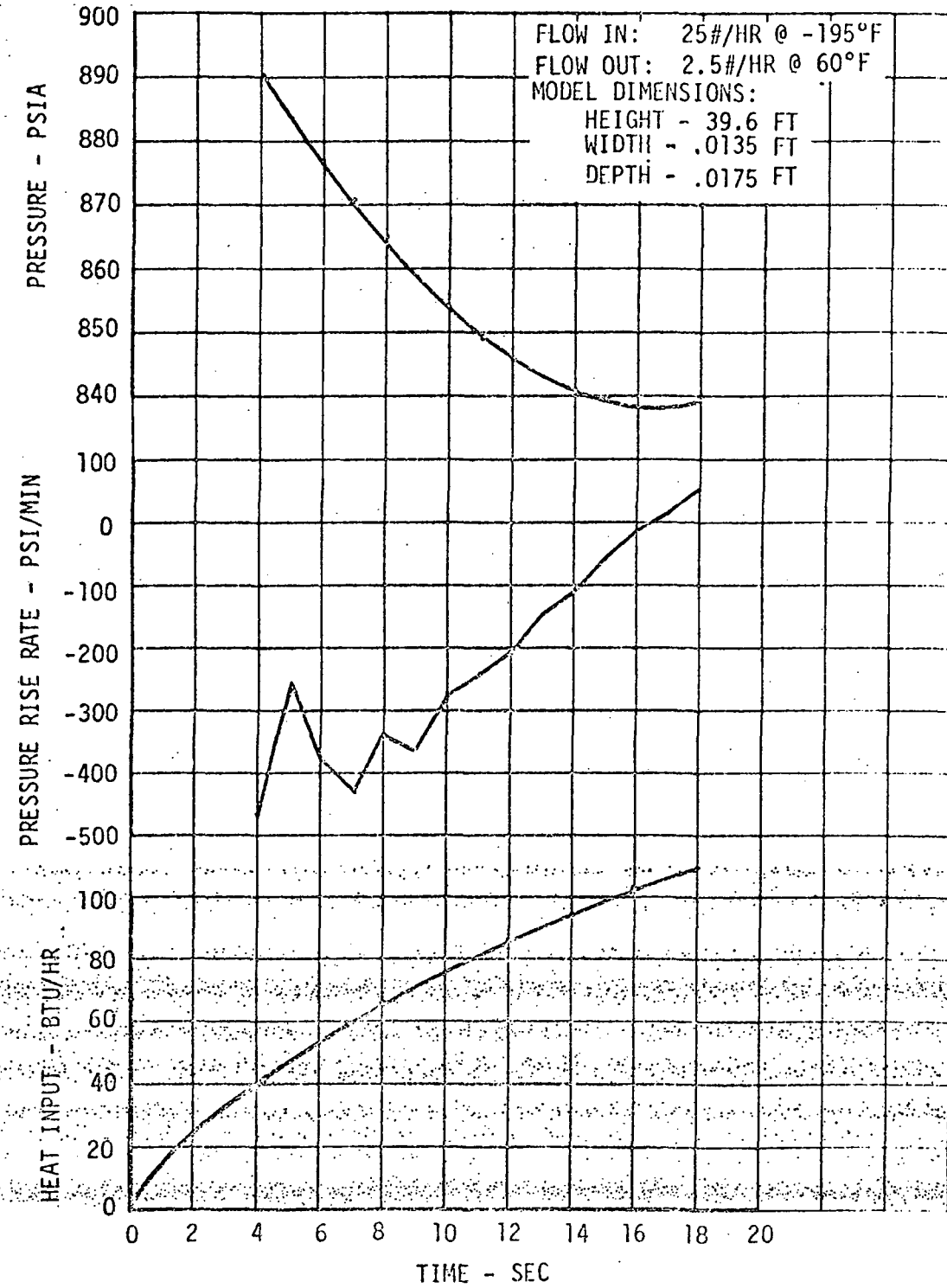

FIGURE 5-6 - PLUMBING SYSTEM PRESSURE RESPONSE WITH HIGH FLOW RATES

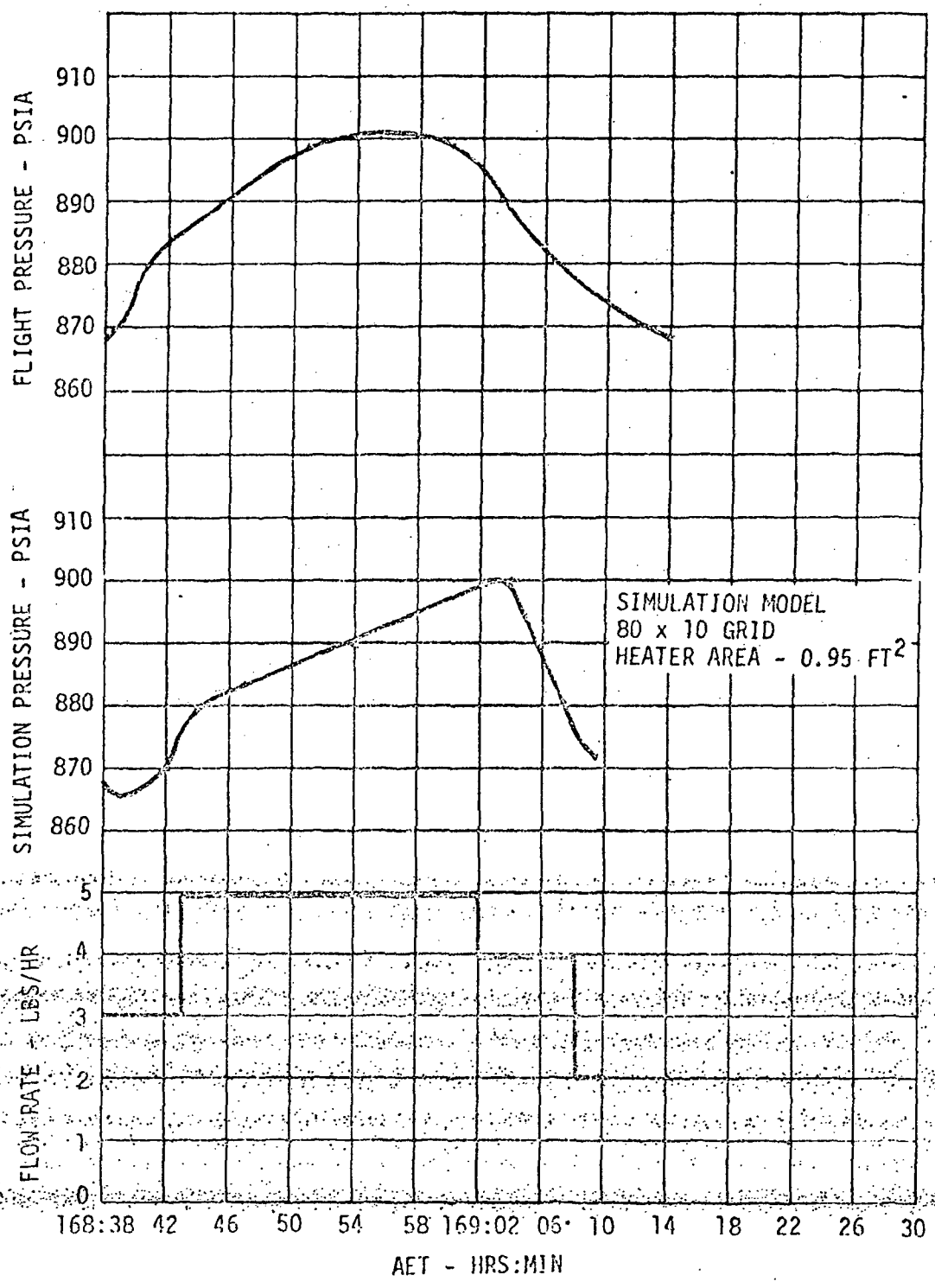

FIGURE 5-7 - TANK 1 TEST SIMULATION WITH PRESSURE DEPENDENT FLOW RATE

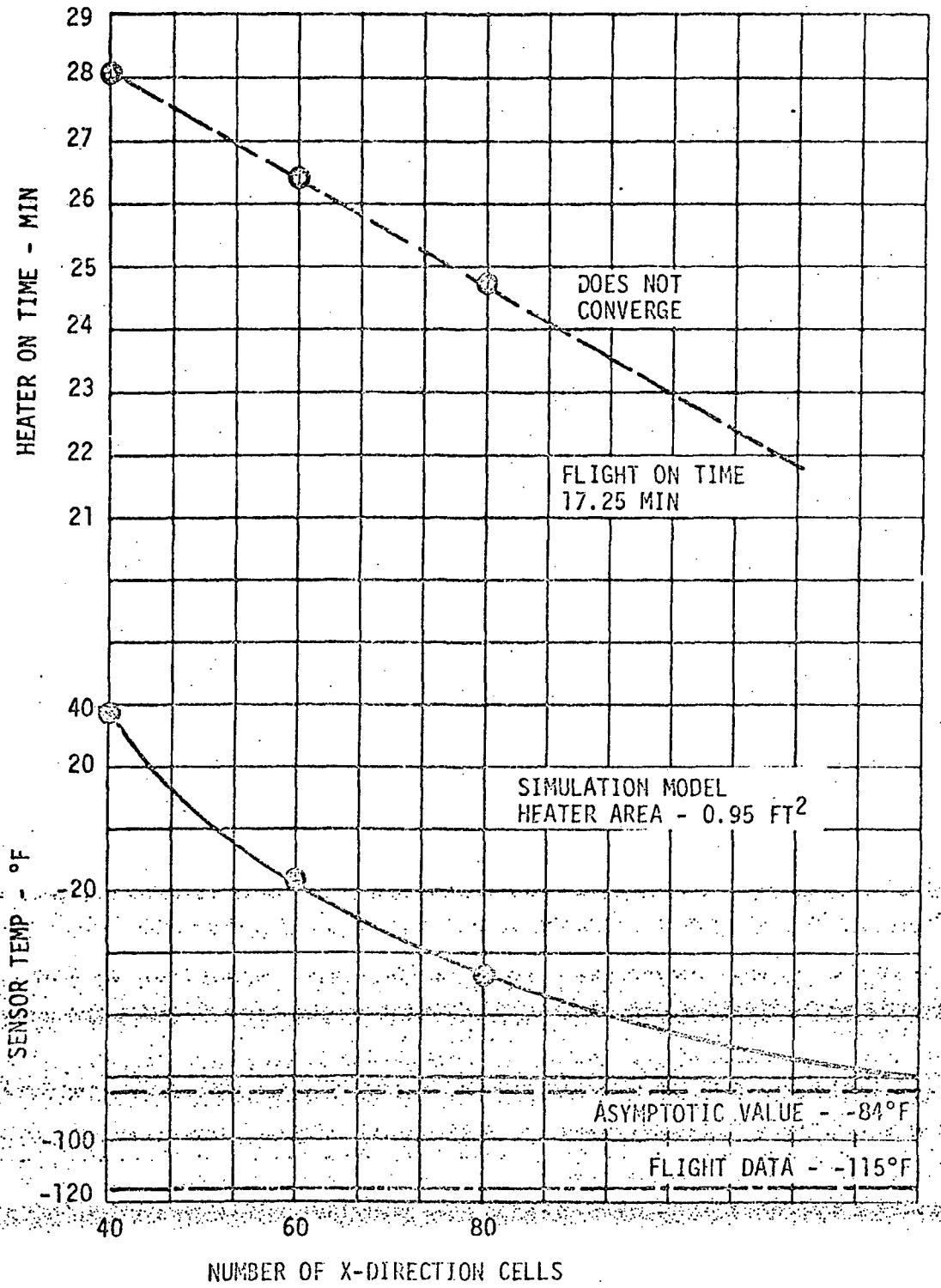

FIGURE 5-8 - TANK 1 TEST CONVERGENCE WITH PRESSURE DEPENDENT FLOW RATE

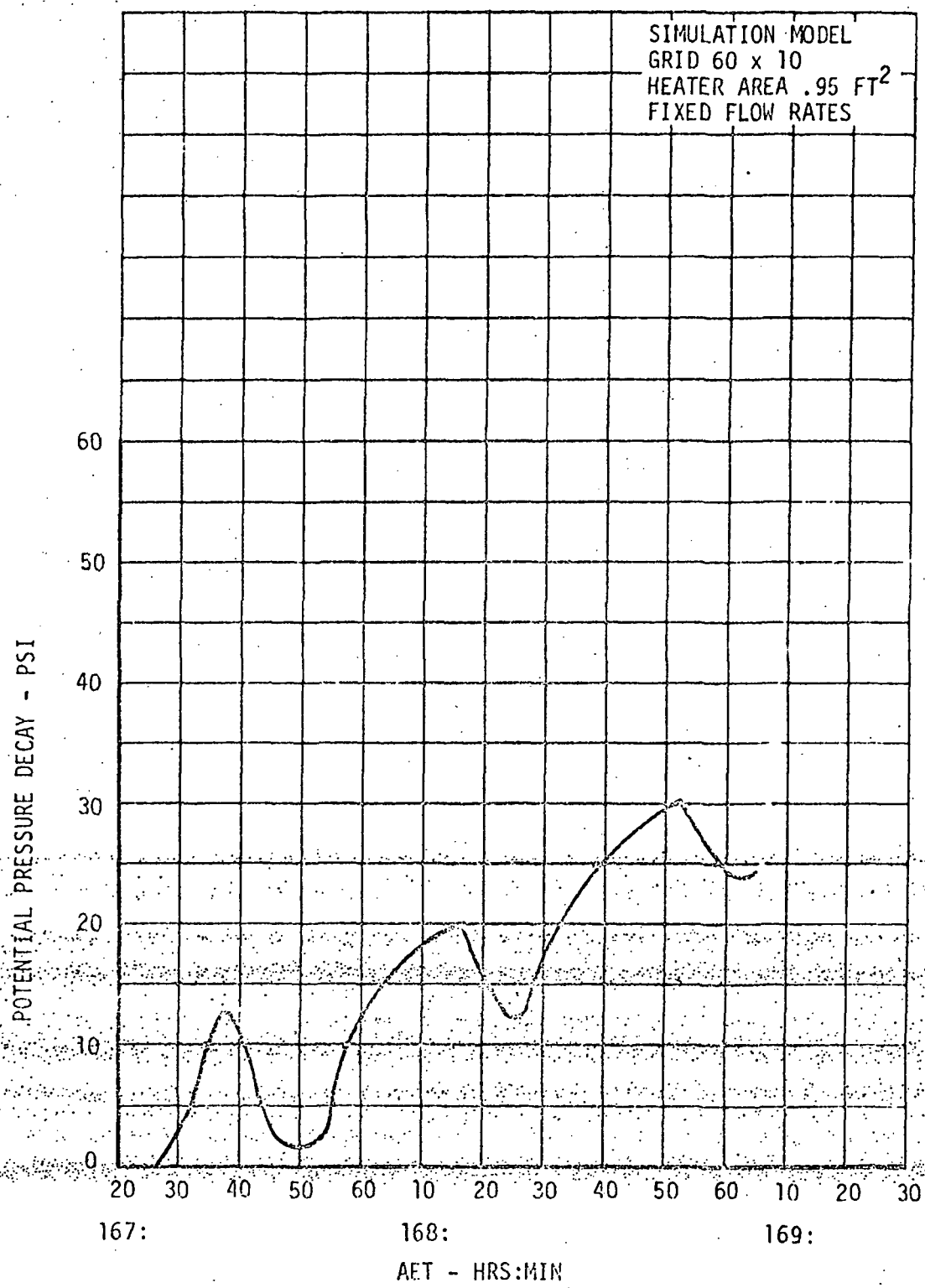

FIGURE 5-9 - TANK 1 POTENTIAL PRESSURE DECAY DURING THE HIGH FLOW TEST

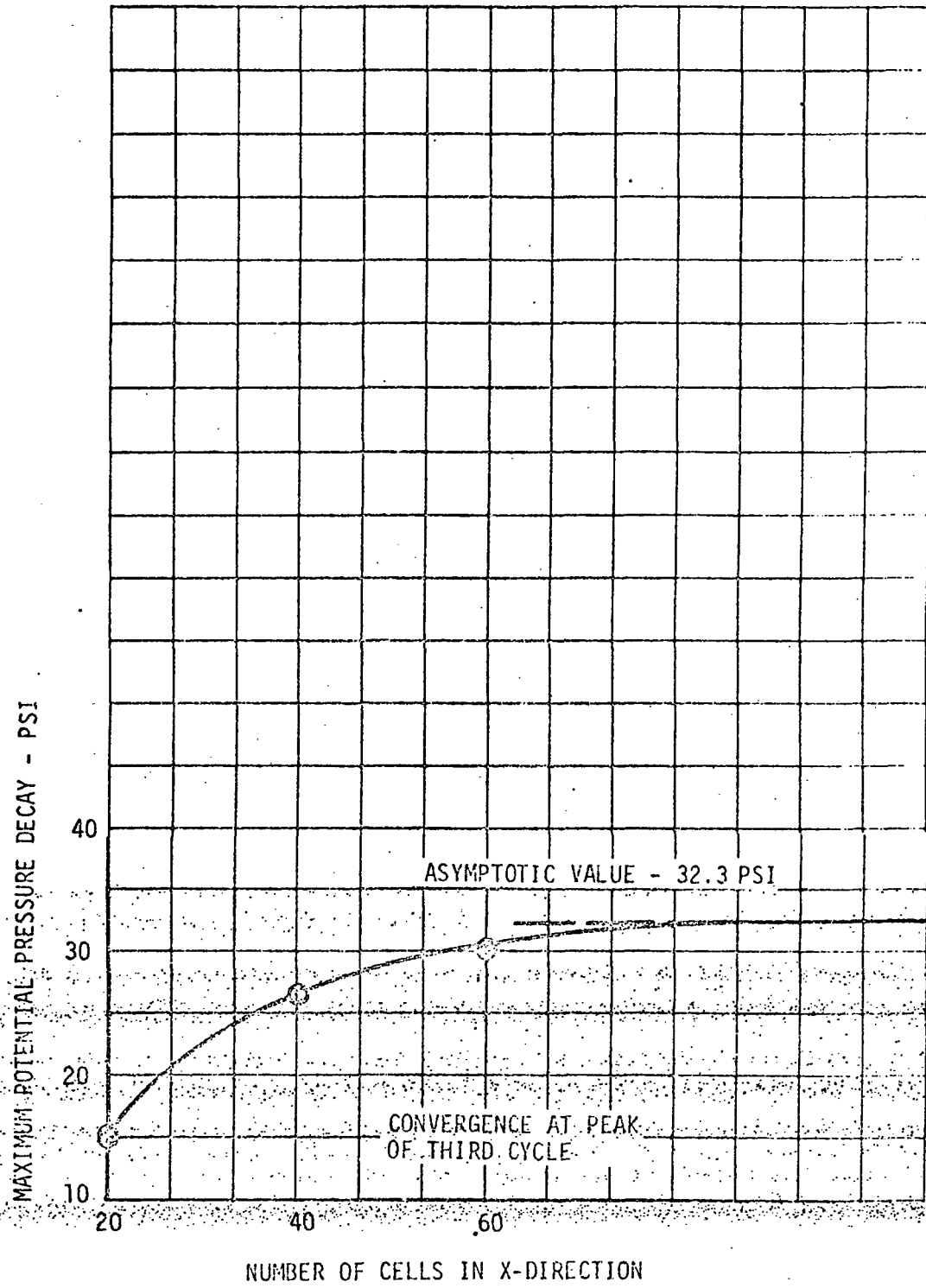

FIGURE 5-10 - CONVERGENCE OF MAXIMUM POTENTIAL PRESSURE DECAY DURING THE HIGH FLOW TEST

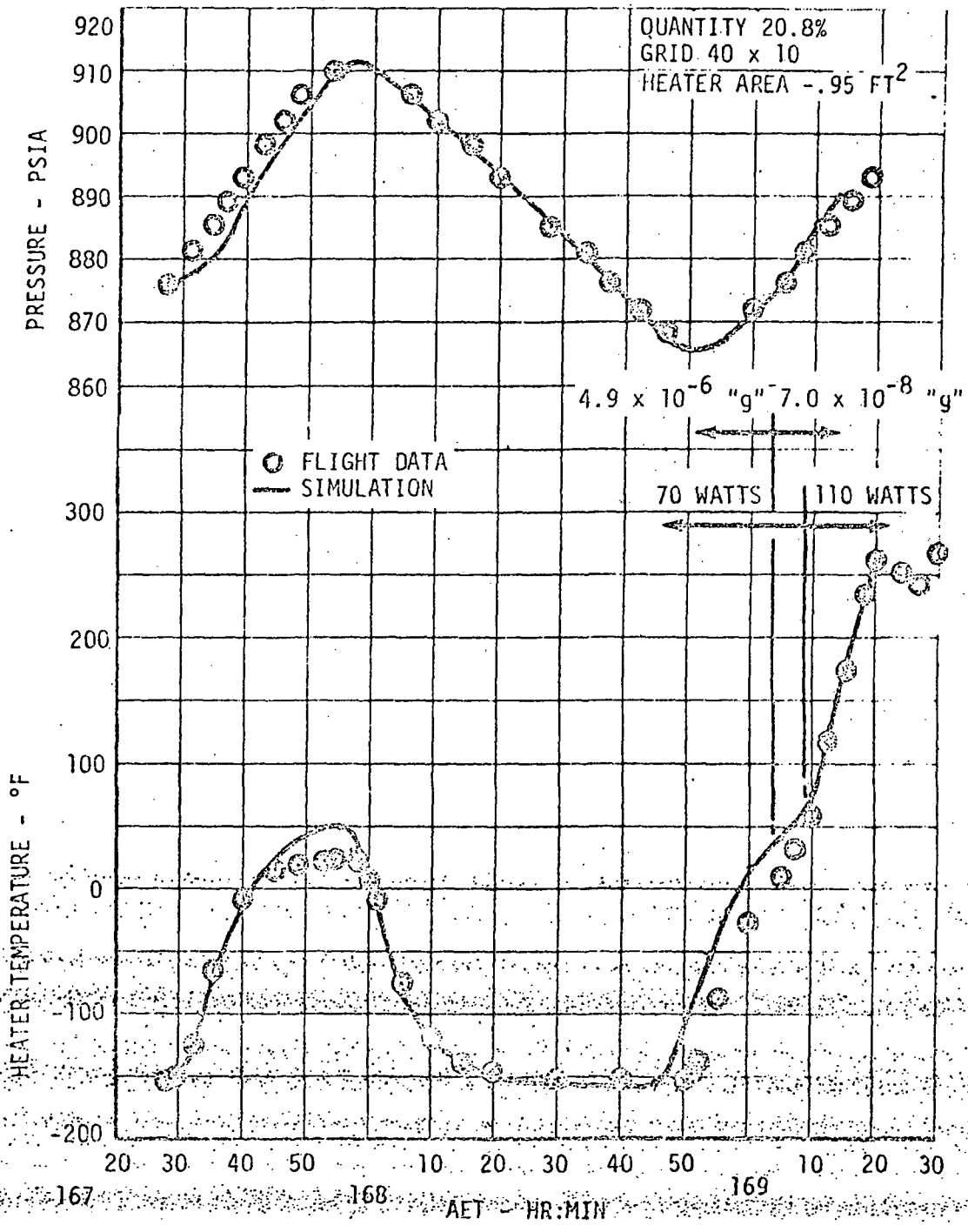

FIGURE 5-11- TANK 3 TEST SIMULATION

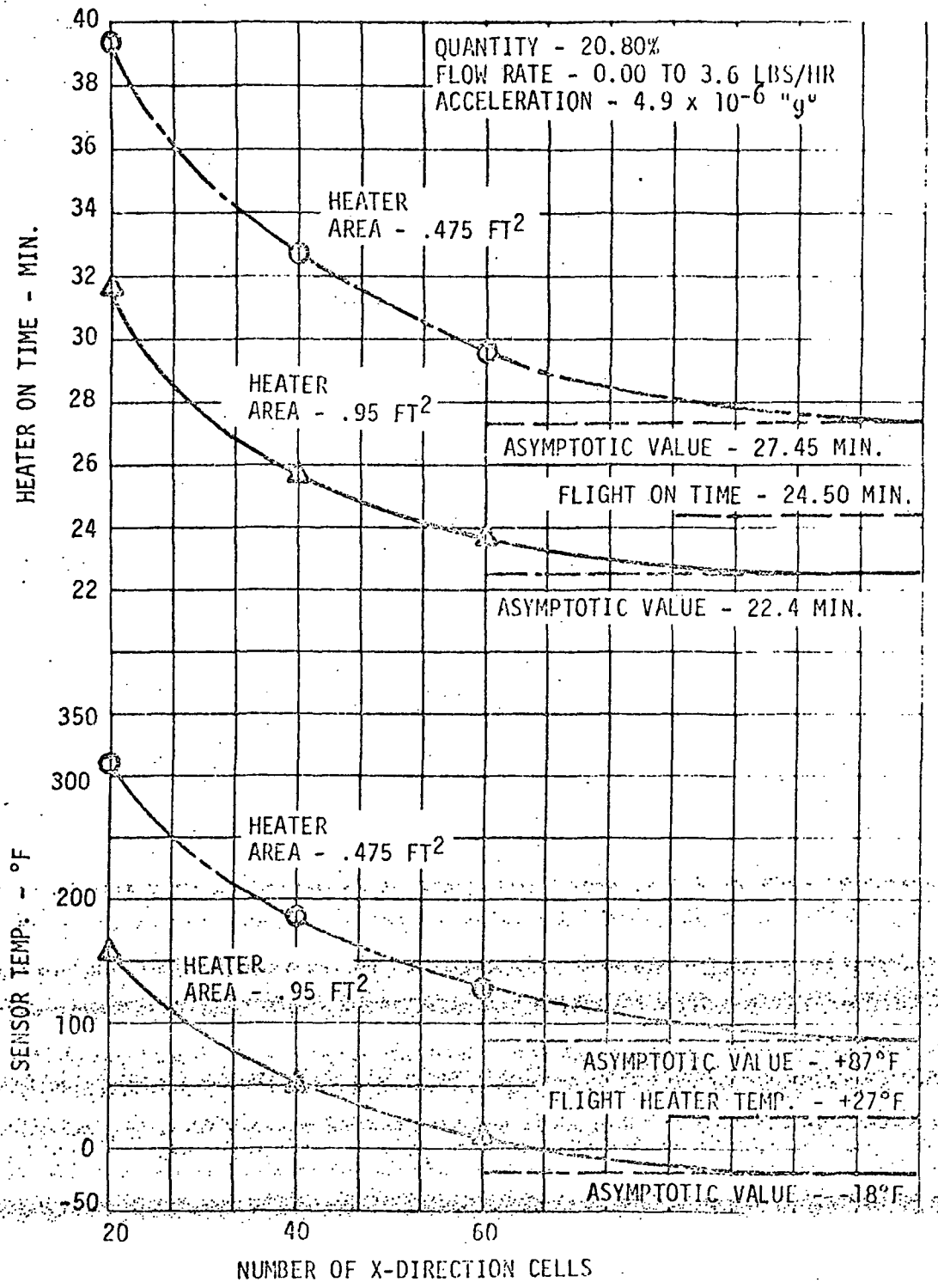

FIGURE 5-12 - TANK 3 TEST CONVERGENCE

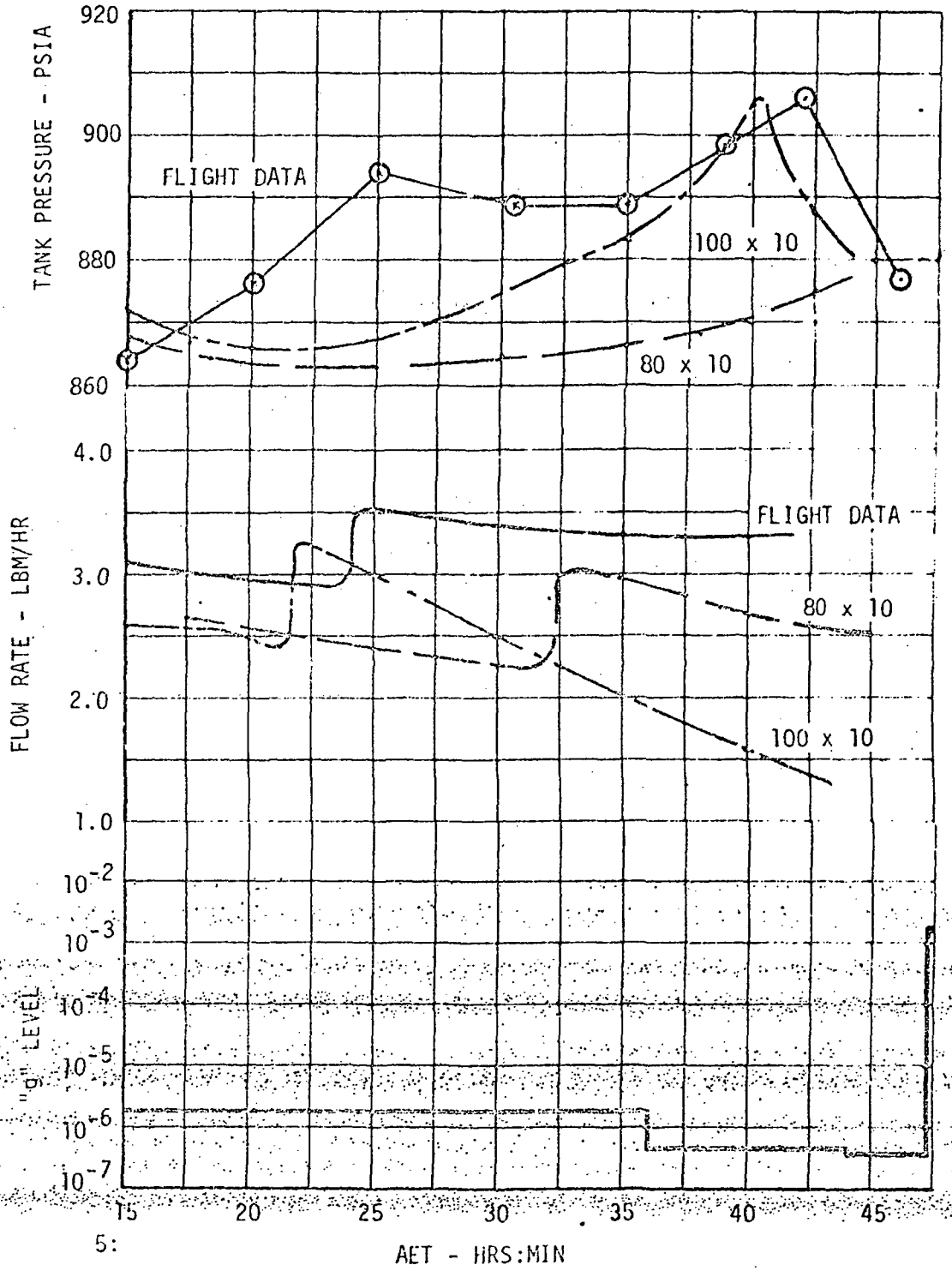

FIGURE 5-13 - SIMULATION OF HEATER CYCLE AT AET 5:15

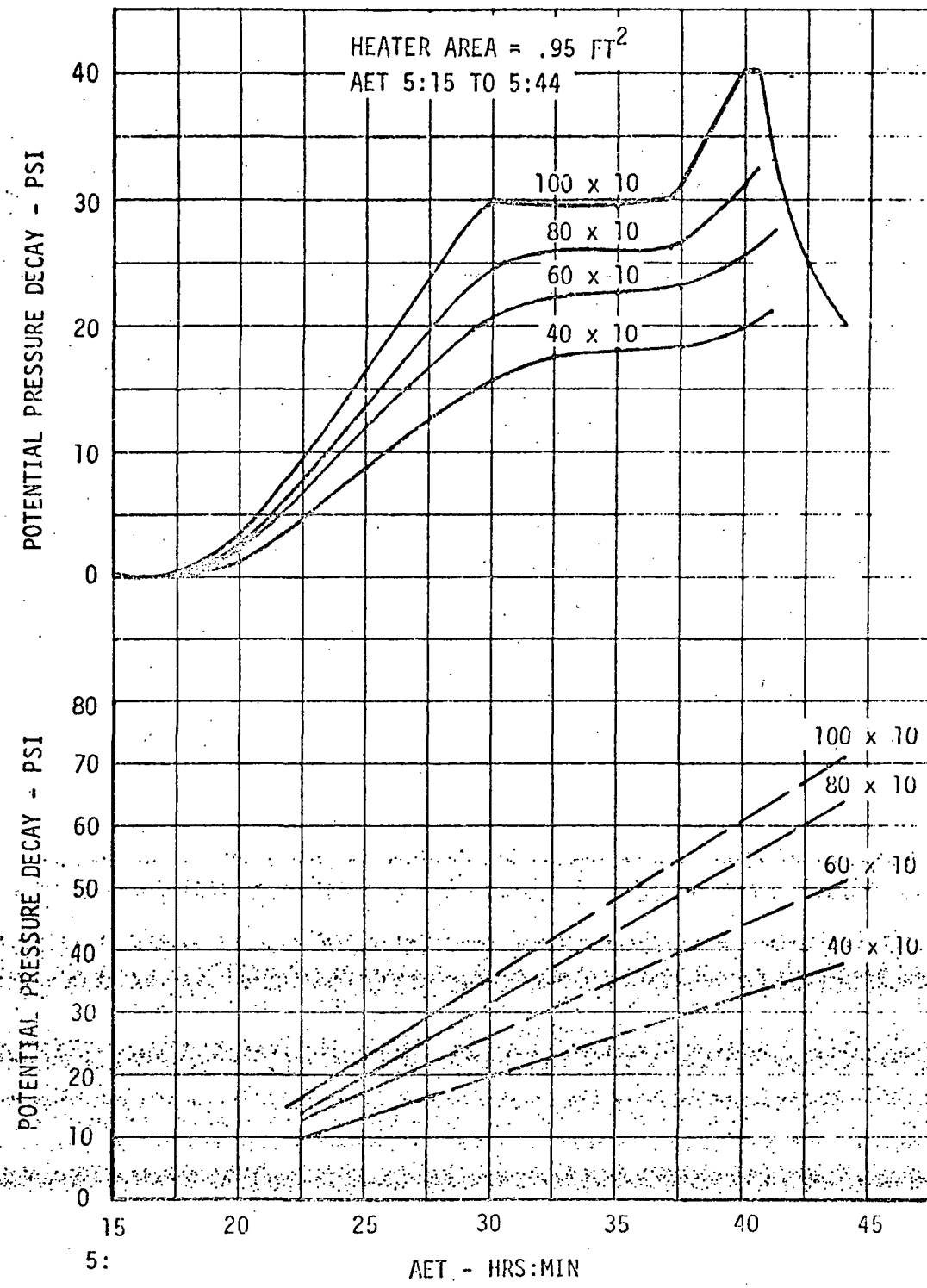

FIGURE 5-14 - POTENTIAL PRESSURE DECAY, .95 FT^2 HEATER AREA

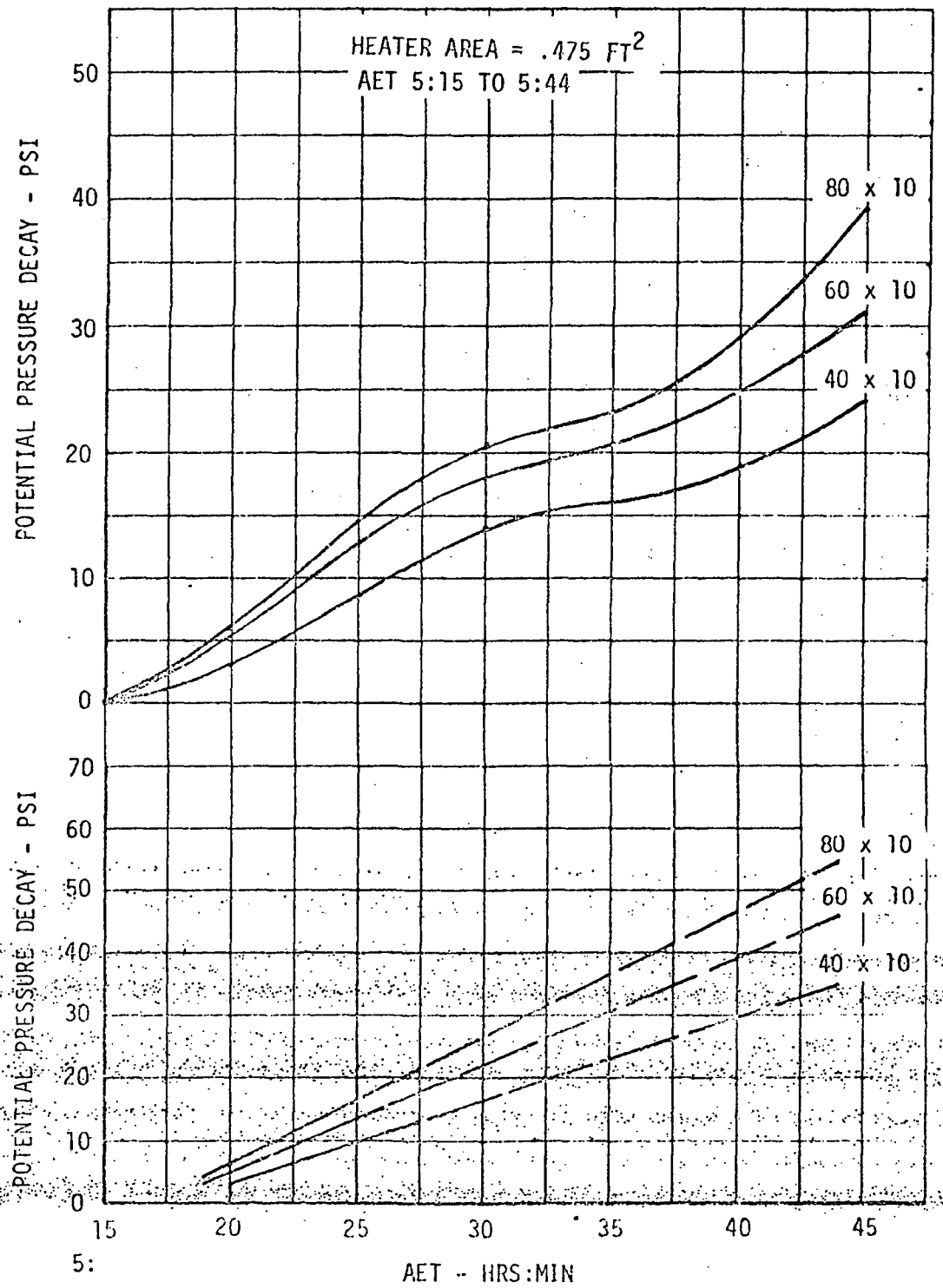

FIGURE 5-15 - POTENTIAL PRESSURE DECAY, .475 FT^2 HEATER AREA

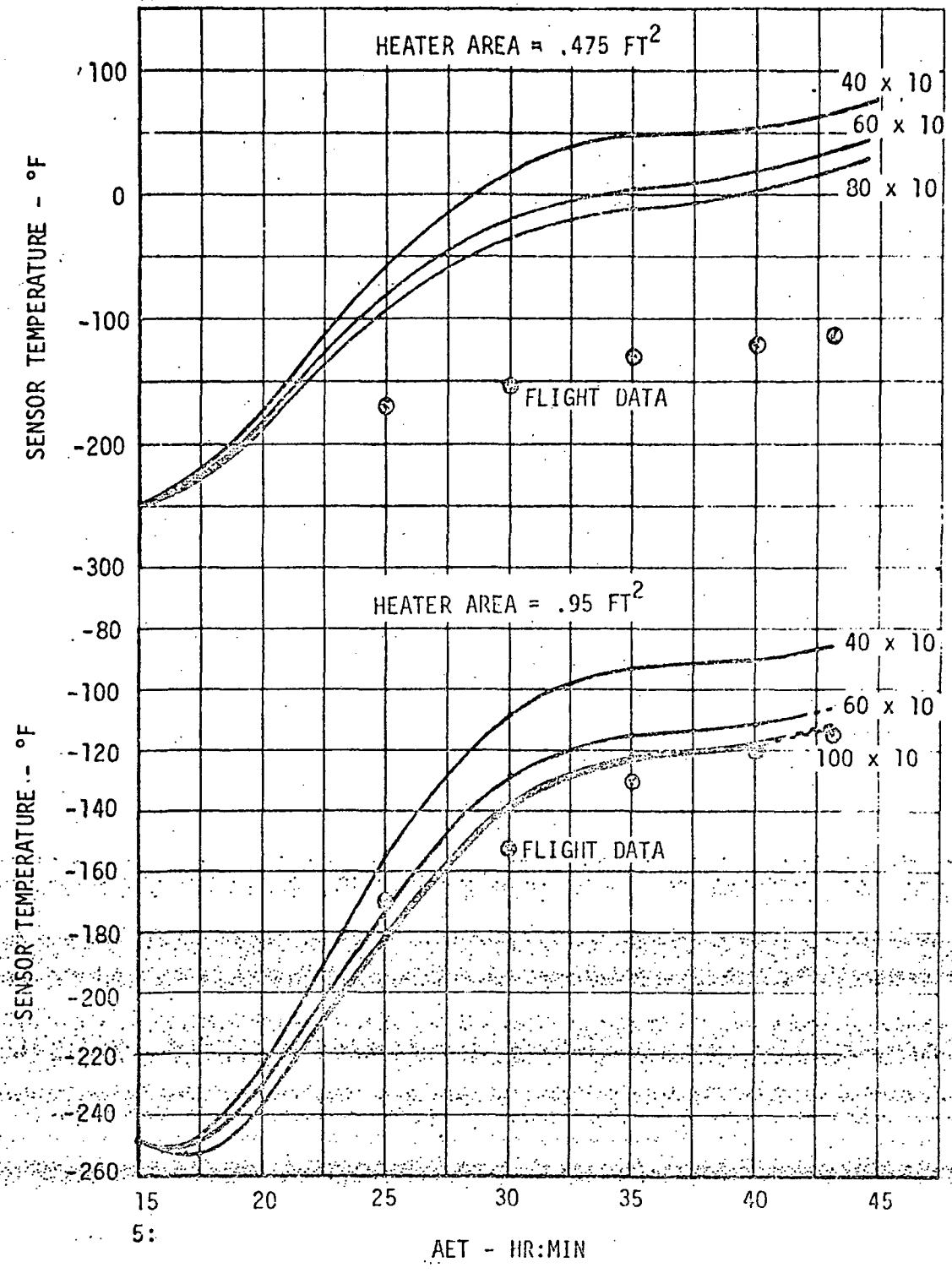

FIGURE 5-16 - HEATER SENSOR TEMPERATURE SIMULATION, AET 5:15 TO 5:44

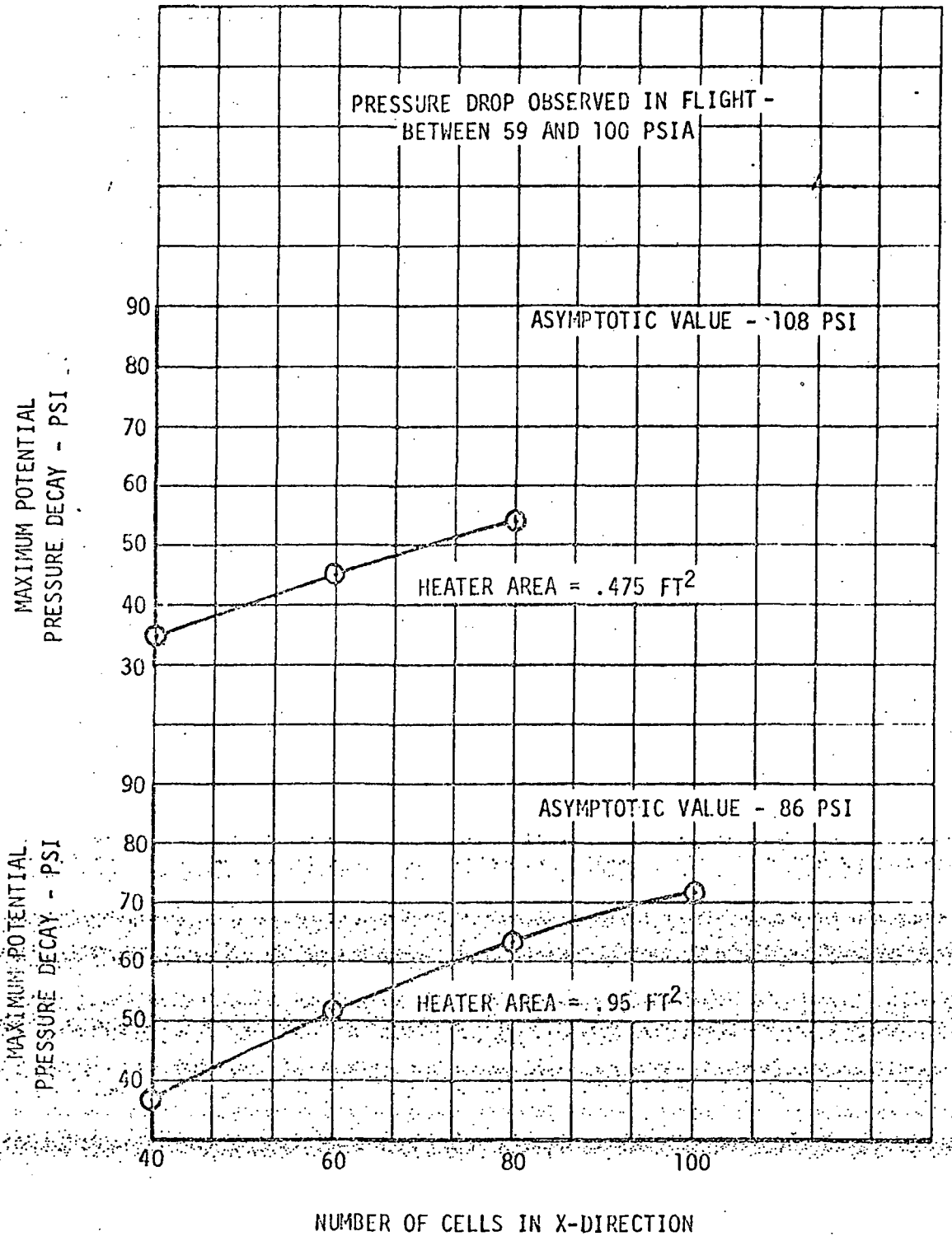

FIGURE 5-17 - CONVERGENCE OF MAXIMUM POTENTIAL PRESSURE DECAY AT AET 5:44

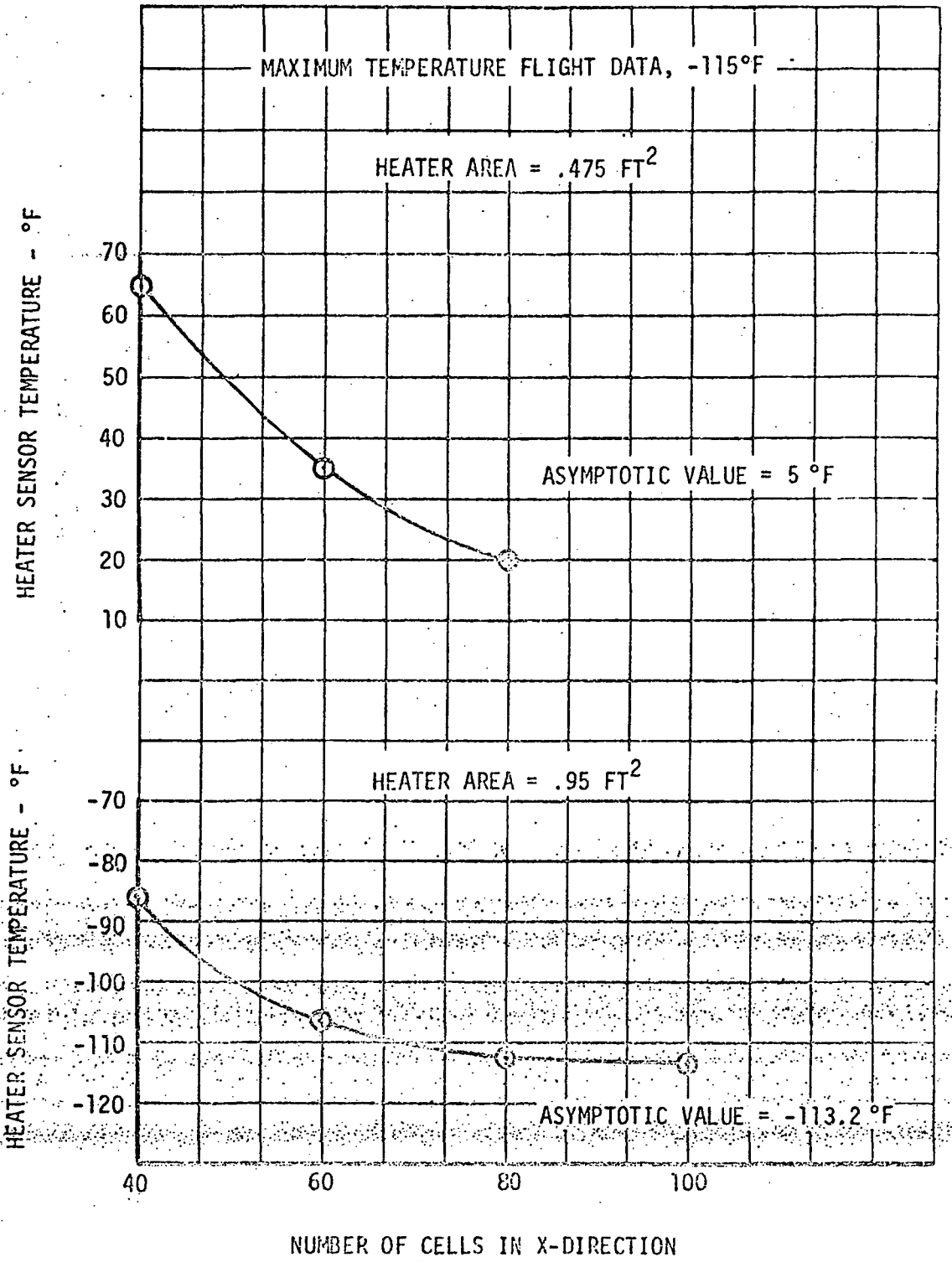

FIGURE 5-18 - CONVERGENCE OF HEATER SENSOR TEMPERATURE AT AET 5:44

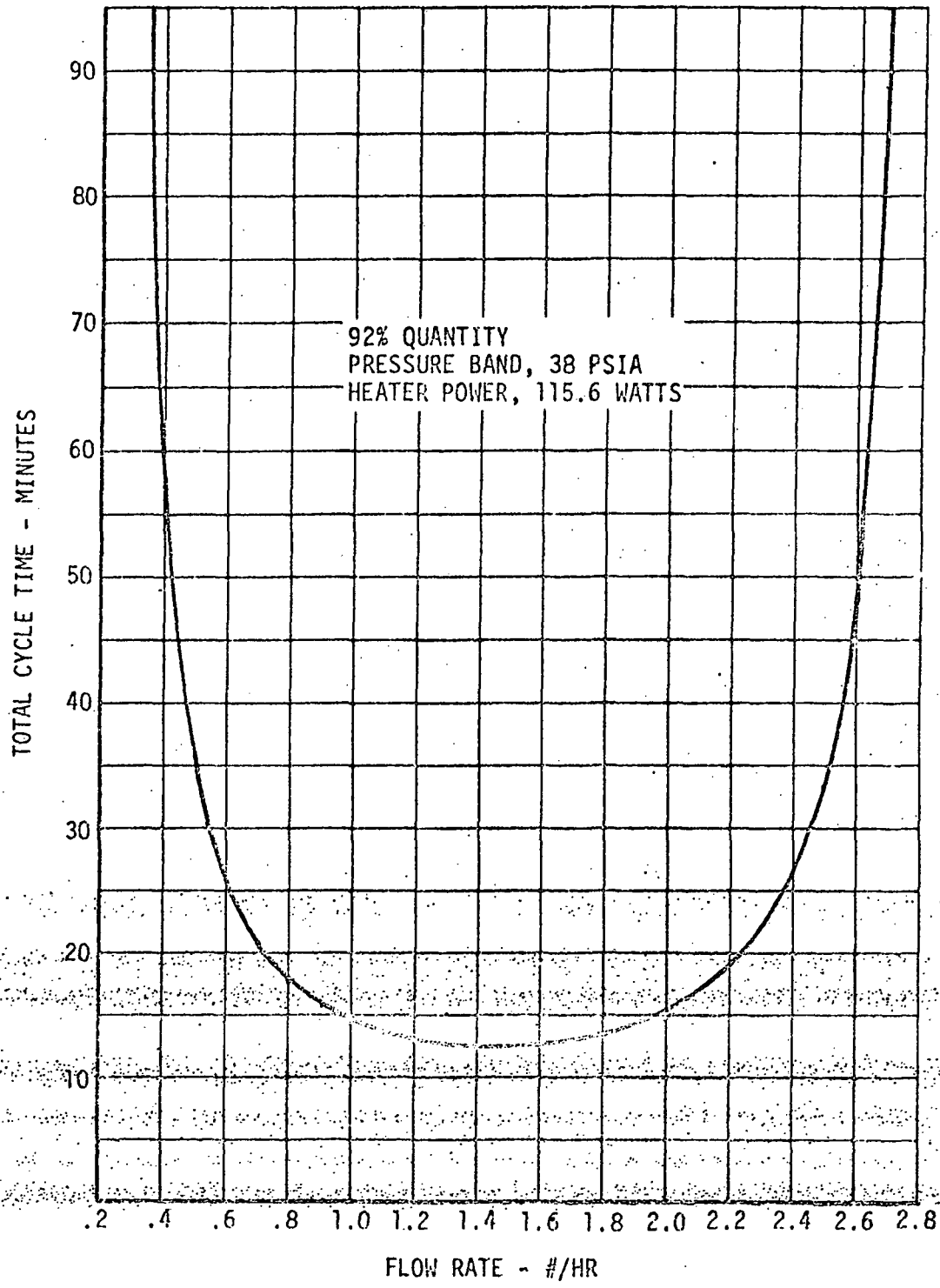

FIGURE 5-19 - LENGTH OF EQUILIBRIUM HEATER CYCLE AT 92% QUANTITY

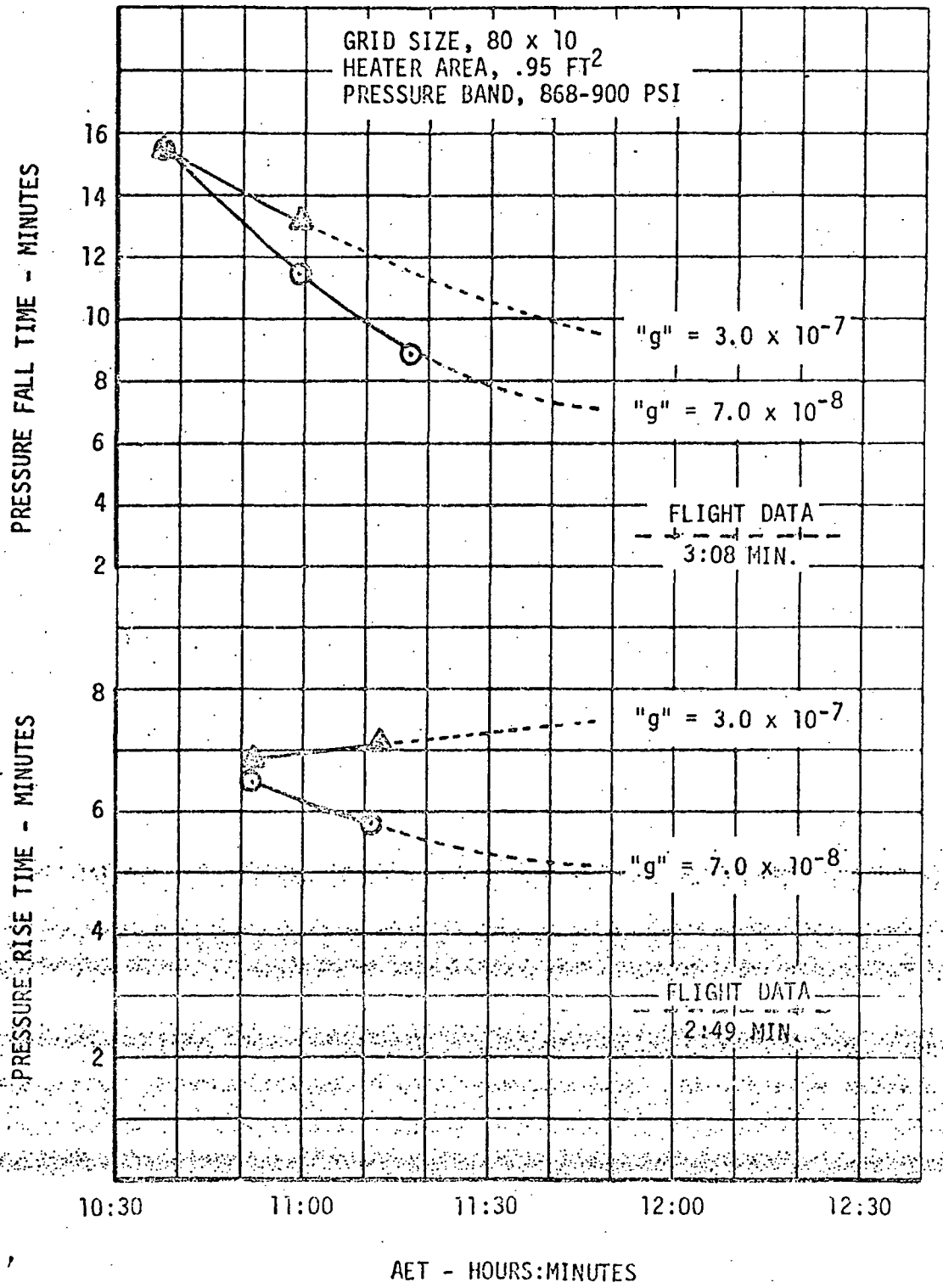

FIGURE 5-20 - EFFECT OF ACCELERATION ON HEATER CYCLES, AET 10:30 - 12:30

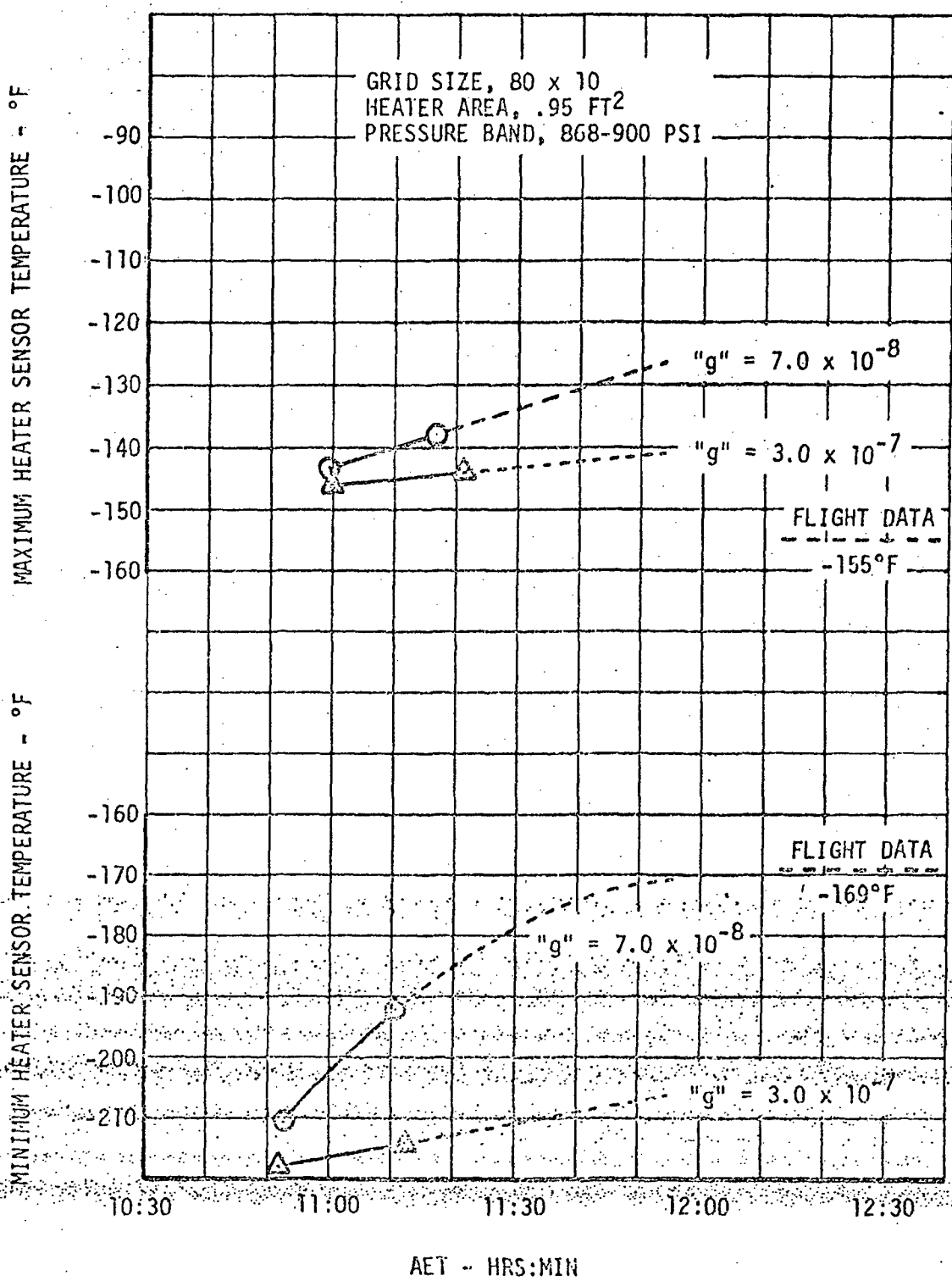

FIGURE 5-21 - EFFECT OF ACCELERATION ON HEATER SENSOR TEMPERATURE, AET 10:30 - 12:30

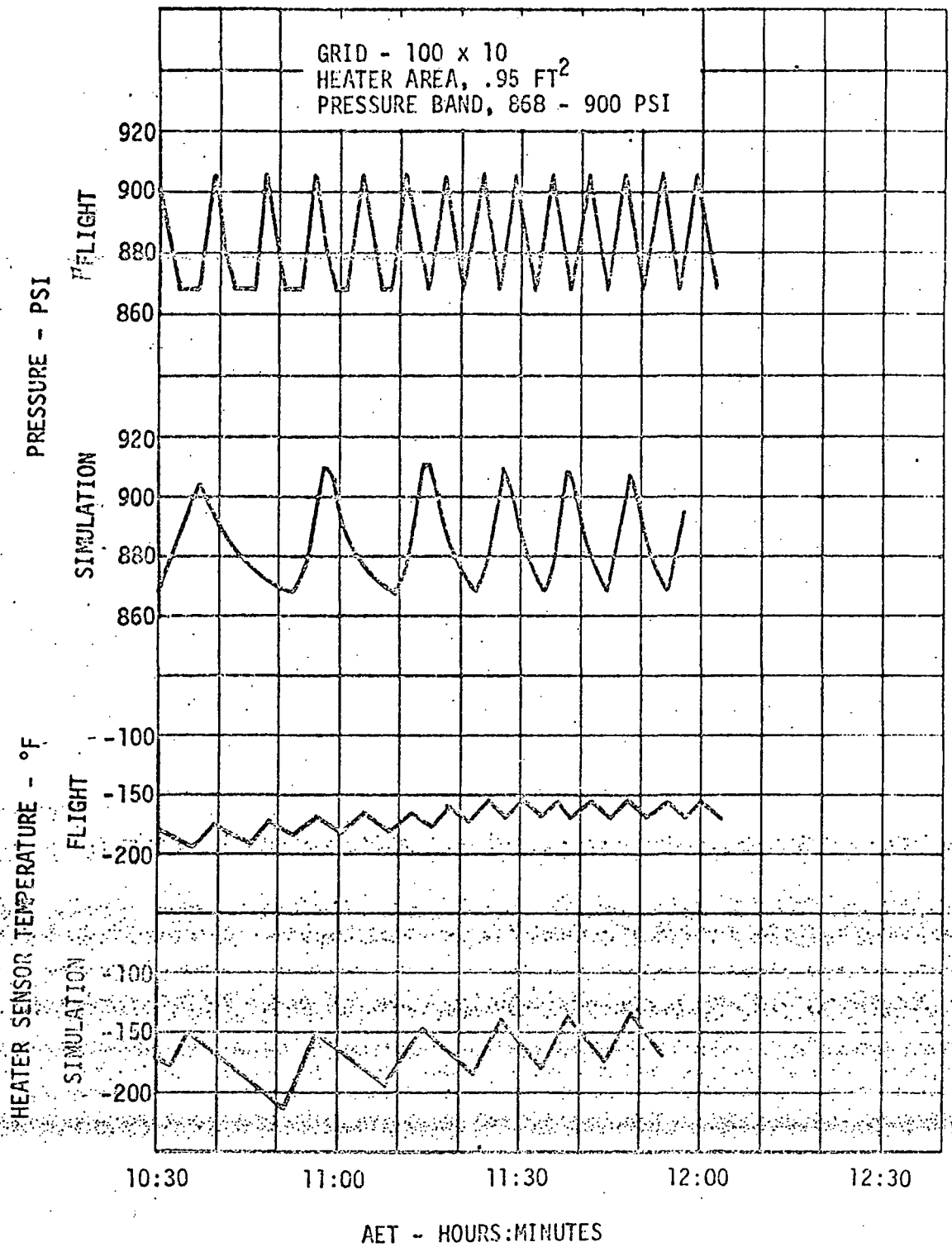

FIGURE 5-22 - SIMULATION OF AET 10:30 TO 12:00 USING 100 x 10 GRID

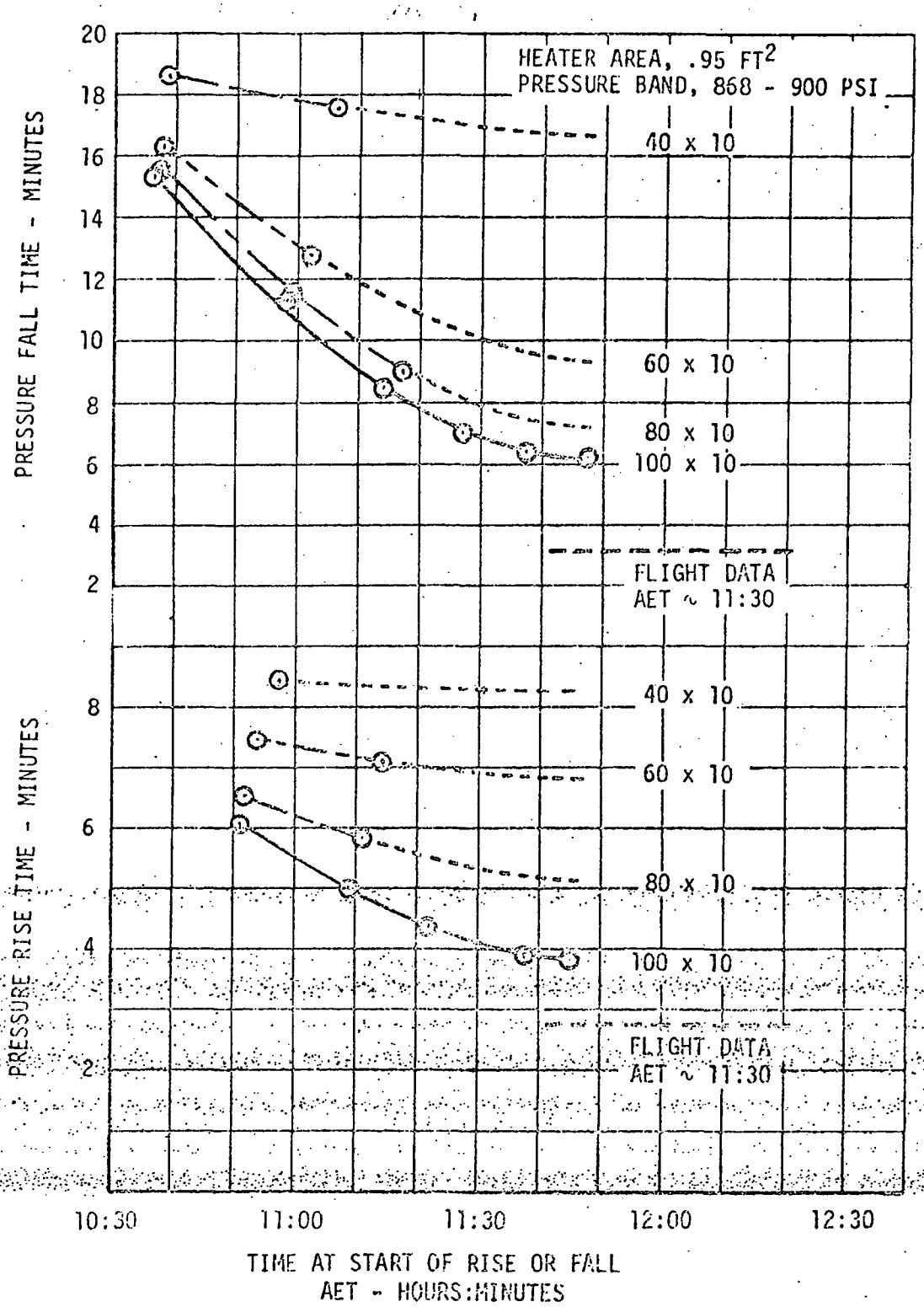

FIGURE 5-23 - EFFECT OF STRATIFICATION ON LENGTH OF HEATER CYCLE

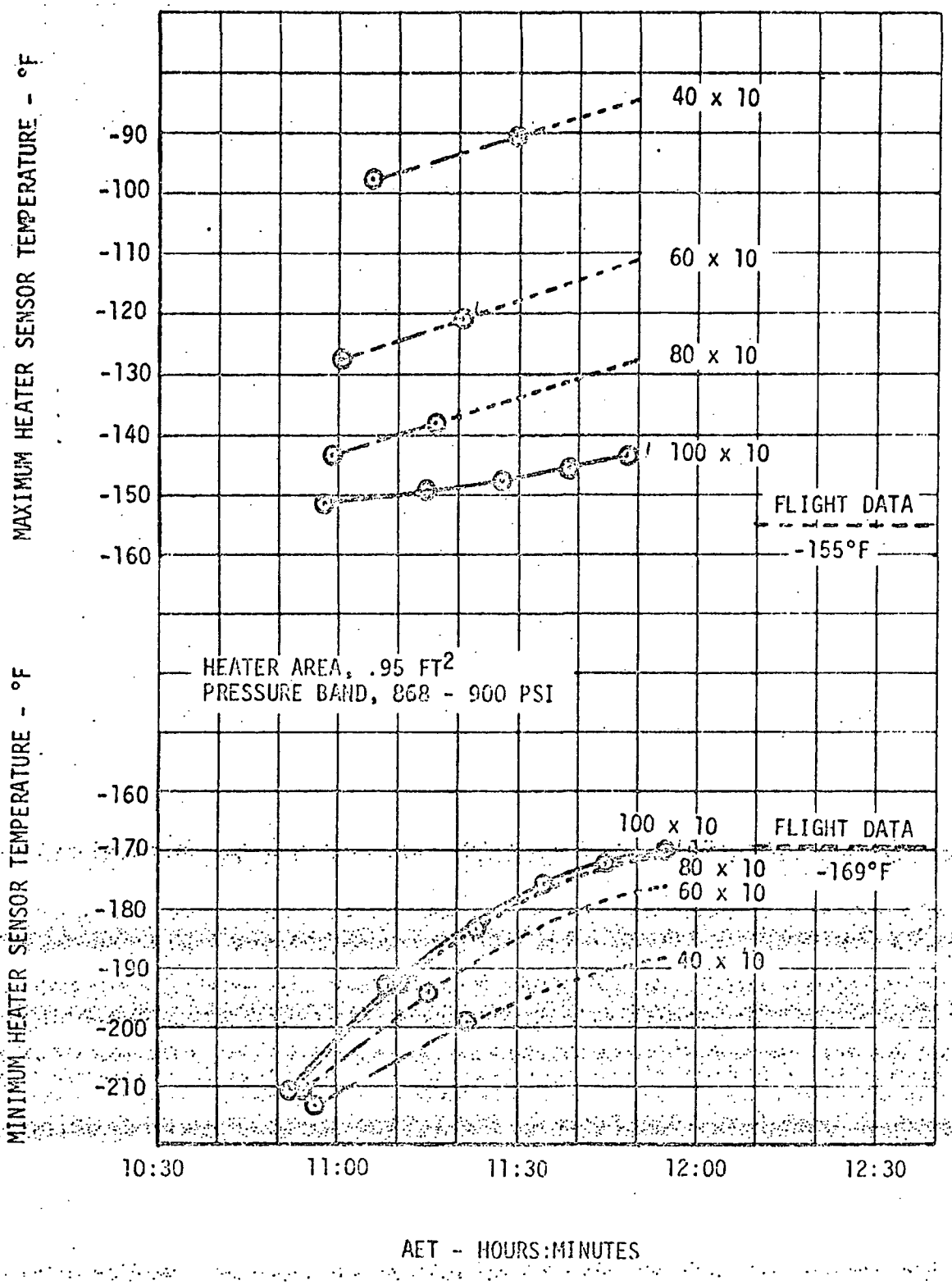

FIGURE 5-24 - EFFECT OF STRATIFICATION ON HEATER SENSOR TEMPERATURE

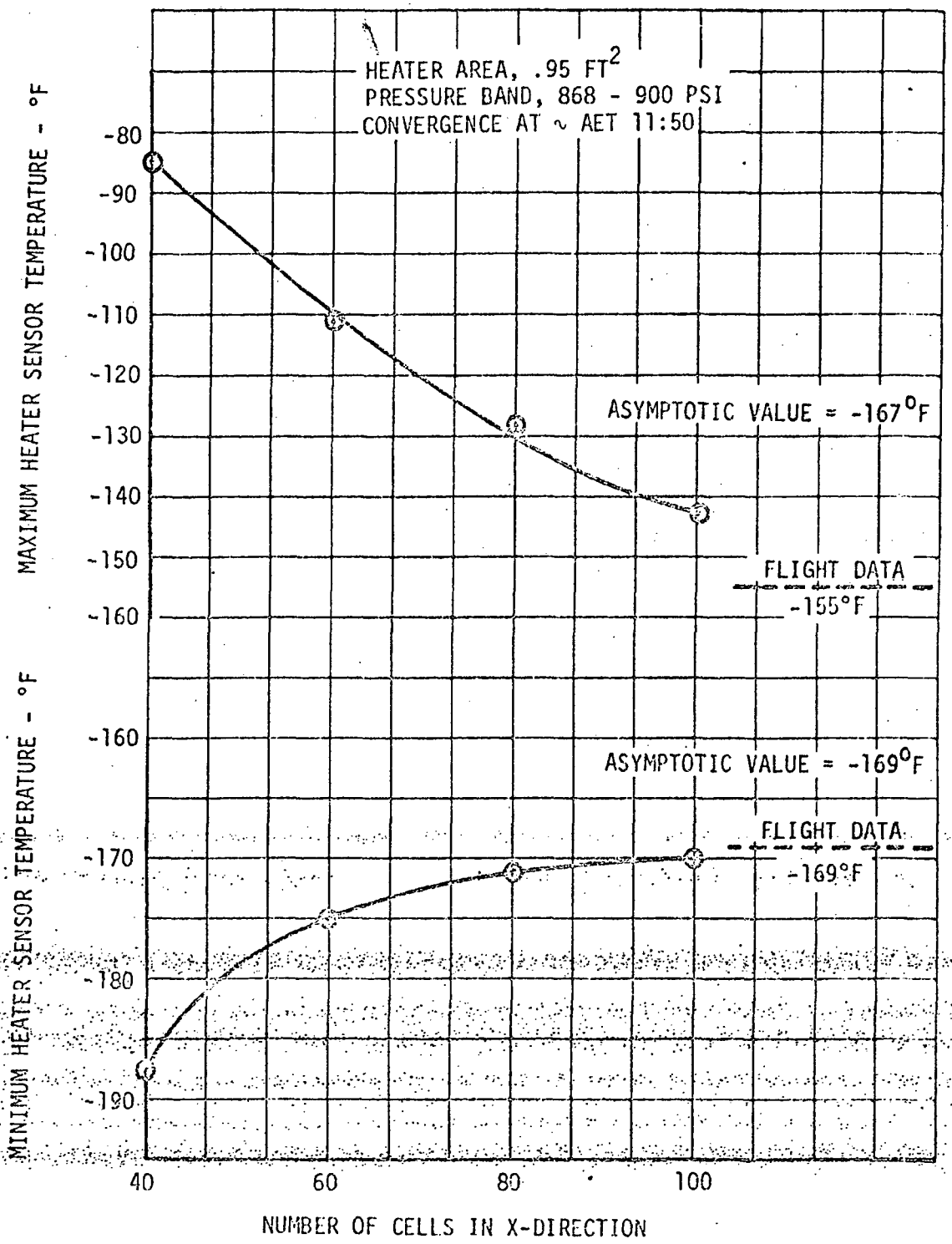

FIGURE 5-25 - CONVERGENCE OF HEATER SENSOR TEMPERATURE AT AET 11:50

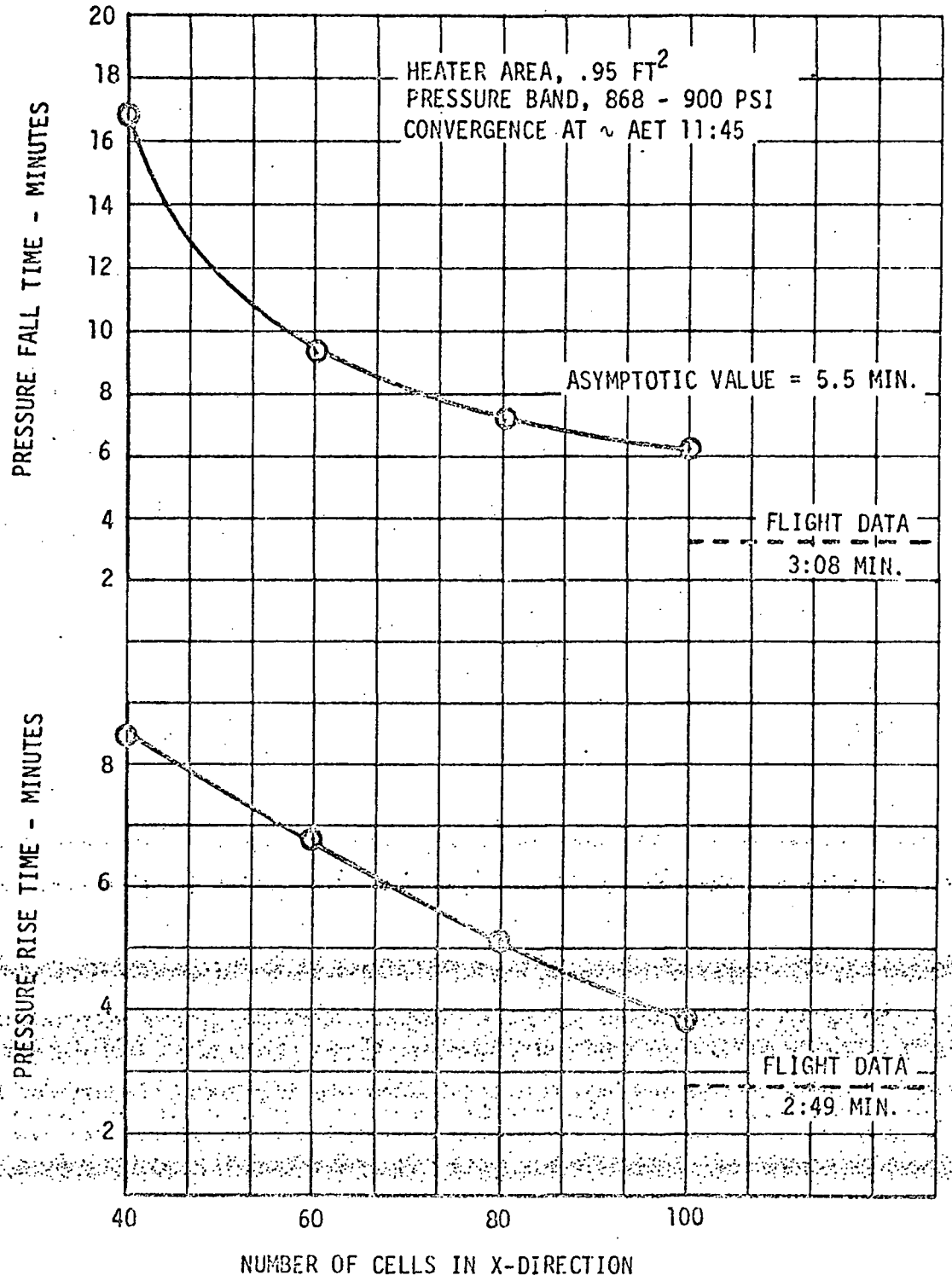

FIGURE 5-26 - CONVERGENCE OF LENGTH OF CYCLE TIME AT AET 11:45

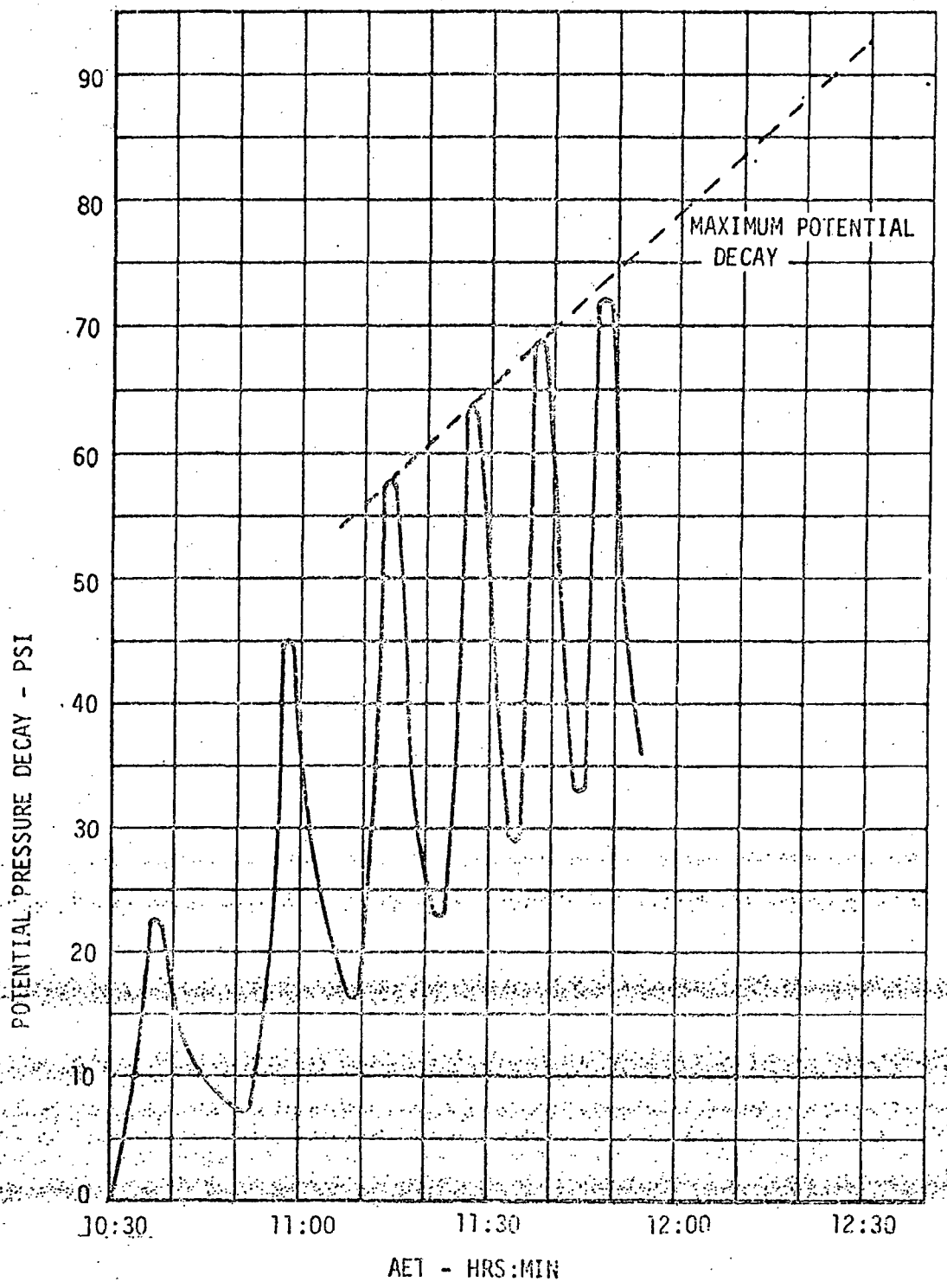

FIGURE 5-27 - BUILD-UP OF POTENTIAL PRESSURE DECAY FROM AET 10:30 TO 12:30

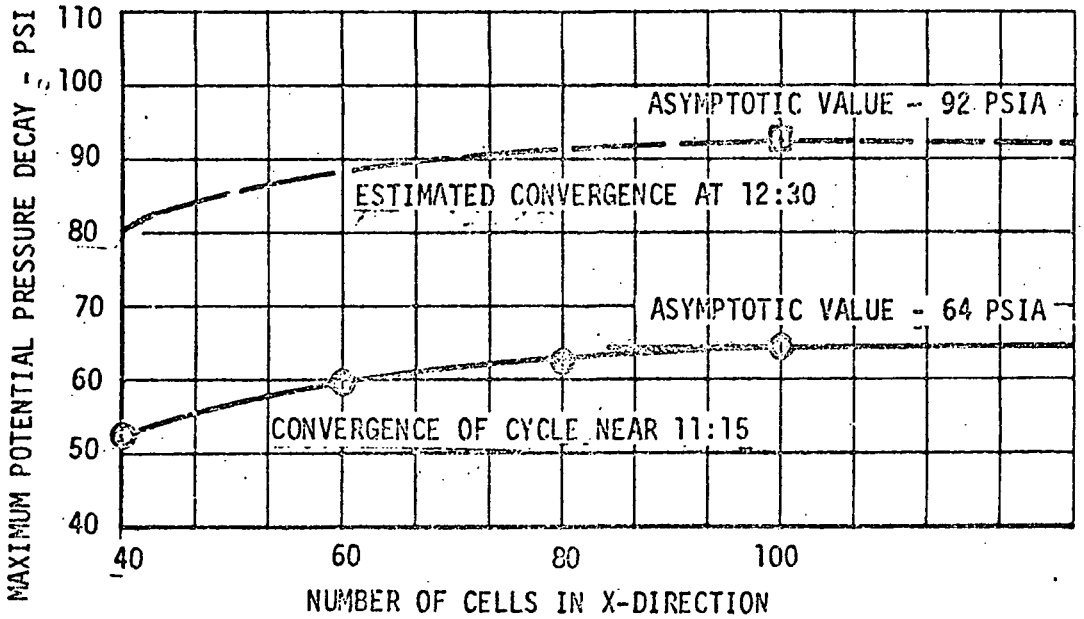

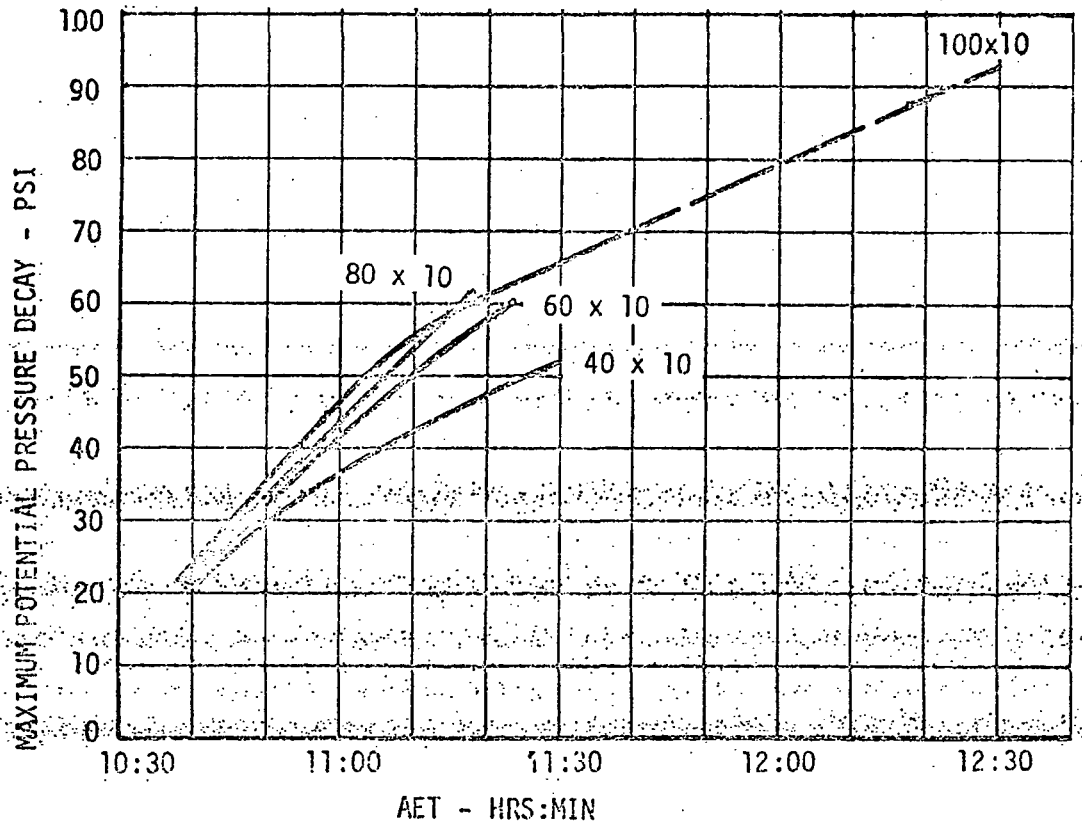

FIGURE 5-28 - CONVERGENCE OF MAXIMUM POTENTIAL PRESSURE DECAY AT AET 12:30

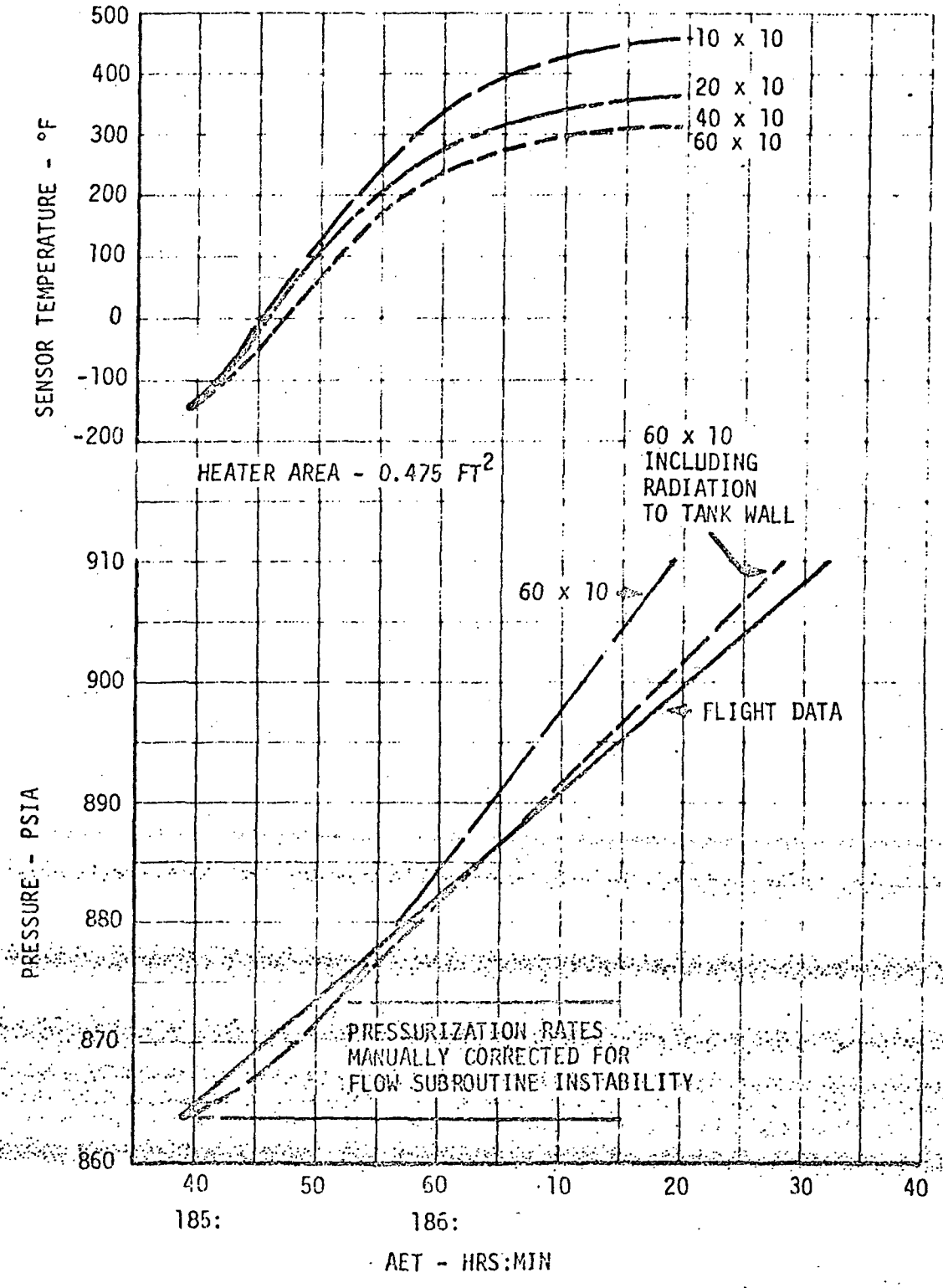

FIGURE 5-29 - LOW DENSITY HEATER CYCLE SIMULATION

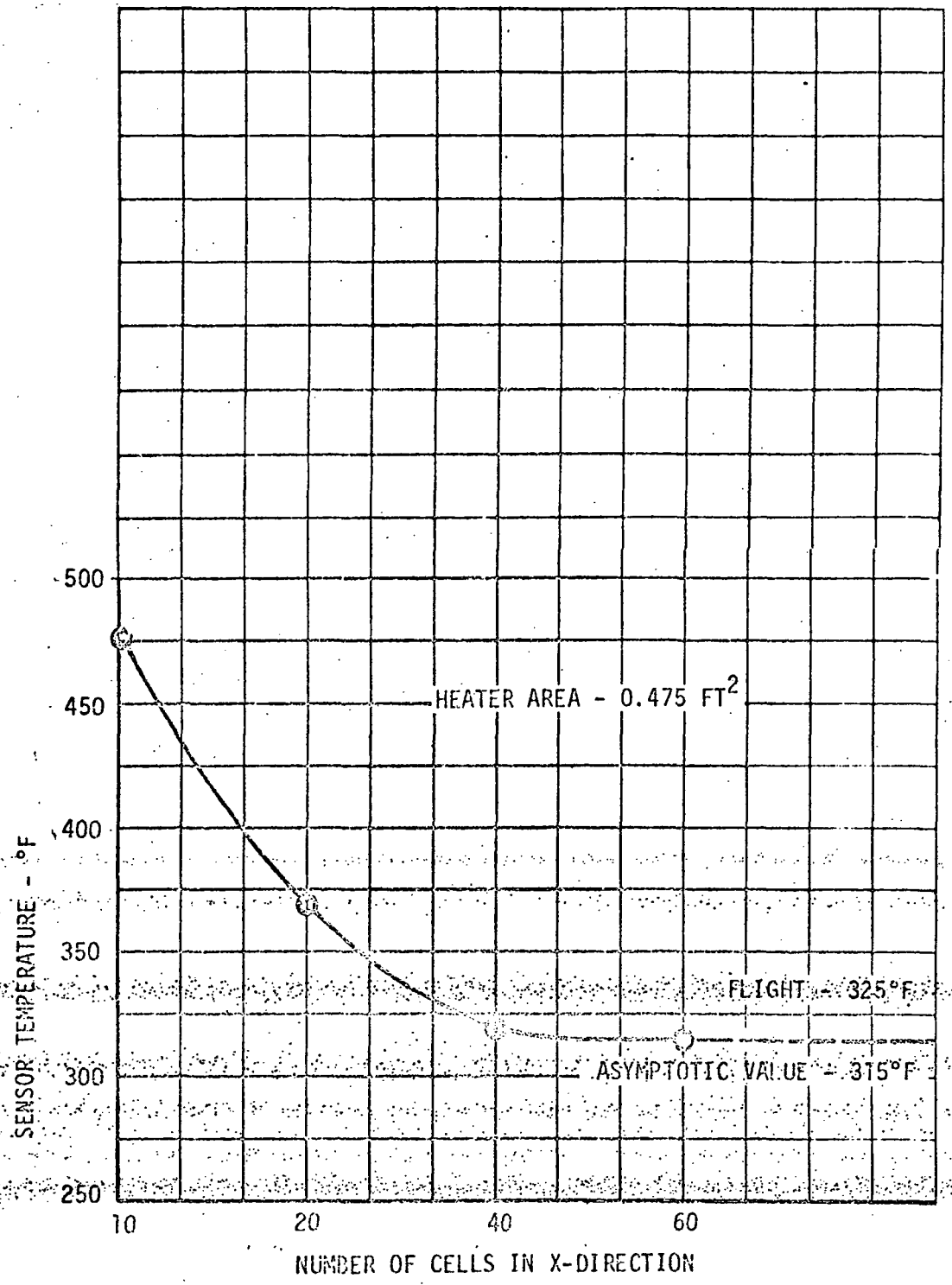

FIGURE 5-30 - LOW DENSITY HEATER CYCLE CONVERGENCE

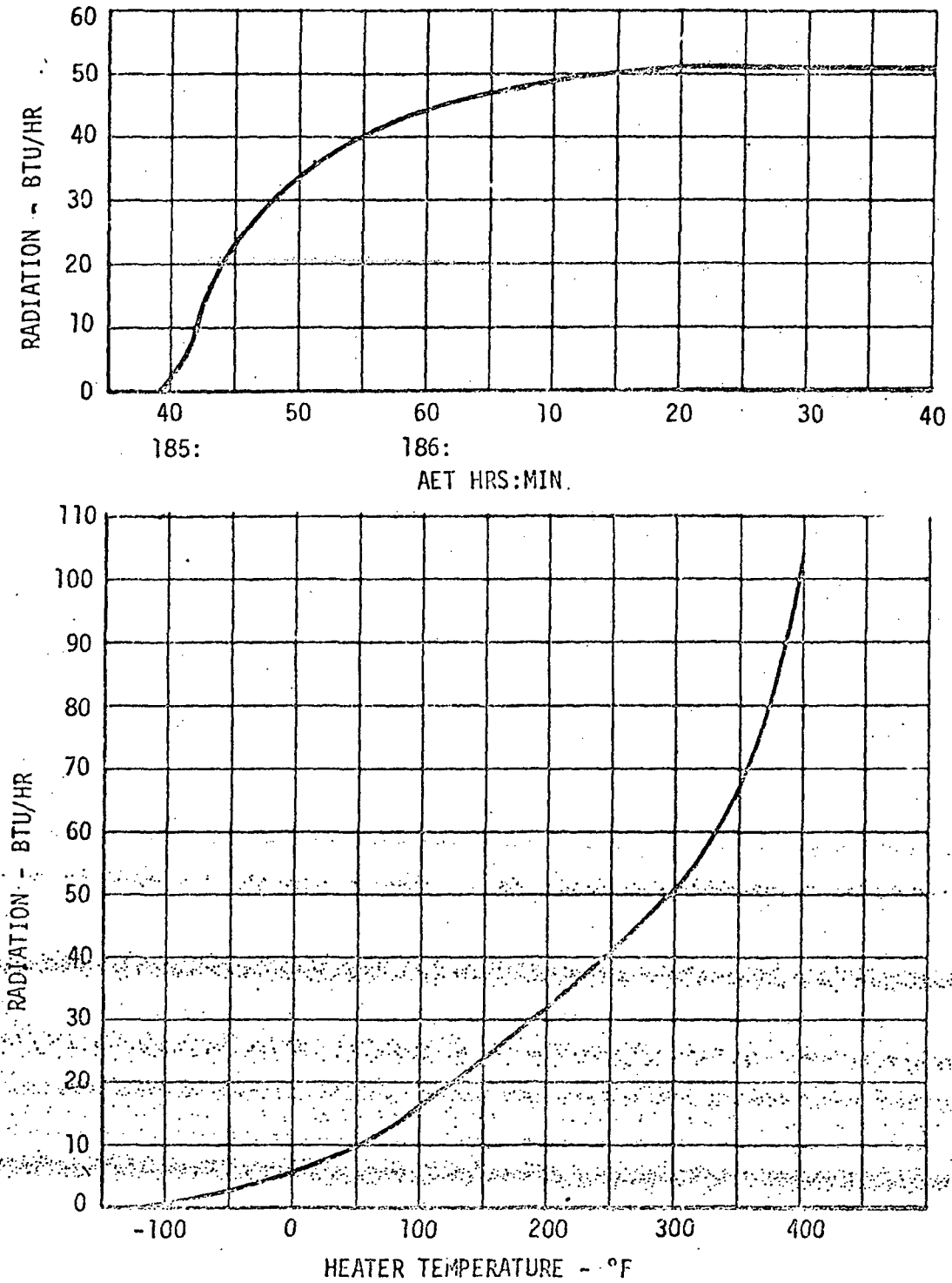

FIGURE 5-31 - RADIANT HEAT TRANSFER DURING LOW DENSITY HEATER CYCLE

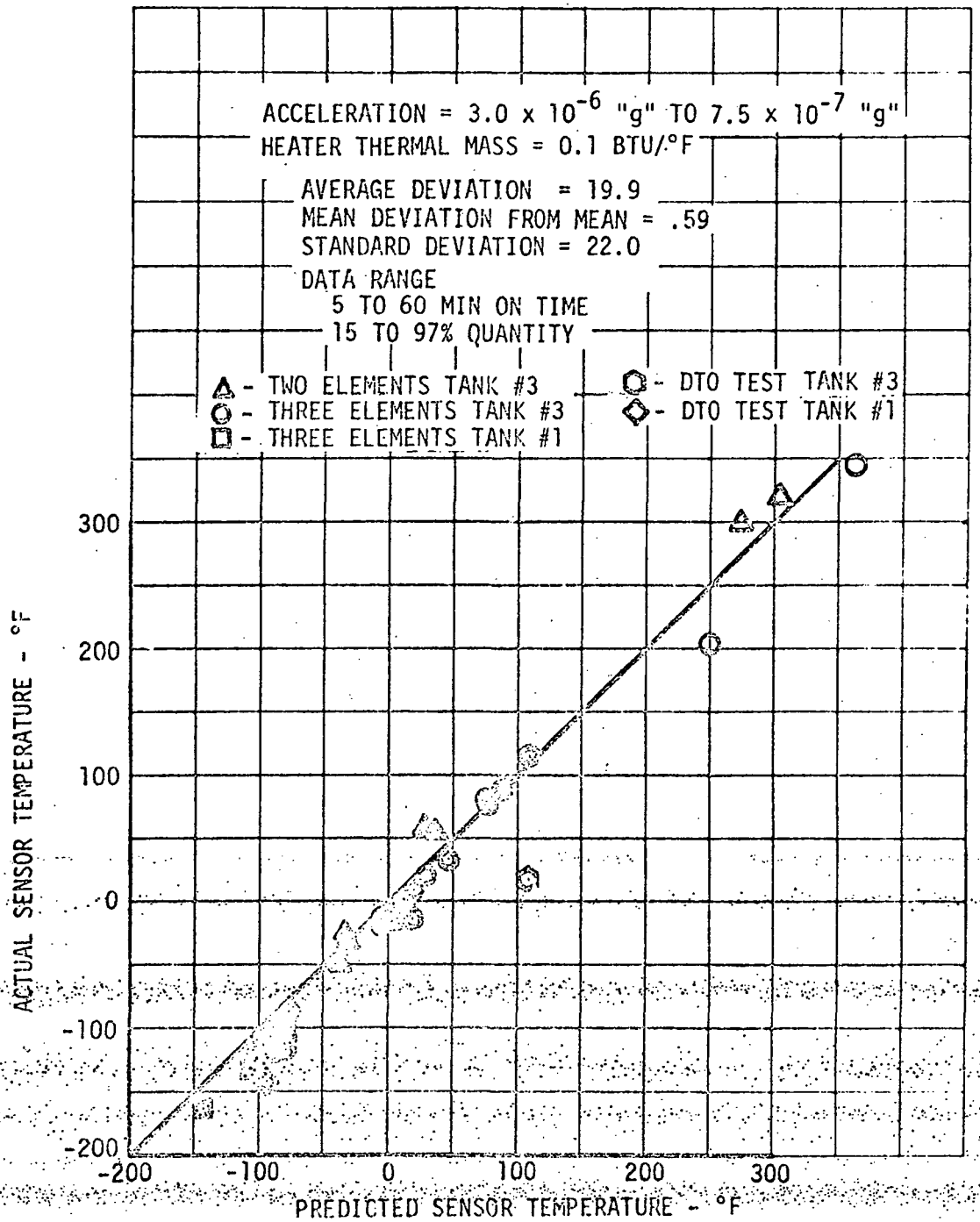

FIGURE 5-32 - TEMPERATURE COMPARISONS SUMMARY

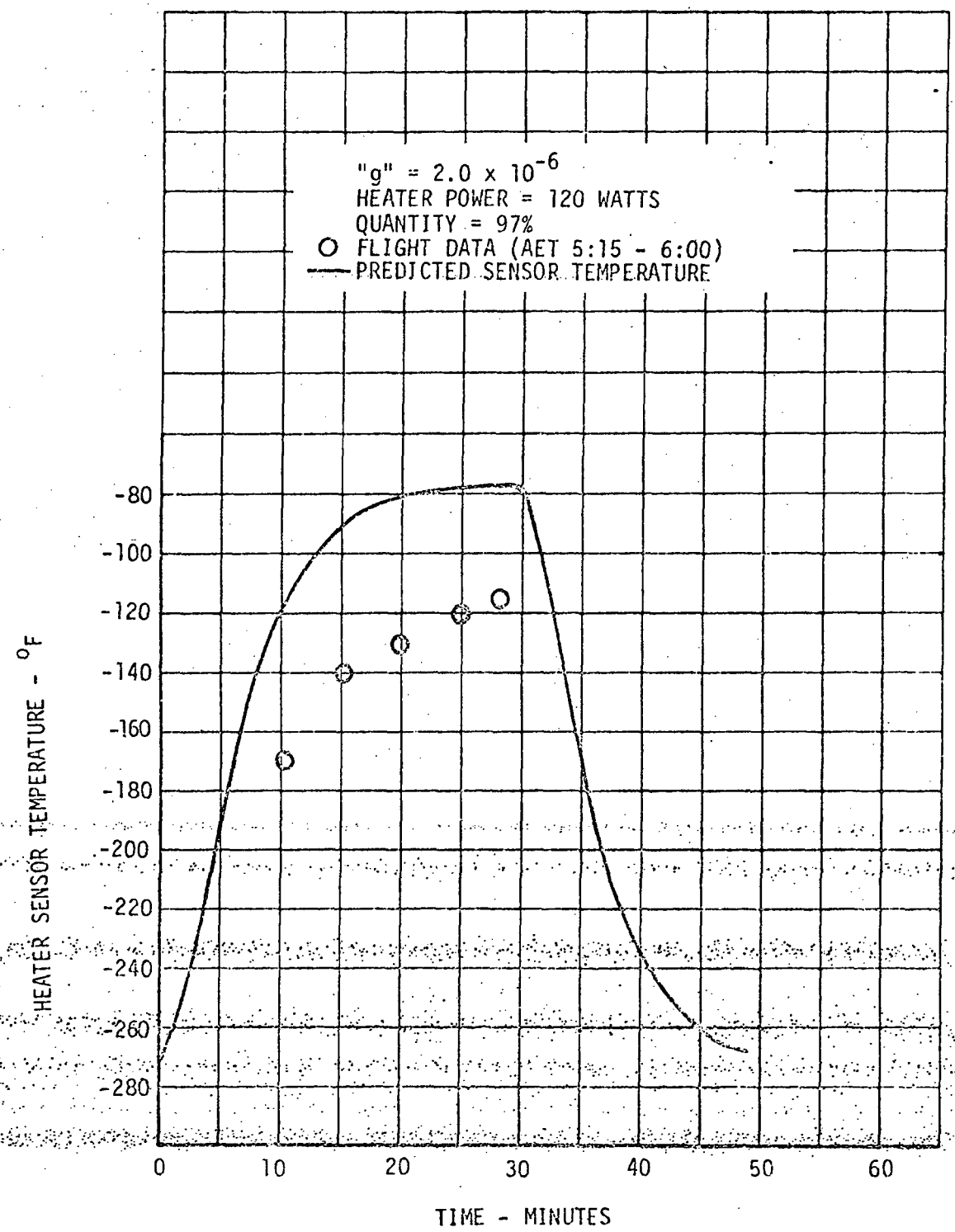

FIGURE 5-33 - EMPIRICAL HEATER RESPONSE, 97% QUANTITY

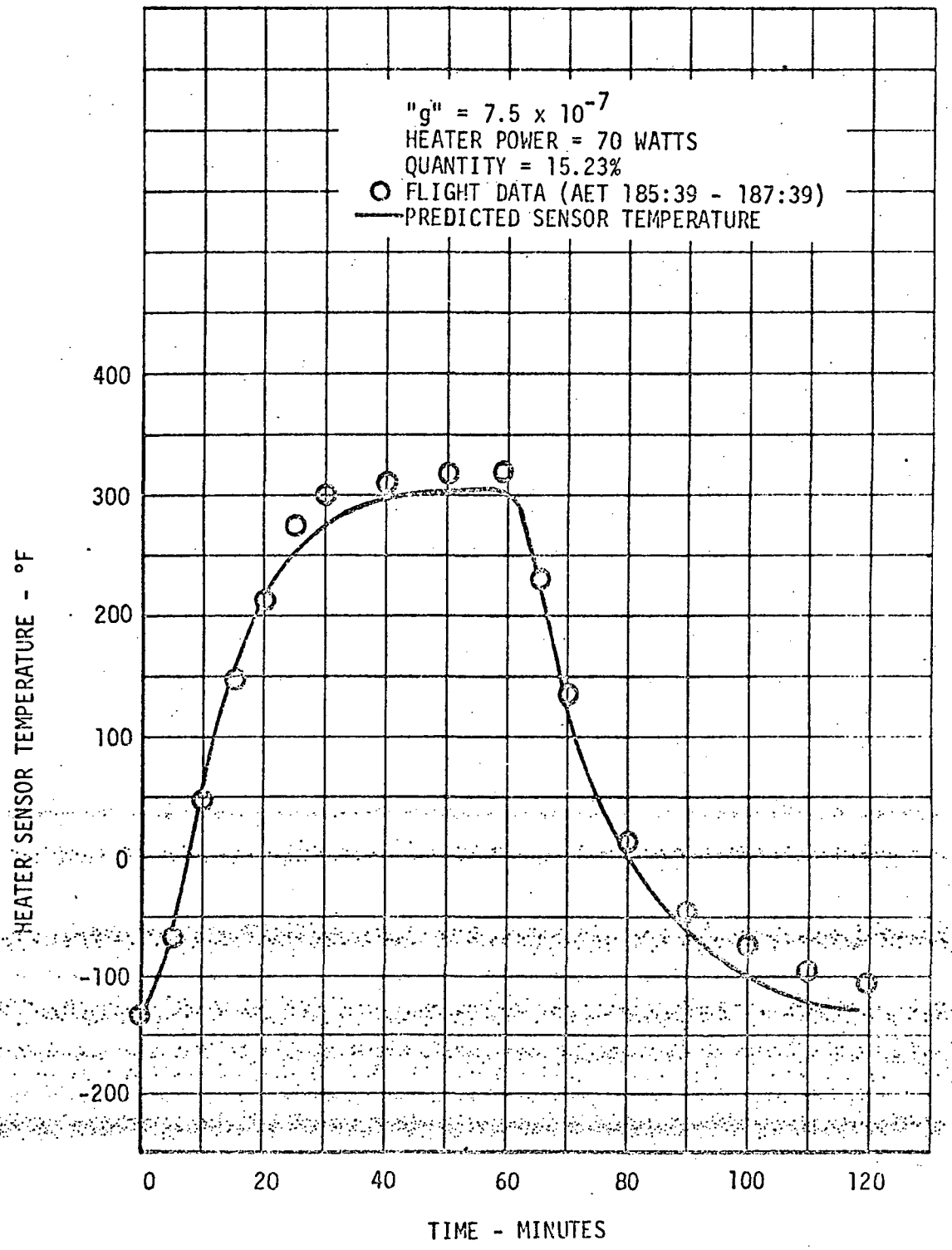

FIGURE 5-34 -- EMPIRICAL HEATER RESPONSE, 15% QUANTITY

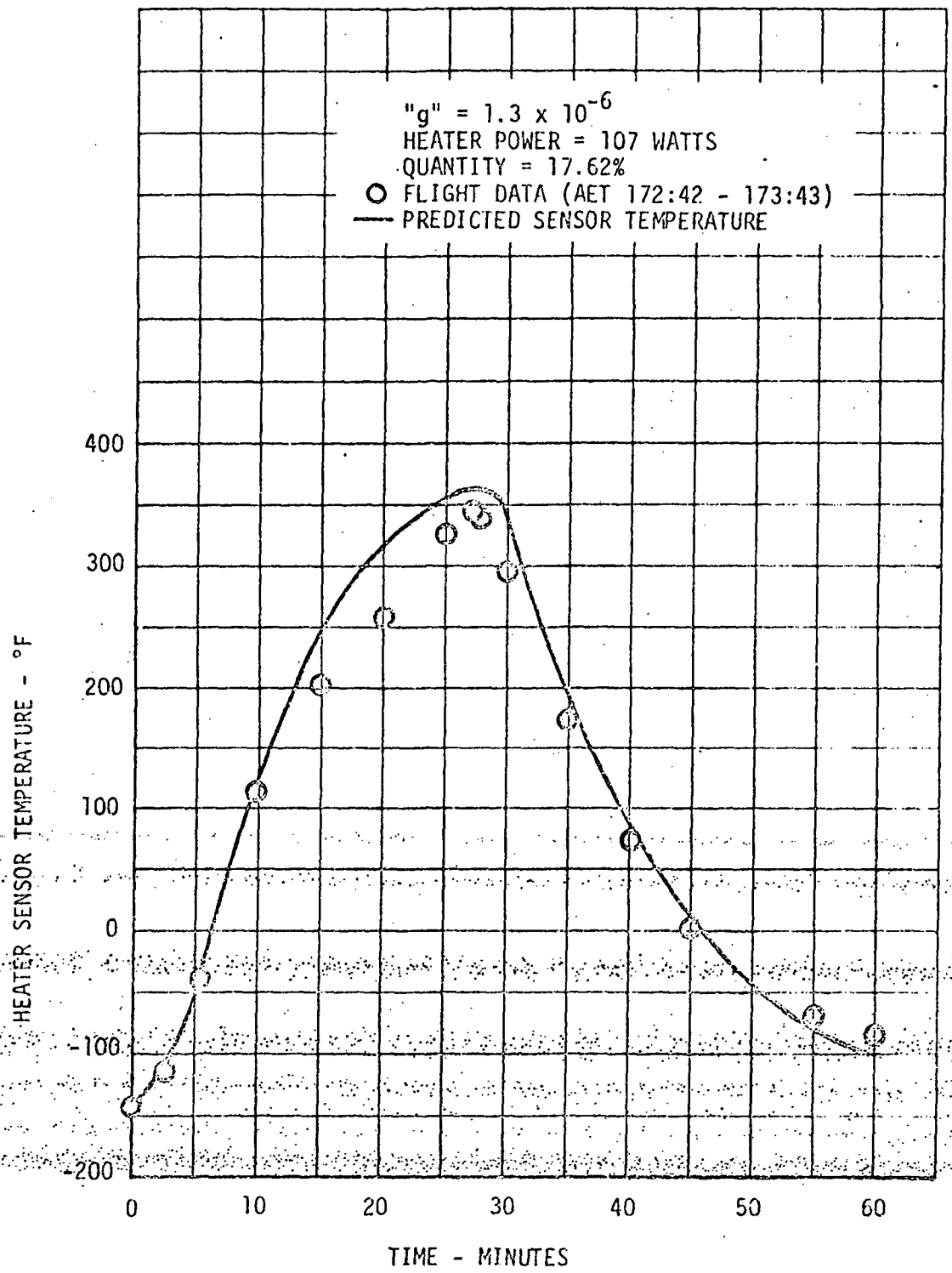

FIGURE 5-35 - EMPIRICAL HEATER RESPONSE, 17% QUANTITY

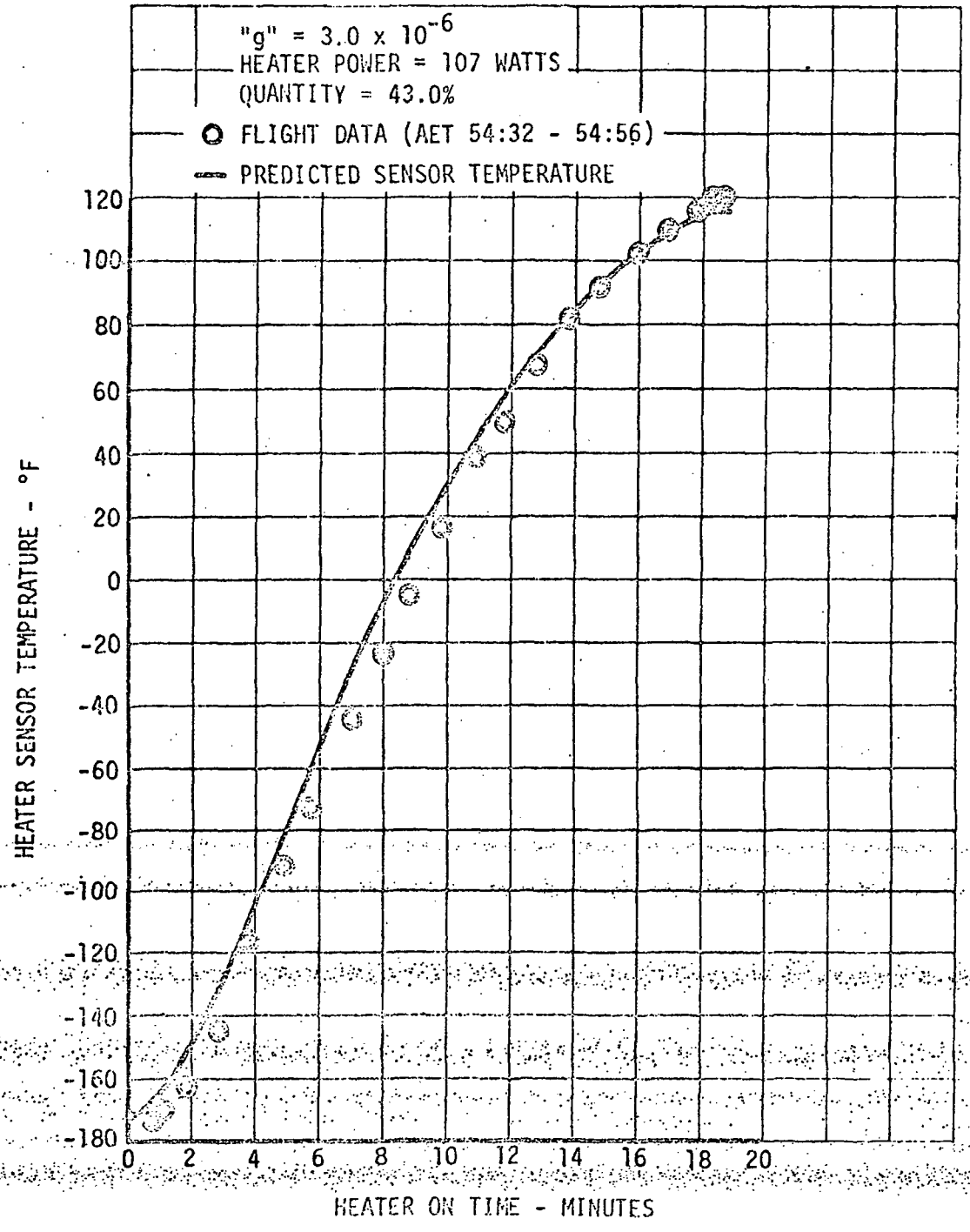

FIGURE 5-36 - EMPIRICAL HEATER RESPONSE, 43% QUANTITY

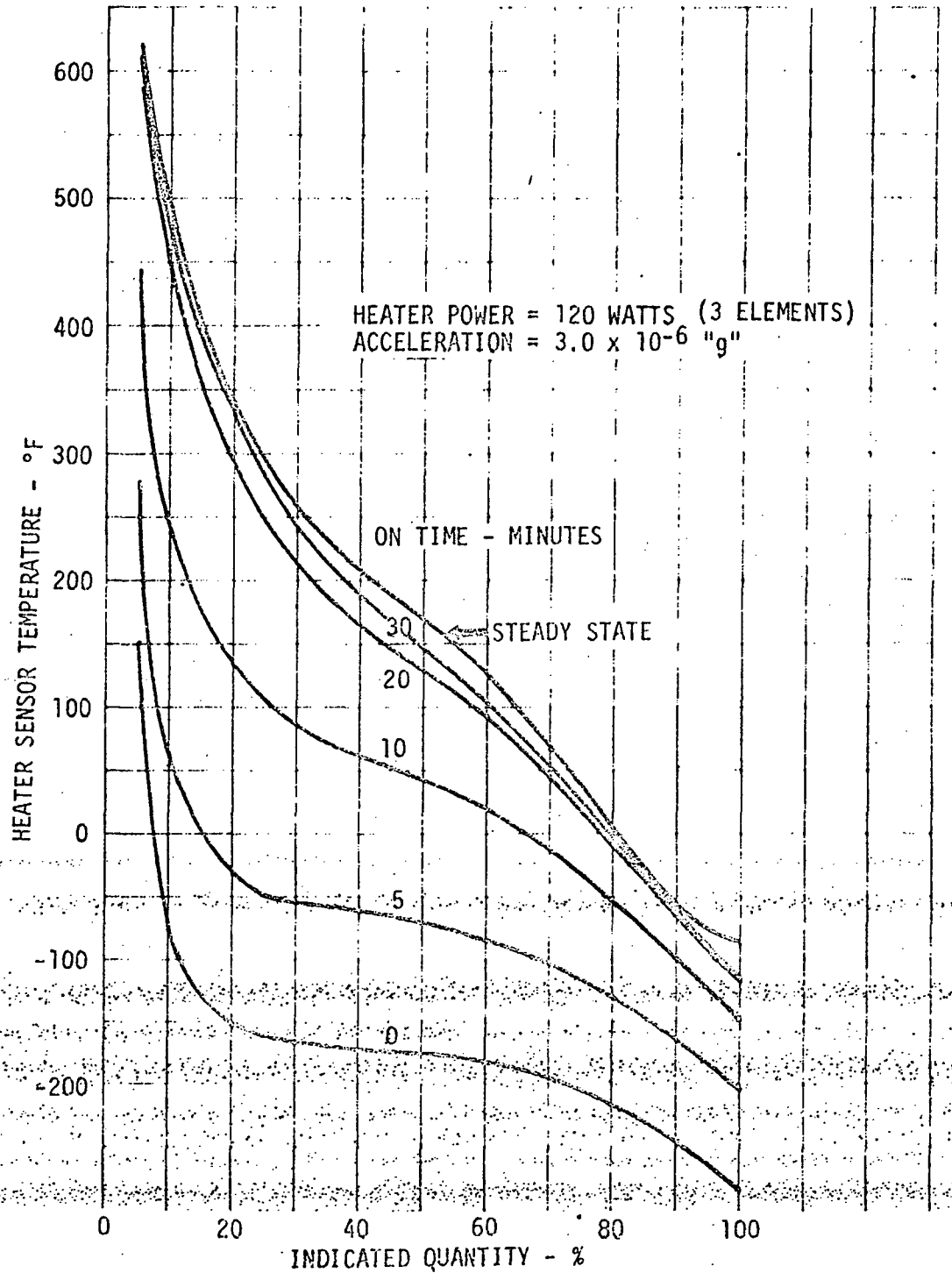

FIGURE 5-37a - PARAMETRIC HEATER RESPONSE

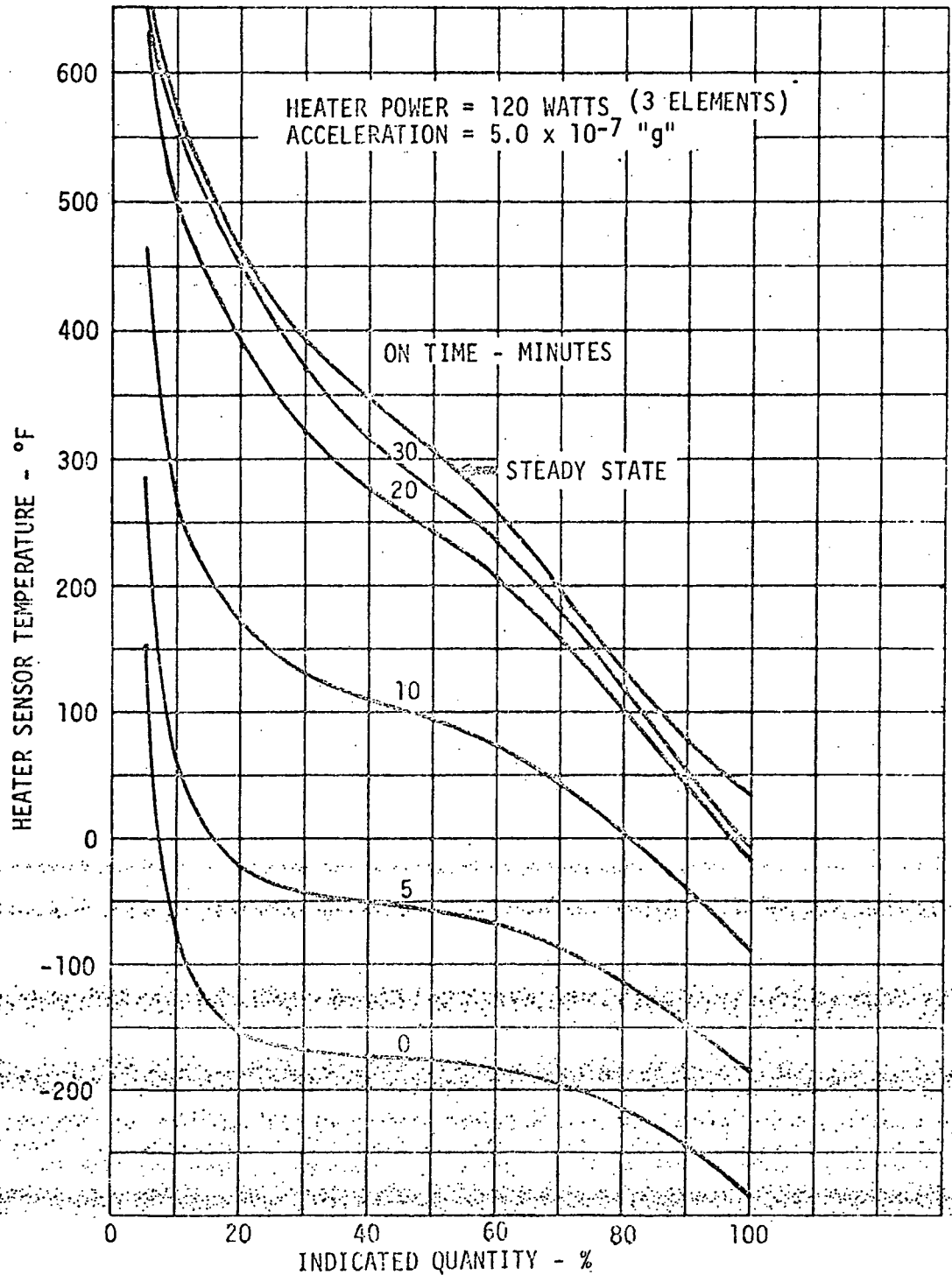

FIGURE 5-37b - PARAMETRIC HEATER RESPONSE

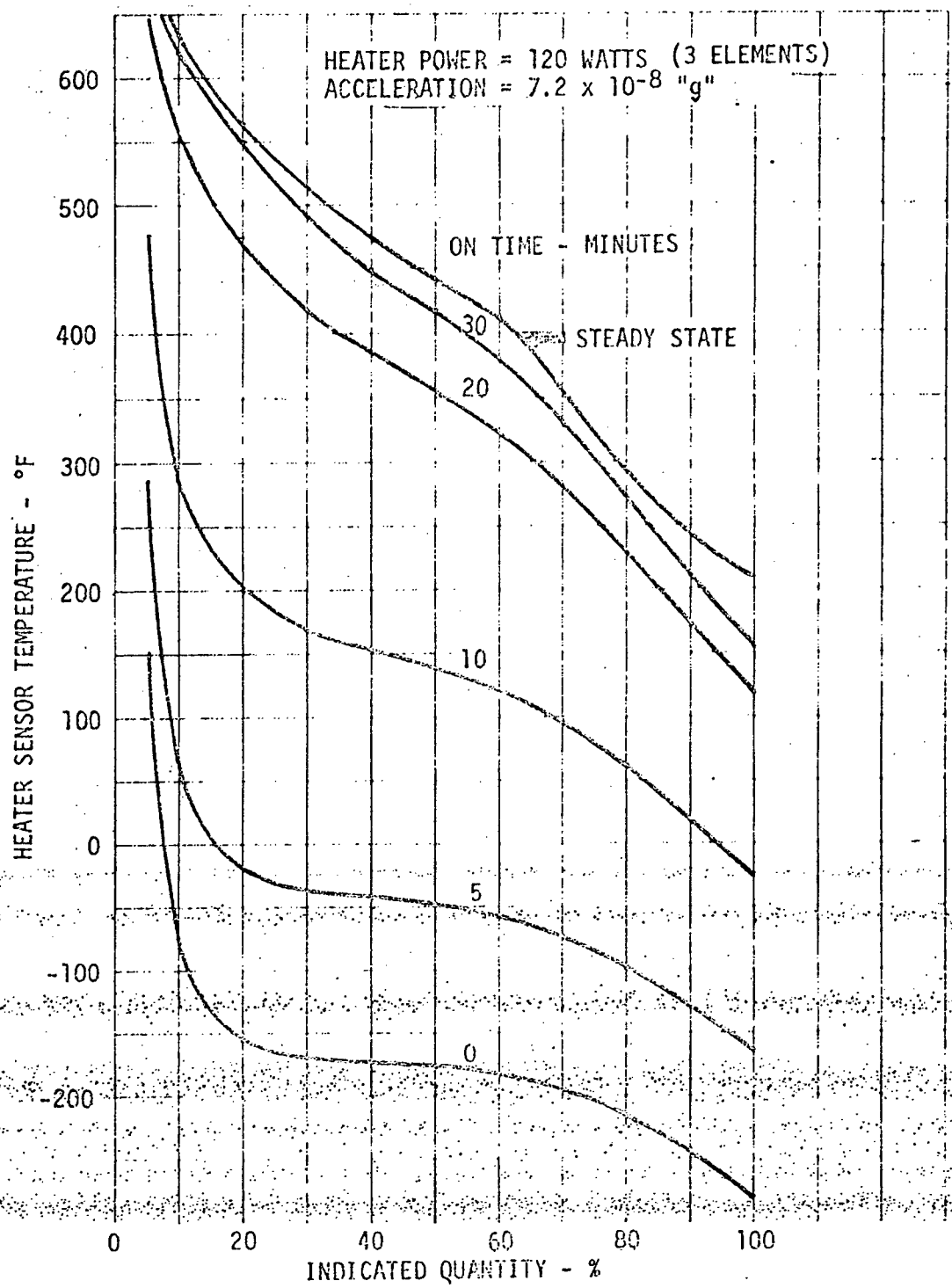

FIGURE 5-37c - PARAMETRIC HEATER RESPONSE

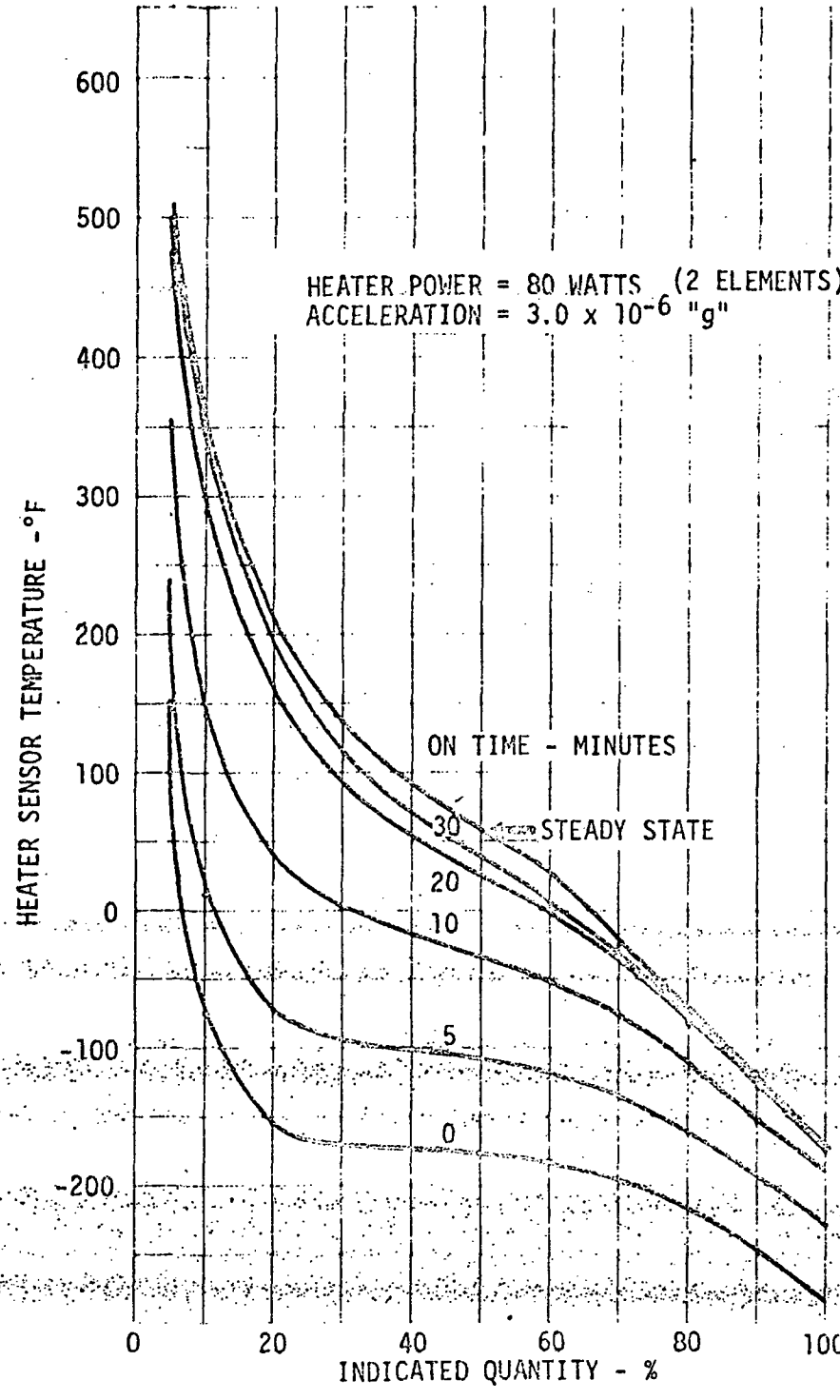

FIGURE 5-37d - PARAMETRIC HEATER RESPONSE

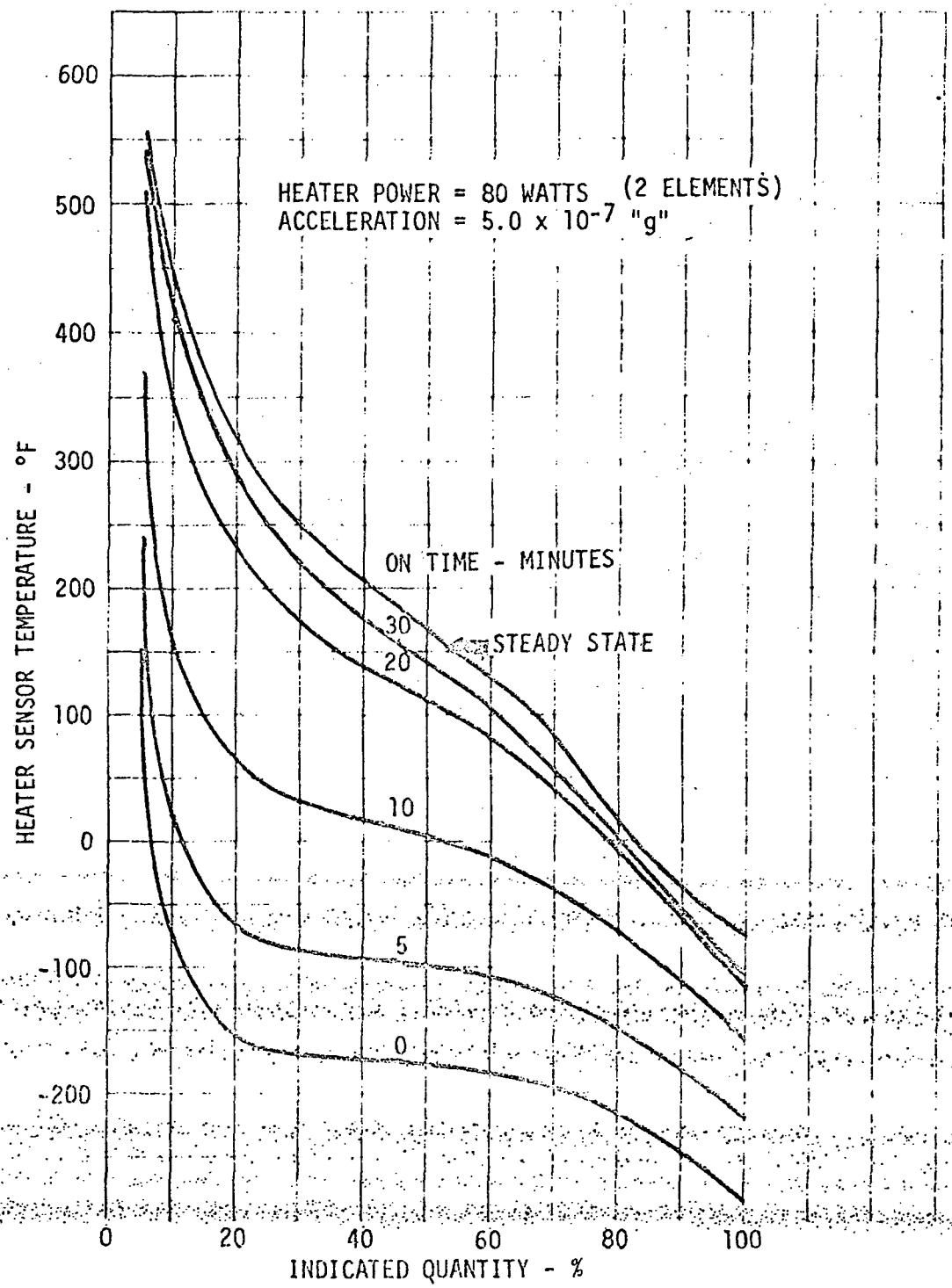

FIGURE 5-37e - PARAMETRIC HEATER RESPONSE

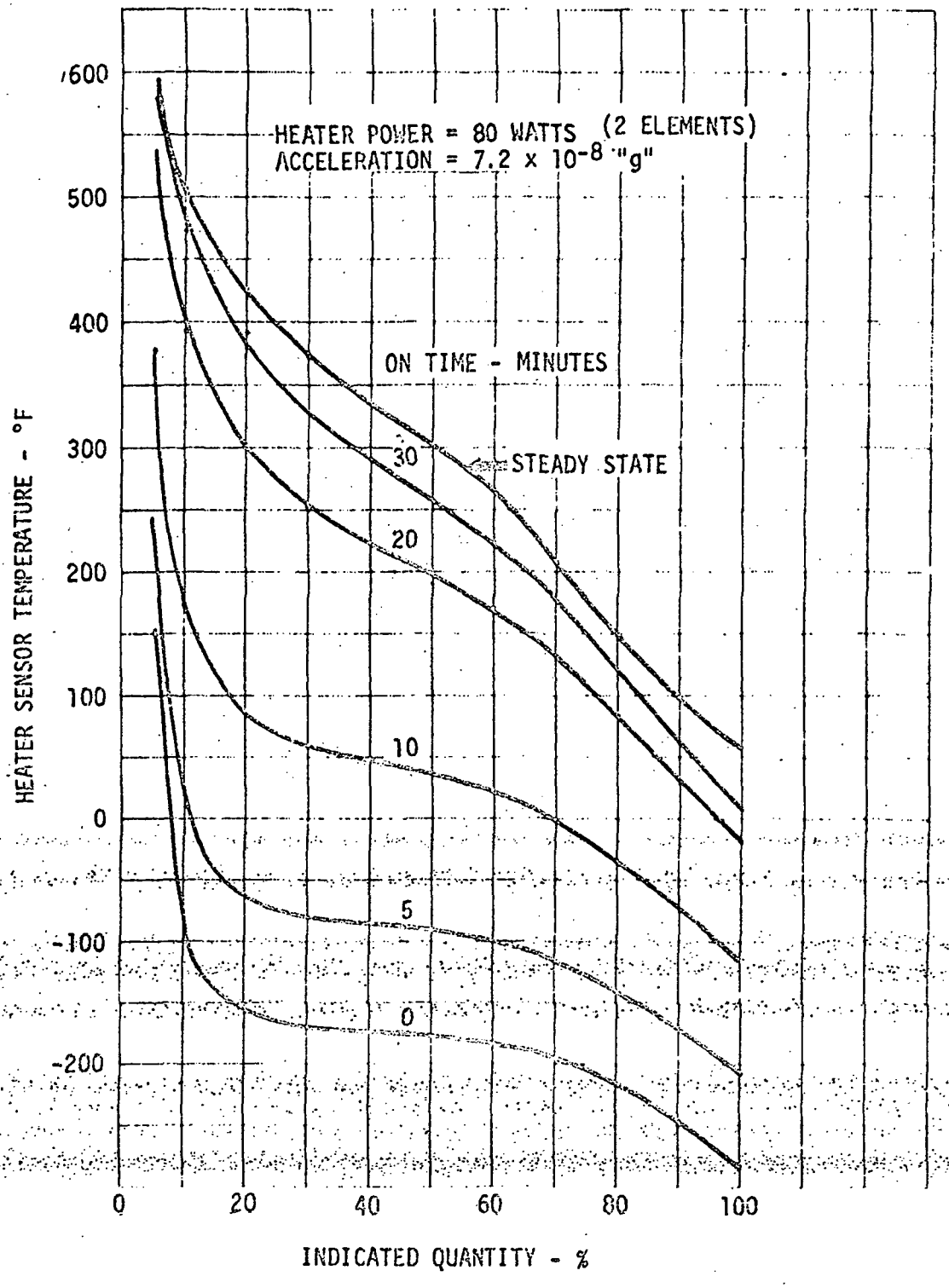

FIGURE 5-37f - PARAMETRIC HEATER RESPONSE

6.0 CONCLUSIONS

Conclusions based on analyses of the flight performance of the redesigned Apollo 14 oxygen tanks are:

1. The tank heaters, sensors, and controls functioned satisfactorily and normally during the mission.

2. The tanks supplied the high flow demands during the test simulating EVA requirements without heater temperatures exceeding the 350°F maximum limit or pressures dropping below normal operating ranges.

3. The heater temperature is strongly affected by the tank acceleration and fluid quantity. Heater power must be reduced by operating less than three elements at low quantities and accelerations to avoid exceeding the 350°F heater temperature limit during long heater-on cycles.

4. The tank accelerations during the high flow test were approximately 5×10^{-6} "g". This relatively high acceleration was caused by the oxygen vented overboard. Tank accelerations during future mission EVA periods will be determined by the astronaut location and suit vent configuration. The average tank acceleration during the EVA is not expected to be less than 7×10^{-8} "g" which is the lowest "g" observed for a long time period.

5. The heater temperatures during the Apollo 15 EVA period will be higher than the heater temperatures during the Apollo 14 high flow test because tank acceleration may be as low as 7×10^{-8} "g". Two heater elements can be used for quantities above 35% without exceeding the 350°F heater temperature limit at this acceleration. Manual control of the heaters can provide the required flow rate (4.5 lbs/hour) for quantities between 20% and 35% without exceeding 350°F heater temperatures.

6. Pressure decays may also occur during later mission EVA periods due to the low acceleration. The maximum pressure decay will be less than 230 psi for the worst case conditions of 4.5 lbs per hour flow for 3 hours duration at 70% quantity and the lowest anticipated acceleration (7×10^{-8} "g").

7. The oxygen tank pressure response and flow rates are strongly affected by heat transfer in the lines for approximately one hour after the initiation of high system flow rates (3-4 lbs per hour per tank).

6.0 CONCLUSIONS (Continued)

8. The stratification math model accurately predicts heater temperature and tank pressure response during drifting flight with tank accelerations from 7×10^{-8} to 5×10^{-6} "g". The simulation accuracy is primarily limited by the accuracy of the tank flow rates and acceleration levels.

9. Heater temperatures can be predicted within 50°F with emperical Rayleigh number heat transfer equations for steady acceleration conditions.

7.0 RECOMMENDATIONS

No hardware or operational changes are recommended for the redesigned oxygen tanks which were found to be adequate for known Apollo mission requirements. Additional analyses recommended to improve prediction accuracies and capabilities for future missions are:

1. Perform post-flight analyses of the tanks performance during the Apollo 15 EVA which will duplicate later mission EVA periods more closely than the Apollo 14 simulation tests.

2. Modify the stratification math model to calculate tank flow rates from system demands for planned configurations and operating modes not included in the present model.

3. Determine model parameters required for accurate simulations when using the improved math model developed under this contract.

APPENDIX A

THE PRESSURE CHANGE EQUATION FOR A CRYOGENIC TANK

The pressure changes in a cryogenic tank resulting from heat addition and mass extraction are usually calculated with the assumption that the tank is a constant volume container. This assumption causes large errors when the fluid is nearly incompressible and the pressure vessel is highly stressed. An error in the pressure change calculation is also caused by flows not usually measured that are required to pressurize plumbing system volumes at ambient temperature. In order to eliminate these errors, the pressure change equation for an equilibrium fluid in an elastic container has been derived and a method for including the external volume effects developed.

The thermodynamic system is bounded by the inside surface of the pressure vessel and is closed at the fluid outlet from the pressure vessel. The volume inside the thermodynamic boundary is not constant since the pressure vessel is elastic. The outflow velocity is assumed to be small enough that the kinetic energy and momentum of the outflow are negligible. The conservation equations for mass and energy, therefore, determine the system response to heat and mass flows.

The conservation of mass:

$$\frac{dM}{dt} = V\frac{d\rho}{dt} + \rho\frac{dV}{dt} \tag{A-1}$$

The conservation of energy:

$$\frac{d}{dt}(\rho VU) = \frac{dQ}{dt} + h\frac{dM}{dt} - P\frac{dV}{dt} \tag{A-2}$$

Expanding A-2 and using the definition of enthalpy

$$\rho V\frac{dU}{dt} + U\left(V\frac{d\rho}{dt} + \rho\frac{dV}{dt}\right) = \frac{dQ}{dt} + \frac{dM}{dt}\left(U + \frac{P}{\rho}\right) - P\frac{dV}{dt} \tag{A-3}$$

Substituting A-1 in A-3 and simplifying

$$\rho V\frac{dU}{dt} = \frac{dQ}{dt} + \frac{P}{\rho}\frac{dM}{dt} - P\frac{dV}{dt} \tag{A-4}$$

The internal energy is taken as a function of pressure and density

$$\frac{dU}{dt} = \frac{\partial U}{\partial P}\frac{dP}{dt} + \frac{\partial U}{\partial \rho}\frac{d\rho}{dt} \tag{A-5}$$

Using A-1 and noting that $M = \rho V$

$$\frac{dU}{dt} = \frac{\partial U}{\partial P}\frac{dP}{dt} + \frac{\partial U}{\partial \rho}\left(\frac{1}{V}\frac{dM}{dt} - \frac{M}{V^2}\frac{dV}{dt}\right) \tag{A-6}$$

Substituting A-6 in A-4

$$\rho V\left[\frac{\partial U}{\partial P}\frac{dP}{dt} + \frac{\partial U}{\partial \rho}\left(\frac{1}{V}\frac{dM}{dt} - \frac{M}{V^2}\frac{dV}{dt}\right)\right] = \frac{dQ}{dt} + \frac{P}{\rho}\frac{dM}{dt} - P\frac{dV}{dt} \tag{A-7}$$

Solving for $\frac{dP}{dt}$ and rearranging

$$\frac{dP}{dt} = \frac{\frac{dQ}{dt} + \frac{P}{\rho}\frac{dM}{dt} - P\frac{dV}{dt} - \rho\frac{\partial U}{\partial \rho}\left(\frac{dM}{dt} - \frac{M}{V}\frac{dV}{dt}\right)}{\rho V\frac{\partial U}{\partial P}} \tag{A-8}$$

Rearranging

$$\frac{dP}{dt} = \frac{\frac{dQ}{dt} + \frac{dM}{dt}\left(\frac{P}{\rho} - \rho\frac{\partial U}{\partial \rho}\right)}{\rho V\frac{\partial U}{\partial P}} + \frac{\rho\frac{\partial U}{\partial \rho}\frac{M}{V}\frac{dV}{dt} - P\frac{dV}{dt}}{\rho V\frac{\partial U}{\partial P}} \tag{A-9}$$

and reducing the last term

$$\frac{dP}{dt} = \frac{\frac{dQ}{dt} + \frac{dM}{dt}\left(\frac{P}{\rho} - \rho\frac{\partial U}{\partial \rho}\right)}{\rho V\frac{\partial U}{\partial P}} + \frac{\rho^2\frac{dV}{dt}\left(\frac{\partial U}{\partial \rho} - \frac{P}{\rho^2}\right)}{\rho V\frac{\partial U}{\partial P}} \tag{A-10}$$

Now define

$$\phi = \frac{1}{\rho\frac{\partial U}{\partial P}} \tag{A-11}$$

and

$$\theta = -\rho\frac{\partial h}{\partial \rho} \equiv -\rho\left(\frac{\partial U}{\partial \rho} - \frac{P}{\rho^2}\right) \tag{A-12}$$

Substituting A-11 and A-12 in A-10

$$\frac{dP}{dt} = \frac{\phi}{V}\left(\frac{dQ}{dt} + \theta\frac{dM}{dt}\right) - \frac{1}{V}\frac{dV}{dt}\rho\theta\phi \qquad \text{(A-13)}$$

Equation A-13 provides a convenient method for calculating pressure response if the volume rate of change is known. The last term is zero for a constant volume system. If the container is elastic so that the volume change is related to the pressure change, some further reduction is possible.

$$\frac{dP}{dt} = \frac{\phi}{V}\left(\frac{dQ}{dt} + \theta\frac{dM}{dt}\right) - \frac{1}{V}\frac{dV}{dP}\frac{dP}{dt}\rho\theta\phi \qquad \text{(A-14)}$$

Again solving for $\frac{dP}{dt}$

$$\frac{dP}{dt} = \frac{\frac{\phi}{V}\left(\frac{dQ}{dt} + \theta\frac{dM}{dt}\right)}{1 + \frac{1}{V}\frac{dV}{dP}\rho\theta\phi} \qquad \text{(A-15)}$$

for a spherical tank

$$\frac{1}{V}\frac{dV}{dP} = \frac{3\ r\ (1-\sigma)}{2\ b\ E} \qquad \text{(A-16)}$$

therefore

$$\frac{dP}{dt} = \frac{\frac{\phi}{V}\left(\frac{dQ}{dt} + \theta\frac{dM}{dt}\right)}{1 + \frac{3\ r\ (1-\sigma)}{2\ b\ E}\rho\theta\phi} \qquad \text{(A-17)}$$

Now the outflow is measured at the end of the distribution lines which contain gas at the same pressure as the tank. The flow across the thermodynamic boundary must include the flow required to pressurize the lines. Two assumptions for determining the flow into the lines may be considered:

1. Fluid expelled from the tanks thermodynamic boundary maintains its density while compressing gas in the lines either adiabatically or isothermally.

2. Fluid expelled from the tank does not affect the temperature distribution from the thermodynamic boundary to the system outlet, but the density in the lines changes adiabatically or isothermally.

The phenomena of assumption 1 can be described by writing the polytropic relationship for the volume of gas in the lines.

$$\frac{V_L}{V_{L_0}} = \left(\frac{P}{P_0}\right)^{-\frac{1}{N}} \qquad \text{(A-18)}$$

Taking logarithms and differentiating we have:

$$\frac{dV_L}{V_L} = \frac{1}{N}\frac{dP}{P} \qquad \text{(A-19)}$$

The flow rate into the tank thermodynamic boundary due to the lines is therefore:

$$\frac{dM_L}{dt} = -\rho_t \frac{V_L}{NP}\frac{dP}{dt} \qquad \text{(A-20)}$$

Where N=1 for isothermal compression and N=1.4 for adiabatic compression.

Now writing A-14 in terms of the demand and line flow rates.

$$\frac{dP}{dt} = \frac{\phi}{V}\frac{dQ}{dt} + \frac{\phi\theta}{V}\frac{dM_L}{dt} + \frac{\phi\theta}{V}\frac{dM_d}{dt} - \frac{1}{V}\frac{dV}{dP}\frac{dP}{dt}\rho\phi\theta \qquad \text{(A-21)}$$

Substituting A-20 in A-21 and again solving for $\frac{dP}{dt}$ we have:

$$\frac{dP}{dt} = \frac{\frac{\phi}{V}\left(\frac{dQ}{dt} + \theta\frac{dM_d}{dt}\right)}{1 + \frac{\rho\theta\phi}{V_t}\frac{dV}{dP} + \frac{\rho\theta\phi}{NP}\frac{V_L}{V_t}} \qquad \text{(A-22)}$$

The relationships for assumption 2 are developed by assuming that the fluid density in the lines is related to the pressure by the polytropic exponent.

$$\rho = \rho_0\left(\frac{P}{P_0}\right)^{\frac{1}{N}} \qquad \text{(A-23)}$$

Again taking logarithms and differentiating we have:

$$\frac{d\rho}{\rho} = \frac{1}{N}\frac{dP}{P} \qquad \text{(A-24)}$$

Therefore, the flow rate into the tank from the lines is:

$$\frac{dM_L}{dt} = -\frac{\rho_L V_L}{NP}\frac{dP}{dt} \tag{A-25}$$

Substituting A-25 into A-14 and solving for $\frac{dP}{dt}$ as before we have:

$$\frac{dP}{dt} = \frac{\frac{\phi}{V}\left(\frac{dQ}{dt} + \theta\frac{dM_d}{dt}\right)}{1 + \frac{\rho_t \phi\theta}{V_t}\frac{dV_t}{dP} + \frac{\rho_L \phi\theta}{NP}\frac{V_L}{V_t}} \tag{A-26}$$

APPENDIX B

STRATIFICATION MATH MODEL

The stratification math model used for these analyses is based on the General Elliptic Method (GEM) developed by Mr. C. K. Forester of Boeing-Seattle to solve finite difference approximations to the mass, momentum and energy conservation equations (Reference 1). The fundamental assumption of the method is that the pressure terms in the energy and momentum equation are not coupled. This assumption is valid for low velocity flows in which acoustic waves do not contribute significantly to the fluid energy. This assumption permits a much longer time step than is otherwise necessary for stability. The uncoupling is accomplished by using only the global (average) pressure in the energy equation to eliminate the effects of acoustic waves. Other assumptions which have been validated by comparing model results with Apollo 12 flight data are:

1. Two dimensional rectangular geometry (Figure B-1)
2. Viscous energy dissipation and kinetic energies are neglected
3. Radiation heat transfer within the fluid is neglected (radiation from the heater surface is included).
4. Acceleration body forces are constant through the tank

The difference equations used by the math model are based on the control volume concept. The rectangular flow field region is subdivided into elementary control volumes or cells. The difference equations are formulated with the mass fluxes defined on the cell boundaries, while the fluid properties are defined at the centers of the cells. This formulation results in conservation of mass for each easily defined cell, whereas formulations with fluxes and state properties defined at the same point do not.

The difference equations are solved by extrapolating an initial set of field variables by a time increment. Preliminary field pressure are calculated at the extrapolated time including the effects of the preliminary energy and mass transfers between cells. The preliminary pressures at the extrapolated time are used to revise the energy and mass transfer in the time increment. The extrapolated pressures are revised to account for the new energy and mass transfers, and the extrapolation procedure repeated until satisfactory convergence is obtained. The field variables at the new time are taken as initial conditions for the next time increment. Successive iterative extrapolations are made to describe the fluid state for the simulated time period.

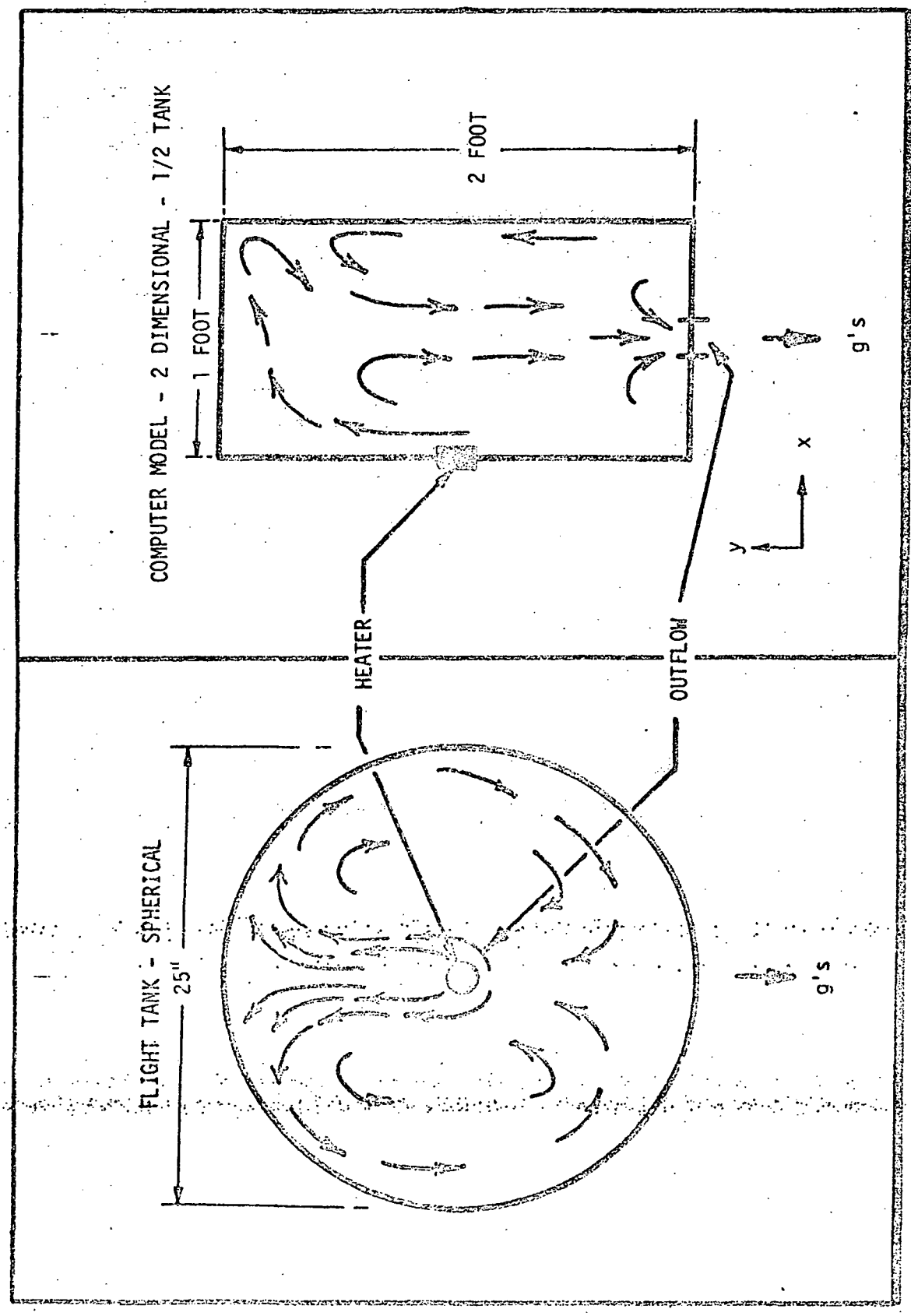

FIGURE B-1 - ANALYTICAL APPROACH - MODEL DESCRIPTION

The difference equations solved by the program are only approximations to the partial differential equations describing the processes in the tank. The quality of this approximate solution improves and approaches the solution of the exact equations as the cell sizes are reduced. The cell sizes required to obtain an adequate approximation can not establish a priori. The effect of cell size on the model results must be investigated for each tank condition simulated to assure that the approximate solutions are convergent. Separate simulations with at least three different cell sizes or grids are required to test the convergence at the solution for each tank condition. Particular parameters, heater temperature for example, are a function of grid size and are extrapolated to "asymptotic" limits. The asymptotic limit, when obtainable, is the exact solution to the controlling partial differential equations. The extrapolation procedure used in these analyses is based on the parameter differences related to the number of cells in the X direction of the model as shown below.

No. of Cells	Parameter-Temperature	Difference
20	60	
40	100	> 40
60	120	> 20
80	130	> 10

The successive differences form a geometric series. The ratio between successive terms is found and the sum of the infinite geometric series determined. The sum of the series of differences is added to the appropriate parameter to obtain the parameter asymptotic limit.

APPENDIX C

HEATER TEMPERATURE CORRELATIONS

Heater temperatures can be determined from the numerical math model, but the computer usage times are excessive for the generation of parametric data and to conduct routine flight analyses. Empirical heat transfer equations were investigated to develop a more convenient tool for heater temperature studies.

The convective heat transfer from a horizontal cylinder is usually determined from a Rayleigh number equation.

$$\frac{dQ}{dt} = \pi \; L \; K \; \Delta T \; C_{ra} \; (R_a)^{1/4}$$

The Rayleigh number is determined from:

$$R_a = \frac{D^3 \; \rho^2 \; 32.174 \; g \; \beta \; \Delta T \; C_p}{\mu K}$$

The fluid properties used to evaluate the Rayleigh numbers are usually taken at the mean film temperatures. This convention is based on tests with simple fluids under 1 "g" conditions. Since the properties of supercritical oxygen may vary by an order of magnitude in the boundary layer, the properties in the Rayleigh number were averaged instead of taken at the mean film temperature. The viscosity, conductivity, and density were taken as the average of their values for the bulk temperature and the heater temperature. The specific heat was evaluated as the difference in the enthalpy at the heater, and bulk temperatures divided by the temperature difference. The coefficient of expansion used was,

$$\beta = \frac{-1}{\rho_b} \frac{\rho_h - \rho_b}{T_h - T_b}$$

The radiation from the heater is also significant and was included in the complete heat transfer equation.

$$\frac{dQ}{dt} = \pi \; L \; K \; \Delta T \; C_{ra} \; (R_a)^{1/4} + \varepsilon \; C_s \; (T_h^{\,4} - T_b^{\,4})$$

Heater temperatures were developed as a function of heater-on time by numerical integration of the equation,

$$\frac{dT}{dt} = \frac{dQ}{dt}\left(\frac{1}{MC}\right)$$

where MC is the heater thermal mass of 0.1 BTU/°F. The heater temperature sensor lag was included in the integration to provide a means of comparison with flight data. The temperature sensor response was determined from:

$$\frac{dT_S}{dt} = C_k\,(T_h - T_S)$$

The constant was estimated as 0.26 minutes^{-1}.